

# **POSITRON IMPACT IONIZATION PROCESSES IN GASES**

A thesis submitted to the University of London  
for the degree of Doctor of Philosophy

Geraint Owain Jones  
Department of Physics and Astronomy  
University College London

September 1991

ProQuest Number: 10611133

All rights reserved

INFORMATION TO ALL USERS

The quality of this reproduction is dependent upon the quality of the copy submitted.

In the unlikely event that the author did not send a complete manuscript and there are missing pages, these will be noted. Also, if material had to be removed, a note will indicate the deletion.



ProQuest 10611133

Published by ProQuest LLC (2017). Copyright of the Dissertation is held by the Author.

All rights reserved.

This work is protected against unauthorized copying under Title 17, United States Code  
Microform Edition © ProQuest LLC.

ProQuest LLC.  
789 East Eisenhower Parkway  
P.O. Box 1346  
Ann Arbor, MI 48106 – 1346

## ABSTRACT

The two experiments that are discussed in this work are both studies of ionization phenomena in gases.

The main body of the work involved the development of an experiment to measure the positron impact ionization cross-section of atomic hydrogen. This experiment utilizes the crossed-beam method wherein a magnetically guided positron beam crosses a diverging jet of highly dissociated hydrogen gas. The suitability of this system to measure relative ionization cross-sections with both positrons and electrons has been demonstrated by measuring the impact ionization cross-sections of molecular hydrogen. Results obtained agree with previously published data to within experimental error.

Preliminary studies have also been made with the atomic hydrogen source in operation and these revealed that high fluxes of photons, protons and electrons are emitted from the gas discharge and detected. These would make it impossible to detect ions at the considerably lower count-rates that are anticipated and their effects have had to be circumvented. This has been done successfully and it is concluded that the measurement of the positron impact ionization cross-section of atomic hydrogen seems possible with this apparatus.

The second experiment has been a study of the times-of-flight of electrons emitted in positron impact ionization of Argon. The purpose of the experiment is to assess the significance of electron capture to the continuum (ECC) as a possible outcome of the ionizing collisions of positrons. Electrons which have been captured into a continuum state of a positron are expected to have a velocity vector equal to that of the positron, one would therefore expect them to have a particular time-of-flight to a detector. A broad peak was observed around the characteristic flight time at all energies indicating that ECC does occur in positron-Ar collisions but quantitative estimates of its likelihood were not possible.

# TABLE OF CONTENTS

Abstract	2	
Table of Contents	3	
Figure Captions	5	
Table Captions	13	
Acknowledgements	14	
CHAPTER 1 INTRODUCTION		
1.1	Historical Background	16
1.2	Basic Properties of the Positron and Positronium	18
1.3	The Development of Slow Positron Beams	22
1.4	The Measurement of Slow Positron Scattering Cross-Sections	33
1.5	The Measurement of Positron Impact Ionization Cross-Sections	46
	1.5.1 Scattering Cell Experiments	48
	1.5.2 Crossed-Beam Experiments	56
1.6	Motivation for this Work	65
CHAPTER 2 THE THEORETICAL CALCULATION OF THE TOTAL POSITRON IMPACT IONIZATION CROSS-SECTION OF ATOMIC HYDROGEN		
2.1	Introduction	67
2.2	Classical Calculations	67
2.3	Quantum Mechanical Calculations	74
	2.3.1 High Energy Approximations	76
	2.3.1.1 The Born Approximation	76
	2.3.2.2 The Glauber Approximation	81
	2.3.2 Distorted Wave Calculations	85
2.4	Summary	93
CHAPTER 3 THE DETERMINATION OF THE TOTAL POSITRON IMPACT IONIZATION CROSS-SECTION OF ATOMIC HYDROGEN - EXPERIMENT		
3.1	General Layout and Principles of Operation	94
3.2	Slow Positron Production and Transport	95
3.3	The Atomic Hydrogen Source	101
	3.3.1 The Gas Handling System	101
	3.3.2 The Radio-Frequency Discharge	104
3.4	The Ion Extraction System	110
3.5	Timing Electronics	114

CHAPTER 4 POSITRON AND ELECTRON IMPACT IONIZATION OF ATOMIC AND MOLECULAR HYDROGEN		
4.1	Preliminary Remarks	118
4.2	Results for Molecular Hydrogen	118
4.2.1	Positron Impact Ionization	119
4.2.2	Electron Impact Ionization	129
4.3	Preliminary Studies with Atomic Hydrogen	129
4.3.1	Positron Impact Ionization	131
4.3.2	Electron Impact Ionization	135
4.4	Summary	136
CHAPTER 5 ELECTRON CAPTURE TO THE CONTINUUM IN POSITRON-ARGON COLLISIONS		
5.1	Introduction	136
5.2	Electron Capture to the Continuum in Positron Impact Ionization	141
5.2.1	Quantum Mechanical Theory	141
5.2.2	Classical Theory	142
5.2.3	Experimental Studies of Capture to the Continuum after Positron Impact	144
5.3	An Experiment to Study the Times of Flight of Electrons Ejected Following Positron Impact Ionization of Argon	145
5.3.1	The Primary Positron Beam	147
5.3.2	The Interaction Region and Timing System	150
5.3.3	Experimental Procedure	156
5.3.4	Results and Discussion	156
CHAPTER 6 CONCLUSION		162
References		167

## FIGURE CAPTIONS

Figure		Page
1.1	The Feynman diagrams for annihilation into one, two, three and four photons and for radiationless annihilation.	21
1.2	The potential energy encountered by a positron at the surface of a metal.	28
1.3	Slow positron yield as a function of the positron work function for Cu (Murray and Mills, 1980).	28
1.4	Source-moderator geometries: (a) Backscattering; (b) Vanes; (c) Mesh; (d) Cup; (e) Transmission	30
1.5	The total cross-section for positrons incident on Helium for energies below 20eV.	36
1.6	The total cross-section for positrons incident on Helium for energies above 20eV.	36
1.7	The excitation cross-section of positrons incident on Helium.	39
1.8	The positronium formation cross-section for positrons incident on helium.	39
1.9	The total cross-section excluding ionization for positrons incident on helium showing contributions from individual channels (Campeanu <i>et al</i> , 1987).	41
1.10	The calculated elastic cross-section of positrons incident on atomic hydrogen.	43

1.11	The positronium formation cross-section of positrons incident on atomic hydrogen (a) up to 14eV, (b) at higher energies.	44
1.12	The cross-sections for excitation of atomic hydrogen by positron impact from its ground state into (a) the 2S level and (b) the 2P level.	45
1.13	Calculated total, elastic, excitation and positronium formation cross-sections for $e^+$ -H scattering. Also shown is the sum of the individual cross-sections for these channels.	47
1.14	The positron impact ionization cross-section of atomic hydrogen determined from partitioning the total cross-section. Directly calculated and measured results are shown for comparison.	47
1.15	The positron impact ionization cross-section of He.	50
1.16	The positron impact ionization cross-section of Ne.	50
1.17	The positron impact ionization cross-section of Ar.	51
1.18	The RP-TOF apparatus used by Sueoka and Mori (1984) to measure the positron impact ionization cross-sections of He, Ne and Ar.	52
1.19	The apparatus used by Diana <i>et al</i> (1985) to measure the positron impact ionization cross-section of He.	52
1.20	The positron impact ionization cross-section of molecular hydrogen.	53

1.21	The apparatus used by Fromme <i>et al</i> (1986, 1988) to measure the positron impact ionization cross-sections of He and H <sub>2</sub> .	53
1.22	The apparatus used by Knudsen <i>et al</i> (1990) to measure the positron impact ionization cross-sections of He, Ne, Ar and H <sub>2</sub> .	55
1.23	The ratio of double-to-single ionization cross-sections of He for e <sup>-</sup> , e <sup>+</sup> , p and p (from the data of Charlton <i>et al</i> , 1988, 1989 and Andersen <i>et al</i> , 1987).	55
1.24	A block diagram of a typical crossed-beam experiment to measure the ionization cross-sections of gases showing the quantities in equations (1.16) and (1.17).	58
1.25	A schematic diagram of the apparatus used by Fite and Brackmann (1958) to measure the electron impact ionization cross-section of atomic hydrogen.	58
1.26	The measured electron impact ionization cross-sections of atomic hydrogen.	60
1.27	A schematic diagram of the apparatus used by Shah <i>et al</i> (1987) to measure the electron impact ionization cross-section of atomic hydrogen.	60
1.28	A diagram of the apparatus used by Spicher <i>et al</i> (1990) to measure the positron impact ionization cross-section.	62
1.29	The measured ionization cross-sections of Spicher <i>et al</i> (1990) for (a)	63
2.1	Electron impact ionization cross-sections of atomic hydrogen calculated using the Binary Encounter Approximation.	69
2.2	A diagram showing the notation that is employed in the discussion of classical calculations in the text.	72

2.3	Positron impact ionization cross-sections of atomic hydrogen calculated using the Classical Trajectory Monte Carlo (CTMC) method.	72
2.4	The notation used in the present discussion of quantum mechanical systems for (a) the pre- and (b) post-collision systems.	76
2.5	Electron impact ionization cross-sections calculated using the first Born approximation which are suitable for consideration in positron scattering (see text).	80
2.6	The electron impact ionization cross-section of atomic hydrogen calculated using the Glauber approximation but allowing for the possibility of exchange.	84
2.7	The positron impact ionization cross-section calculated using the indicated models (see text) by Ghosh <i>et al</i> (1985).	88
2.8	The positron impact ionization cross-section of atomic hydrogen calculated using different models (for details see text) by Mukherjee <i>et al</i> (1987).	88
2.9	The results of distorted wave calculations of the positron impact ionization cross-section of atomic hydrogen using different forms of the polarization potential $V_{POL}$ , see text for details.	91
2.10	The positron impact ionization cross-section of atomic hydrogen calculated using different models incorporating final state correlation by Campeanu (1990).	91
3.1	A cut-away diagram of the source/moderator holder showing the brass plug on which the source is held and the W moderator meshes.	96
3.2	A schematic diagram of the evacuated positron beam system.	98

3.3	The acceptance angle (see text for definition) of the positron beam transport system over a range of positron energies.	101
3.4	A schematic diagram of the microchannel plates used for positron detection in this experiment.	102
3.5	(a) A schematic diagram of the Pd-Ag hydrogen gas leak valve. (b) A graph showing the variation of hydrogen pressure in the gas handling system with current passing through the Pd-Ag leak valve.	103
3.6	A schematic diagram of the radio-frequency discharge tube used in this experiment.	107
3.7	A diagram of the resonator cavity cut away to show the helical inner conductor.	110
3.8	A schematic diagram of the electrostatic ion extraction system used in this experiment, the nozzle of the RF discharge tube is located centrally between the ion extraction plates.	112
3.9	A diagram of the trajectories of H <sup>+</sup> ions after extraction from different parts of the interaction region, showing the spatial focusing properties of the extraction optics.	113
3.10	A block diagram of the timing electronics.	115
3.11	A circuit diagram of the pulser unit that applies $\pm 100\text{V}$ pulses to the ion extraction plates on the input of a shaped output pulse from the positron detector.	116

4.2	The measured ion yield as a function of gas pressure at different positron energies (a) below 150eV, (b) above 200eV.	121
4.3	A plot of the measured ion yield against positron energy, having normalized all points to the data of Knudsen <i>et al</i> (1990) at 100eV which is shown smoothed (---).	123
4.4	The H <sub>2</sub> <sup>+</sup> ion yield shown as a function of extra delay added to the onset time of the extraction pulse.	123
4.5	The H <sub>2</sub> <sup>+</sup> ion yield shown at different energies as a function of the potential applied to the positron extraction tube.	126
4.6	The H <sub>2</sub> <sup>+</sup> ion yield plotted over a range of energies having normalized it to the data of Knudsen <i>et al</i> (1990) at 100eV, this being shown smoothed (- - -).	126
4.7	The H <sub>2</sub> <sup>+</sup> ion yield plotted against electron beam intensity for an electron energy of 300eV.	127
4.8	Ion yields measured over a range of energies with an electron beam, the data has been normalized to the corrected data of Rapp and Englander-Golden (see text) which is shown smoothed (- - -).	128
4.9	A coincidence spectrum taken with the discharge on and a 100eV positron beam showing the peaks due to H <sup>+</sup> ions and, at longer time, H <sub>2</sub> <sup>+</sup> .	132
4.10	The H <sup>+</sup> ion yield plotted as a function of the magnitude of the dc offset potential applied to the ion extraction plates.	134
5.1	The calculated doubly differential cross-section for electron emission of Macek (1970) for 300 keV protons incident on He. The experimental data of Rudd <i>et al</i> (1966) is shown for comparison.	137

5.2	The reduced cross-section $\sigma_c$ for capture to a continuum state of Rödbro and Andersen (1979) compared with reduced cross-sections for capture to bound states derived from literature.	137
5.3	The energy distribution of electrons emitted at $0^\circ$ in positron impact ionization of H at 100eV as calculated by Mandal <i>et al</i> (1986).	143
5.4	The energy distribution of electrons emitted at $0^\circ$ in the ionization of H atoms by 1keV positrons, as calculated by Brauner and Briggs (1986).	143
5.5	The energy distribution of electrons emitted in the ionization of H by 100eV positrons, calculated at various angles by Schultz and Reinhold (1990). Also shown are the scaled $0^\circ$ results of Mandal <i>et al</i> (1986).	144
5.6	The emitted electron count versus retarding potential reported by Coleman (1986) for positron impact ionization of Helium.	146
5.7	Electron count versus retarding potential for positron impact ionization of neon reported by Charlton <i>et al</i> (1987) (●) shown with the integrated results of Brauner and Briggs' (1986) (□).	146
5.8	A cut-away diagram of the source region	148
5.9	A schematic diagram of the experimental apparatus showing the primary positron beam transport and electron collection and detection systems.	149
5.10	A graph showing the acceptance angle of the electron detection system used in this experiment for both magnetic field strengths (a) 15 Gauss and (b) 25 Gauss.	151

5.11	A schematic diagram of the interaction region.	152
5.12	A schematic diagram of the timing electronics.	155
5.13	The time-of-flight spectra of electrons detected after the ionization of Argon atoms by 100eV positrons in magnetic fields of (a) 15 Gauss and (b) 25 Gauss	157
5.14	(a) A plot of the observed positions of the peaks in the electron energy distributions against those values of electron energy expected from theory at 15 Gauss. (b) A plot of the observed positions of the peaks in the electron energy distributions against those electron energies expected from theory at 25 Gauss.	160
6.1	Curves drawn through the relative positron (- - -) and electron (---) ionization cross-sections of H <sub>2</sub> measured in this experiment to illustrate comparisons made in the text.	163

## TABLE CAPTIONS

Table		Page
1.1	Developments in slow positron moderators.	24
1.2	A table showing the possible reactions in $e^+$ -H scattering which give rise to ions and the notation that is used for the cross-section of each.	65
5.1	A table showing the potentials that are applied to parts of the CEMA2 assembly when detecting $e^-$ or $e^+$ .	153

## ACKNOWLEDGEMENTS

I would like to express my gratitude to those who have supported, encouraged and helped me over the course of my postgraduate work.

For their supervision and tuition I would like to thank Drs Mike Charlton and Nella Laricchia and Prof Ceiri Griffith.

For their invaluable technical assistance I must thank Ivan Rangué, Ted Oldfield, Brian Humm, Bill Lenihan and Niall Murphy.

I should also acknowledge the advice given on particular aspects of the work by Prof J A Slevin, Drs A C H Smith, D L Moores and À Kövér.

Neither can I overlook the contributions of the following to my general welfare over the last few years: Zoe, Bing, Dave, Howel, Nevs, Dave, Annette, Jon, Mogens, Jeremy, Iain, Nazrene (especially for juggling my thesis so expertly) and Síle.

Finally and foremost I wish to thank my parents Beryl and John Jones without whose ceaseless encouragement and support throughout the course of this work and before, it would never have been accomplished.

I Mam, Dad a Nain  
ag er cof am Taid

# CHAPTER 1

## INTRODUCTION

### 1.1 Historical Background

The existence of antimatter was first predicted by Dirac (1930a) when proposing a physical interpretation of solutions to his relativistic wave equation requiring electrons to have negative total energies. Dirac formulated his model by considering Einstein's relation between the energy  $E$  of a particle of rest mass  $m_0$  and its momentum  $p$ , with  $c$  being the speed of light *in vacuo*

$$E^2 = m_0^2 c^4 + p^2 c^2 \quad (1.1)$$

One can then assume that all energy states below  $-m_0 c^2$  ( $-m_0 c^2 \geq E \geq -\infty$ ) are filled with electrons. The Pauli exclusion principle then forbids the transition of free electrons from the positive states to the occupied negative states. However, if an electron in the negative levels gains enough energy it can go to a positive level leaving a hole in the negative "sea of electrons". This hole will behave as a positive particle. Dirac's reluctance to propose the existence of a new particle led to his suggestion that these holes corresponded to protons but Weyl (1931) showed that the new particle had to have the same mass as an electron. The particle became known as the positron,  $e^+$ .

Experimental confirmation of its existence was subsequently obtained by Anderson (1932) in cloud chamber studies of cosmic ray showers. His results were subsequently corroborated in an experiment by Blackett and Occhialini (1933).

Initially, considerable interest was shown in positrons as the only available example of antimatter. Although this has paled somewhat with the discovery of other

antiparticles the ready availability of positrons from radio-isotopes has ensured their rapid development as probes of atomic interactions in gases and of the bulk and surface properties of condensed matter. The complementarity of these investigations to those employing electrons is a consequence of the different charge signs but equal masses of the particles. This leads to the distinguishability of projectile positrons from target atom electrons unlike the electron case where exchange effects must be taken into account.

Another difference is the possibility of annihilation with one of the electrons in the target with the emission of  $\gamma$ -rays. Observation of this phenomenon in swarm experiments involving positrons allows the determination of the momentum distributions of electrons in solids and the study of the interaction mechanisms of positrons with gas atoms. Reviews of such experimental work for gases can be found in Griffith and Heyland (1978) and Charlton (1985) and for solids in Schultz and Lynn (1988).

Of great importance is the attractive nature of the positron-electron Coulomb interaction. This can lead to a high degree of correlation between the particles if they are free with the possible outcome of forming a quasi-stable bound state-positronium, Ps. Its existence was predicted by Mohorovicic (1934) and confirmed experimentally by Deutsch (1951). The simplicity and purely leptonic nature of this system has led to extensive theoretical treatments with a view to testing the accuracy of the bound state aspects of Quantum Electrodynamics (QED) (e.g. Wheeler, 1946 and Fulton and Martin, 1954).

Another bound state system involving a positron whose synthesis would be of great value is antihydrogen ( $\bar{\text{H}}$ ). This bound state of two antiparticles, the positron and antiproton, would again be a candidate on which stringent tests of QED could be performed. Its study would also allow the most accurate tests of CPT invariance to date, this is the symmetry that states that the laws of physics are the same for matter

and antimatter and is integral to gauge field theories. Current experimental efforts to produce antihydrogen are discussed in detail by Charlton (1989) and Poth (1989).

The study of positron scattering processes developed significantly in the late 1960s with the advent of slow positron beams. On the implantation of fast  $\beta^+$  particles certain solids were found to emit positrons with energies of a few eV. Their subsequent acceleration and collimation allows the energy dependence of individual atomic scattering processes to be ascertained. The main body of this work will detail such a study.

## 1.2 Basic Properties of the Positron and Positronium

The mutual annihilation of positrons and electrons is likely to result in the emission of a number of  $\gamma$ -ray photons. If both are at rest their total energy will be the sum of their rest mass energies, 1.022MeV. Conservation of charge parity,  $P_c$  determines the number of photons,  $n_\gamma$  that are emitted. Since a single photon has  $P_c = -1$ , a system of  $n_\gamma$  photons will have

$$P_c = (-1)^{n_\gamma} \quad (1.1)$$

Using symmetry arguments Yang (1950) has showed that, in positron-electron annihilation

$$P_c = (-1)^{L+S} \quad (1.3)$$

where L is the total angular momentum and S is the total spin of the system. The detection of annihilation radiation therefore yields information on the relative states of the annihilating pair.

The probability of any given number of photons being emitted can be deduced from the Feynman diagrams for the interaction. Figure 1.1 shows the diagrams for

annihilation into zero, one, two, three and four photons. The probability of an interaction occurring is given approximately by  $\alpha^m$  where  $\alpha$  is the fine structure constant ( $\alpha \approx 1/137$ ) and  $m$  is the number of vertices on the Feynman diagram i.e. the number of points where photons interact with other particles. Both cases (a) and (c) in Fig. 1.1, for annihilation into one and three photons respectively have  $m=3$  but the required presence of a third body in case (a) to conserve momentum makes case (a) less likely to occur by a factor  $\alpha^3$ . Of cases (a) to (c) case (b) is therefore the most likely, followed by case (c). Case (d)-annihilation into four photons-with four vertices is less likely still but, nevertheless, has been observed recently (Adachi *et al*, 1990). Radiationless annihilation, depicted in case (e), was first proposed by Brunings (1934). Here a positron annihilates with a bound electron and the energy liberated releases another electron from the atom. Its branching ratio was subsequently calculated more accurately by Massey and Burhop (1938) and their conclusion was that, although rare compared to the other annihilation modes, it should still be observable. It is clear from these considerations that annihilation into two  $\gamma$ -rays is the most probable, in fact Ore and Powell (1949) have calculated that the ratio of the cross-section for annihilation into two  $\gamma$ -rays to that into three  $\gamma$ -rays is 1:372 for free positrons.

Dirac (1930b) derived the following expression for the cross-section for the annihilation into two  $\gamma$ -rays of a non-relativistic positron with a free electron,  $\sigma_{2\gamma}$

$$\sigma_{2\gamma} = \frac{\pi r_0^2 c}{v} \quad (1.4)$$

where  $v$  is the positron velocity and  $r_0 = e^2/4\pi\epsilon_0 m_0 c^2$  is the classical electron radius with  $\epsilon_0$  being the permittivity of free space,  $m_0$  being the electronic mass. If there is a number density,  $n_e$  of electrons present one can write from (1.4) for the observed rate of annihilation of positrons into two  $\gamma$ -rays,  $\lambda_{2\gamma}$

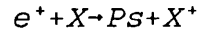
$$\lambda_{2\gamma} = \pi r_0^2 c n_e \quad (1.5)$$

In a gas of number density,  $\rho$  this can be written

$$\lambda_{2\gamma} = \pi r_0^2 c Z_{\text{eff}}(v) \rho \quad (1.6)$$

where  $Z_{\text{eff}}$  is the effective number of electrons per atom seen by a positron of velocity  $v$ . It differs from the atomic number,  $Z$  because of the polarization of the atom by the approaching positron. As this is only significant at low positron energies  $Z_{\text{eff}}$  approaches  $Z$  at energies commonly encountered in positron beam experiments. At these energies it has been shown that  $\sigma_{2\gamma}$  is  $\sim 10^{-26} \text{cm}^2$  so the likelihood of positron annihilation is negligible compared to that of the other scattering channels that are investigated in beam experiments.

An alternative reaction to annihilation in which the positron can participate is the formation of Ps given by the reaction



where  $X$  is any atom or molecule. The threshold energy for this reaction,  $E_{Ps}$  is given by

$$E_{Ps} = (E_I - 6.8) \text{eV} \quad (1.7)$$

with the binding energy of ground state Ps being 6.8eV, half that of hydrogen with the Bohr radius being correspondingly double (1.05Å). Ps has a finite lifetime depending on the relative spins of its component particles, this is again governed by equation (1.3). If the particles' spins are parallel ortho-positronium (o-Ps) is formed, this state has  $L+S=1$  and has therefore three magnetic substates. Equation (1.3) then predicts that it will annihilate with the emission of an odd number of photons, three

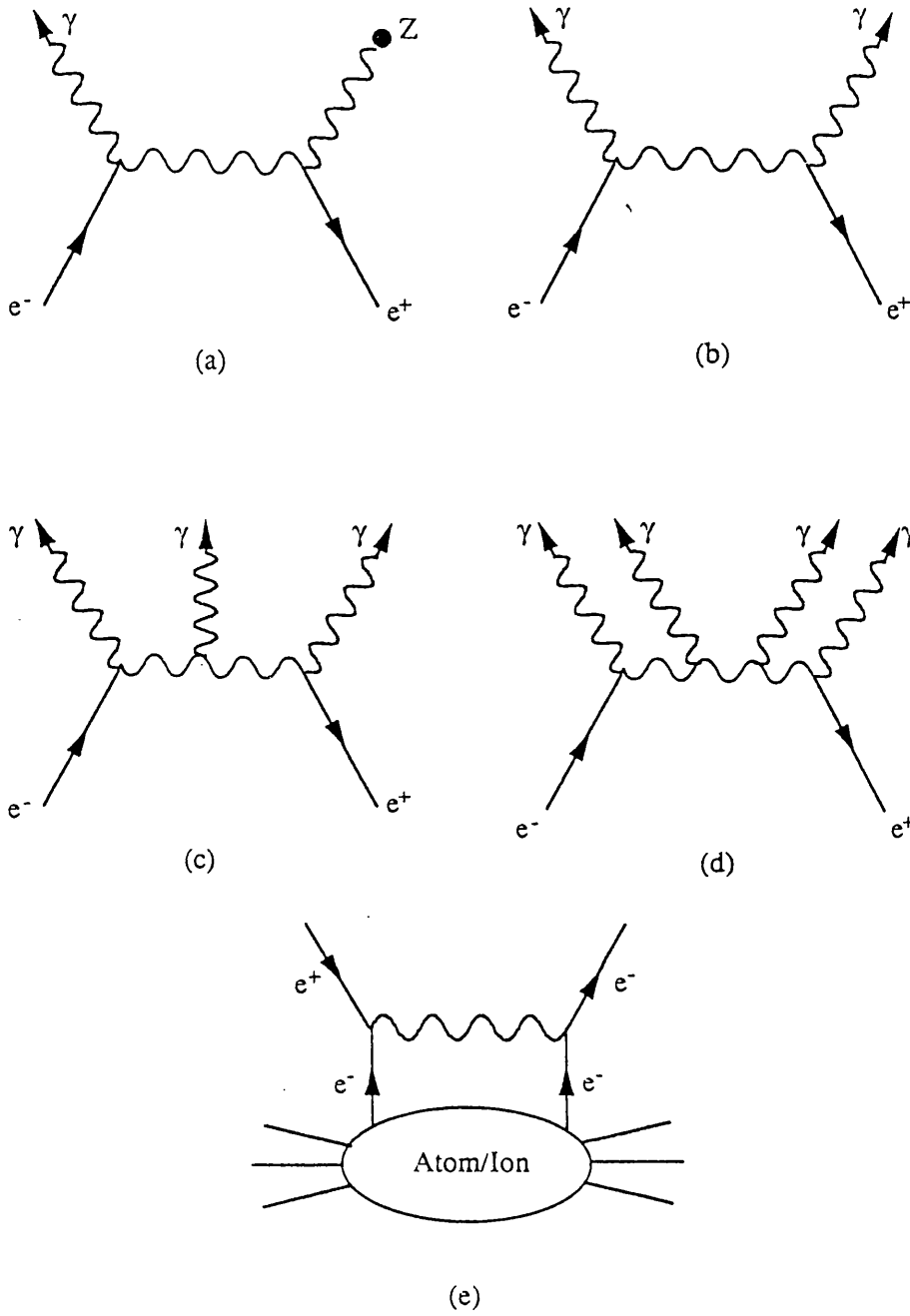


**Fig 1.1** The Feynman diagrams for annihilation into one, two, three and four photons and for radiationless annihilation.

being the most likely. This gives it a longer lifetime than the singlet state ( $L+S=0$ ) para-positronium (p-Ps) which is most likely to emit two colinear photons. Calculations have borne this out with Harris and Brown (1957) finding the self-annihilation rate of p-Ps to be  ${}_0\lambda_{p-Ps}=7.9852\text{ns}^{-1}$  compared to Caswell and Lepage's (1979) result for o-Ps of  ${}_0\lambda_{o-Ps}=(7.0386\pm 0.0002)\mu\text{s}^{-1}$ . The short lifetime of p-Ps makes the experimental determination of its decay rate difficult but Gidley *et al* (1982) employed the Zeeman effect to mix it with the  $m=0$  substate of o-Ps in a magnetic field and obtained a result in accordance with theory. The most accurate measurement to date for o-Ps is however  $(7.0482\pm 0.0016)\mu\text{s}^{-1}$  by Nico *et al* (1991) which is significantly different to theory; the authors cannot ascribe this discrepancy to systematic effects but suggest that the calculation may be inadequate and suggested the need for higher order corrections.

### 1.3 The Development of Slow Positron Beams

In this section the development over the last forty years of increasingly efficient sources of slow positrons shall be reviewed. The milestones in this field are summarized for convenience in Table 1.1.

Although early positron swarm experiments proved valuable in the discovery of positronium, Ps (Deutsch, 1951) and as probes of gaseous and solid media the limitations imposed on the amount of information derivable by the broad positron energy distribution became apparent. A technique involving positrons that was analogous to the widely used electron beams was required hence the need for a variable energy, monochromatic positron beam. The possibility that positrons with thermal energies could be obtained on implanting fast  $\beta^+$  particles from a radioactive source into a solid and allowing them to diffuse back to the surface was first suggested by Madansky and Rasetti (1950). They correctly predicted that the efficiency of such a "moderator" of the positrons' energies was given by the ratio of the diffusion length of the positrons to the implantation depth in the solid. This they

calculated to be  $\sim 10^{-3}$  for their experiment in which samples of various materials were irradiated by a  $^{64}\text{Cu}$  source. Positron detection was to be by means of  $\gamma$ -ray detectors observing the annihilation of positrons on an Al plate 80 cm away from the moderator sample in an axial magnetic field. They obtained a null result for each sample which is now thought to be due to the poor resolution of the experiment and the quality of the samples although at the time it was claimed that it was due to Ps formation and  $e^+$  trapping in bulk defects and at the surface-two phenomena that are now known to be of great significance.

The first observation of slow positron production in this manner was from a Cr covered mica surface by Cherry (1958). In this experiment the positrons were extracted electrostatically and the moderation efficiency,  $\epsilon$  was measured to be  $3 \times 10^{-8}$ . The significance of this work was not realized until Madey (1969) performed a similar experiment with a polyethylene sample and Groce *et al* (1968) used gold.

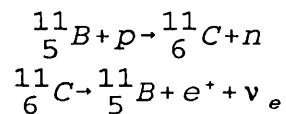
Greater understanding of the process of positron moderation was abetted by the study of Costello *et al* (1972a) of the energy distribution of positrons emitted from gold. The experiment involved producing fast positrons by pair production from bremsstrahlung  $\gamma$ -rays emitted on the slowing down of 55MeV electrons from a linear accelerator (LINAC). These positrons were implanted into gold coated mica and CsBr crystals. This work revealed that the positron work function,  $\phi_+$  for Au was negative. This concurs with the theoretically determined result of Tong (1972) who postulated that positrons would be ejected from metals with a negative positron work function and would have an energy  $\phi_+$ . Tong also predicted negative values of  $\phi_+$  for Al, Mg and Cu. Although subsequent experimental work has shown that this model is valid, Lynn (1980, unpublished) has measured  $\phi_+$  for Au to be positive suggesting that the results of Costello *et al* (1972a) cannot be explained by this mechanism. Possible explanations are that these positrons may not have thermalized in the sample or that surface impurities made  $\phi_+$  negative.

Moderator	Experimental Arrangement	Efficiency $\epsilon$	$\Delta E$ [eV]	Reference
Pt, K, Ga	Transmission	0	-	Madanski & Rasetti (1950)
Cr/Mica	Transmission	$3 \times 10^{-8}$	-	Cherry (1958)
Au/Mica	Transmission	$10^{-7}$	2	Costello <i>et al</i> (1972)
MgO coated Au	Backscattering /Vanes	$3 \times 10^{-5}$	2.3	Canter <i>et al</i> (1972)
B	Self-moderator	$10^{-7}$	0.15	Stein <i>et al</i> (1974)
Al(100)	Backscattering	$3 \times 10^{-5}$	0.1	Mills <i>et al</i> (1978)
Cu(111)+S	Backscattering	$9 \times 10^{-4}$	0.3	Mills (1979)
W	Backscattering /Vanes	$7 \times 10^{-4}$	1.3	Dale <i>et al</i> (1980)
W(110)	Backscattering	$3 \times 10^{-3}$	0.7	Vehanen <i>et al</i> (1983)
W(100)	Transmission, High vacuum	$6 \times 10^{-4}$	3	Lynn <i>et al</i> (1985)
Ne	Transmission	$7 \times 10^{-3}$	0.58	Mills & Gullikson (1986)
W(100)	Transmission, High vacuum	$5.9 \times 10^{-4}$	-	Gramsch <i>et al</i> (1987)
Ni(100)		$6.6 \times 10^{-4}$		
Mo		$7.5 \times 10^{-5}$		
W(100)	Transmission, Low vacuum annealing	$8.8 \times 10^{-4}$	1.7	Zafar (1990)
Ni(100)		$6.5 \times 10^{-4}$	0.3	
Mo	Transmission/ Low vacuum annealing	$4 \times 10^{-4}$	0.8	Andrikoupoulos, Avdi & Laricchia (1991)
Diamond	Field assisted/ Backscattering	$7 \times 10^{-3}$	-	Brandes <i>et al</i> (1991)

Table 1.1 Developments in slow positron moderators.

A far more efficient positron moderator was discovered by Canter *et al* (1972). An efficiency of  $3 \times 10^{-5}$  was achieved using MgO coated gold vanes-this then prompted the increasing use of positron beams to measure total cross-sections (see section 1.4). The model of Tong (1972) could not however explain the effectiveness of this moderator. It was suggested that slow positron production from this moderator was an indirect process in which a positron formed excited positronium,  $\text{Ps}^*$  which subsequently broke up. Field ionization in a charge layer at the non-conducting surface due to liberated electrons was proposed as the mechanism for Ps break-up (Griffith *et al*, 1978). Jacobs (1951) had previously postulated that such a charge layer was responsible for an observed enhancement in secondary electron emission from oxide layers upon electron bombardment-a concept which was supported by later experimental results. There have been subsequent studies of other non-conducting moderators, most notably solid rare gases by Gullikson and Mills (1986). These moderators have yielded results which are not in accordance with this model and are discussed fully below.

A new development in moderator technology came in 1974 when Stein *et al* used a self-moderating source. Here, a boron target was bombarded with 4.75 MeV protons from a Van de Graaf generator to produce  $^{11}\text{C}$  by the reaction



The fast positrons produced here are moderated in the bulk of the B and are emitted with a very low energy spread ( $\sim 0.1\text{eV}$ ) and an efficiency of  $10^{-7}$ . By virtue of this Kauppila *et al* (1976) observed a Ramsauer-Townsend minimum in the  $e^+$ -Ar total cross-section using this source-moderator arrangement.

While these different types of moderators were being developed, metallic moderators

were still under investigation. Pendyala *et al* (1976) studied the emission properties of various polycrystalline samples and achieved their maximum efficiency with Cu. But this work did not add greatly to the understanding of moderators and the moderation process because the structure and purity of the samples were not known. This situation was rectified by Mills *et al* (1978) who investigated the moderating properties of various pure well-characterized samples. These included Al(100), Cr and Si(100), where the numbers denote the orientation of the crystal face. Efficiencies of  $3 \times 10^{-5}$  were achieved. Following this study, the authors deduced the mechanism of slow positron emission from metals, a brief discussion of which now follows.

On implantation in the bulk of the moderator material a fast  $\beta^+$  particle loses energy to electrons in the solid. It loses energy via processes such as plasmon emission and electron-hole pair creation. Whilst thermalizing, a fast positron can diffuse towards the surface of the moderator but for stopping distances that are typical for high energy  $\beta^+$  particles most thermalize before reaching the surface. Therefore those which do diffuse to the surface before annihilating will arrive there thermalized. Thermal positrons at the surface of a solid can undergo one of four processes: Ps formation, trapping in a surface state, reflection or ejection into the vacuum. The latter process which is that of slow positron emission from solids requires the material to have a negative positron work function. The work function of any material is defined as the minimum energy necessary to remove a particle from a point just inside to one just outside the surface. For electrons it was defined by Lang and Kohn (1971) as the difference between the surface dipole barrier,  $\delta$  and the bulk chemical potential,  $\mu_+$

$$\phi_+ = \delta - \mu_+ \quad (1.7)$$

Tong (1972) analogously expressed the positron work function as

$$\phi_+ = -\delta - \mu_+ \quad (1.8)$$

where  $\mu_+$  is the bulk chemical potential for a positron. The potentials that a positron encounters at the surface of a solid are shown in Figure 1.2. Tong (1972) represented the contribution of ion cores in the bulk to the potential a particle experiences at the surface with "jellium": an uniform positive background which is calculated as the mean potential a particle feels at an interstitial site in the lattice from the ion cores. The bulk chemical potential,  $\mu_+$  is the sum of this and the potential of the uniform electron gas in the bulk. The electron gas "spills out" into the vacuum at the surface and gives rise to a negative charge just outside the interface. This forms a dipole with the positive charge inside whose electrostatic interaction with a particle is expressed as  $\delta$  as shown in Figure 1.2. This helps bind electrons to the solid but because of their opposite charge sign it tends to eject positrons from the material as it can cancel out  $\mu_+$  in equation (1.8) and even make  $\phi_+$  negative. In adiabatic conditions the maximum energy an emitted positron can then have is  $\phi_+$ . In practice the thermal motion of surface atoms gives rise to a small energy spread around  $\phi_+$  in the emitted positron energy distribution. Murray and Mills (1980) have investigated the dependence of moderation efficiency on  $\phi_+$ . They did this for Cu and Al samples by changing the crystal orientation, changing the amount of surface coverage by sulphur and heating the sample. Their results are shown in Figure 1.3 and show a clear increase as  $\phi_+$  is made more negative thus lending support to the above model of slow positron emission from metals.

Dale *et al* (1980) then studied the dependence of moderation efficiency on the structural characteristics of the moderator. A variety of metal samples were treated in different ways prior to installation in an electrostatic positron beam system. The best yield obtained was  $7 \times 10^{-4}$  from an arrangement of W vanes. These had previously been etched chemically and annealed by resistive heating to 2200°C. On

$$\phi_+ = -\delta - \mu_+$$

$$\phi_- = +\delta - \mu_-$$

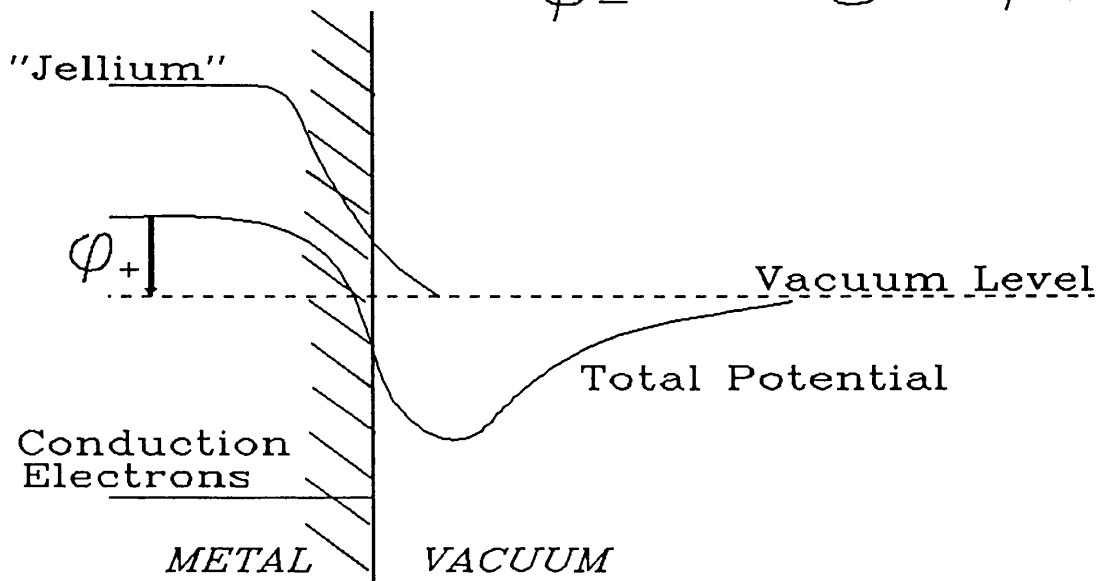


Fig 1.2 The potential energy encountered by a positron at the surface of a metal.

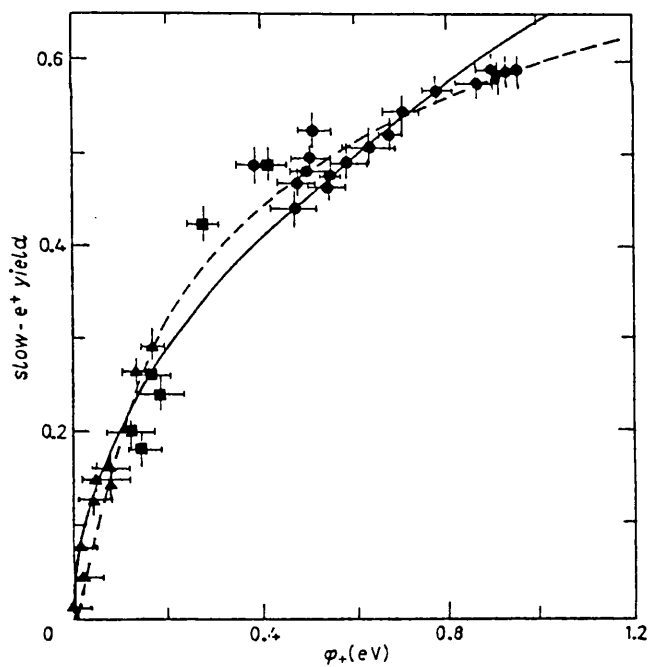


Fig 1.3 Slow positron yield as a function of the positron work function for Cu (Murray and Mills, 1980).

further investigation it transpired that the annealing process was a far more significant process in increasing the yield than the removal of surface contaminants by chemical etching. This was because, on heating, the lattice structure of the W relaxed and then recrystallized as it cooled. Defects in the crystalline structure are thus removed and there being fewer sites for diffusing positrons to be trapped, the diffusion length, and hence the moderator efficiency, is increased.

It was also discovered in the study of Dale *et al* (1980) that the annealing of W removes all adsorbed O from its surface. During subsequent exposure to air the extent of adsorption will not exceed about two monolayers of O - it was concluded that this inertness made W a very useful positron moderator especially when working in non-UHV conditions. Using a single crystal sample instead of the polycrystalline W used above Vehanen *et al* (1983) obtained an efficiency of  $3 \times 10^{-3}$ , close to the maximum expected efficiency for W of  $4 \times 10^{-3}$  calculated by Vehanen and Mäkinen (1985).

The extraction of slow positrons from the source-moderator arrangement is clearly highly dependent on its geometry. All the systems described thus far have employed backscattering or vane geometries for the moderator, these are depicted in Figure 1.4 (a) and (b) respectively. Another widely used arrangement is the mesh moderator - this is shown in Figure 1.4 (c). In cases (b) and (c) the dimensions of the source are unimportant but in case (a) this is not so because the source obscures part of the moderator and therefore intercepts some of the re-emitted positrons. The size of the source must therefore be kept to a minimum when using the backscattering geometry so radioactive isotopes with a high specific activity (activity per unit mass) such as  $^{58}\text{Co}$  must be used to maintain a high flux of  $\beta^+$  particles. When this is not a consideration  $^{22}\text{Na}$  with a lower specific activity but a conveniently long half-life of 2.6 years (more than 13 times that of  $^{58}\text{Co}$ ) is normally used.

Figure 1.4 (d) shows the cup geometry onto which Mills and Gullikson (1986)

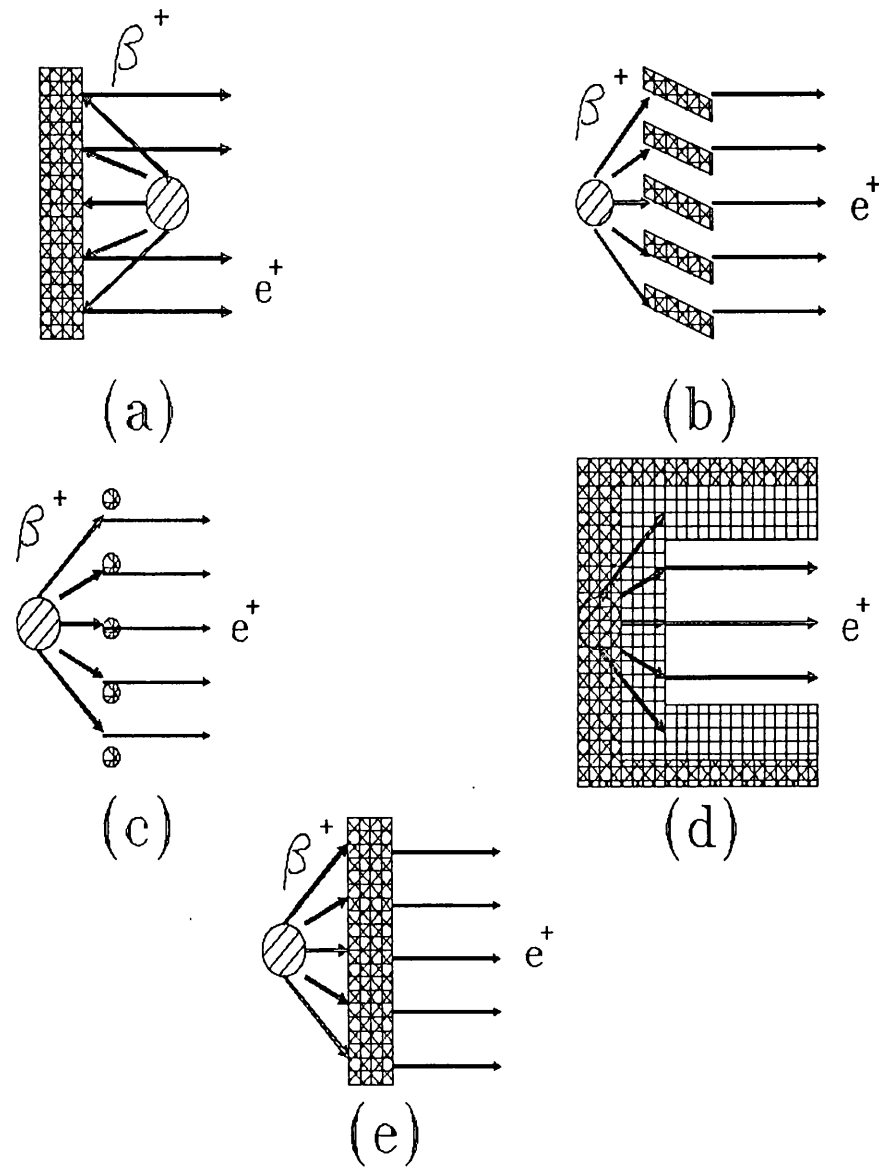


**Fig 1.4** Source-moderator geometries: (a) Backscattering; (b) Vanes; (c) Mesh; (d) Cup; (e) Transmission

condensed the rare gases Ne, Ar, Kr and Xe to make the first solid rare gas moderators. The maximum efficiency achieved was  $(7.0 \pm 0.2) \times 10^{-3}$  with a layer of solid Ne deposited on the cup. This was the most efficient slow positron moderator then produced. The authors explain their results in terms of the "hot positron" model which assumes that the positrons are not thermalized prior to emission. They postulate that implanted positrons will lose energy by making inelastic collisions involving electronic transitions until their energy falls below the threshold for these processes. Subsequent energy loss will be via phonon emission but since the maximum phonon energy is small (e.g. 8.3meV for Ar) positrons diffuse a long distance before thermalizing ( $\sim 5000 \text{ \AA}$  in Ar) and some are likely to reach the surface and be emitted if their energies are greater than the positron work function  $\phi_+$  ( $\phi_+ > 0$  for rare gas solids). On measuring the slow positron yield over a range of implantation energies the authors deduced the variation of yield with positron implantation depth. Extrapolation of this yield to zero implantation depth revealed that slow positron emission was considerably more probable than the formation of  $\text{Ps}^*$  at the surface-this contradicts the field-ionization model of Griffith *et al* (1978).

Figure 1.4 (e) shows the transmission geometry as first used by Chen *et al* (1985). This has the advantage over the other geometries of a smaller energy spread for the emitted positrons as with the backscattering case but without the associated problem of source shadowing. In the study of Chen *et al* (1985) single crystal W(100) films of varying thicknesses were grown epitaxially on a MgO/Mo substrate which was subsequently removed by chemical etching. These films were then annealed *in situ* to remove defects and surface contaminants. The FWHM of the emitted positron energy distribution was found to be less than half an eV. In a later study Lynn *et al* (1985) report an efficiency of  $4 \times 10^{-4}$  for a W(100) film prepared in this manner.

These results encouraged further investigation of the properties of thin film transmission moderators. Samples which have been studied and were demonstrated

to be potentially useful moderators include W, Ni and Mo. Specific references and results are cited in Table 1.1 but it is of interest to note the recent work of Andrikoupolos, Avdi and Laricchia (1991) with single crystal Mo in which it was ascertained that half of the observed energy spread of  $\sim 800\text{meV}$  arises from the wide angular distribution of emitted positrons. This complements the study of Gullikson *et al* (1985) which revealed a similar effect for W(110) and Ni(100) except that in the UHV conditions used and accordingly less surface contamination the observed energy spread was almost entirely the result of the angular distribution of positrons. These experiments therefore support the theory that positron emission from metals is an elastic process which, in adiabatic conditions, would produce mono-energetic positrons with energy  $\phi_+$ .

Although these developments are leading to more well-defined positron beams their spatial spreads are still too broad for many applications e.g. some surface studies such as low energy positron diffraction. Focussing on its own cannot overcome these difficulties since, as pointed out by Mills (1980), Liouville's theorem states that in a conservative field the volume occupied by a swarm of particles in phase space remains constant. This implies the constancy of the quantity  $d^2E\sin^2\theta$  for a beam of particles of energy  $E$  which has a minimum diameter  $d$  and angular divergence  $\theta$ . If the beam is of intensity  $I$  one can define the brightness per unit energy as

$$B(E) = \frac{I}{d^2E\sin^2\theta} \quad (1.10)$$

Focussing would therefore improve one or more of  $d, \theta$  or  $E$  at the expense of worsening others. Mills (1980) went on to suggest that the non-conservative process of moderation might produce a brighter flux without diminishing  $d^2$  or  $\theta$  but with, of course, a decrease in  $I$ . This, he suggested, could be achieved by focussing high energy positrons onto smaller areas on successive re-moderators thus increasing  $B(E)$  by several orders of magnitude. The first experimental demonstration of this process,

brightness enhancement, was by Frieze *et al* (1985) but a more recent experiment by Brandes *et al* (1988) increases  $B(E)$  by a factor of 500. Such work aids the development of positrons as probes of surfaces and bulk media, a purpose for which they are potentially valuable sources of information.

#### 1.4 The Measurement of Slow Positron Scattering Cross-Sections

The first positron scattering cross-section to be measured was the total cross-section of He by Costello *et al* (1972b) but this data is now known to be inaccurate. As sources of slow positrons became more efficient several other groups measured total cross-sections for various gases. Experiments to measure the total cross-section for scattering processes in gases generally involve observing the attenuation of a beam of particles through an extended region in which the gas is confined. In these circumstances the total cross-section  $\sigma_T$  can be defined

$$I = I_0 \exp(-\rho l \sigma_T) \quad (1.9)$$

where  $I_0$  is the intensity of a beam entering a gas column of length  $l$  and number density  $\rho$  and  $I$  is the intensity of the beam leaving the scattering region. The gas density,  $n$  can be related to the measurable quantities pressure and temperature by simple relations deriving from kinetic theory. In total cross-section measurements with positrons the attenuation was either observed directly or inferred from time-of-flight spectra with and without gas present.

Shown in Figure 1.5 are the low energy total cross-sections measured for He by Canter *et al* (1972), Stein *et al* (1978), Coleman *et al* (1979), Mizogawa *et al* (1985) and Wilson (1978), the latter being corrected by Sinapius *et al* (1980). It is notable that the narrow energy spread of the positron beam ( $< 0.1\text{eV}$ ) of Stein *et al* permitted

the measurement of  $\sigma_T$  at energies as low as 0.5eV allowing therefore the first observation of a Ramsauer-Townsend minimum in the  $e^+$ -He total cross-section. This was subsequently confirmed in the very low energy measurements (1-6eV) of Wilson (1978) and Mizogawa *et al* (1985). The Ramsauer-Townsend minimum is familiar in low energy electron scattering but arises in a slightly different fashion for positrons. The static interaction with an atom is repulsive for positrons but the polarization interaction is attractive as for electrons, at low energy where the polarization interaction is strong there will be a point at which the interactions cancel out, there will then be a minimum in the total cross-section.

All experimental measurements shown in Figure 1.5 are in reasonable agreement above the Ramsauer-Townsend minimum but differ around the minimum itself. Figure 1.5 also show the theoretical calculations of the elastic scattering cross-section below the threshold for inelastic processes. These are as follows: the Kohn variational calculations of Humberston (1979) for s-wave scattering, Humberston and Campeanu (1980) for p-wave, Drachman (1966) for d-wave and the Born approximation result of O'Malley *et al* (1961) for higher order phase shifts all summed by Wadehra (1981); the many-body calculation of Amusia *et al* (1976) and the polarized orbital method of McEachran *et al* (1977) which followed the work of Temkin and Lamkin (1961). It can be seen that all calculations apart from those of McEachran *et al* (1977) are slightly higher than the measured values around the Ramsauer-Townsend minimum but subsequently are in agreement up to the Ps formation threshold (17.8eV). Those of McEachran *et al* (1977) do not reproduce the shape of the cross-section very well at low energies.

The work of Stein *et al* (1978) was extended up to  $\sim 800$ eV by Kauppila *et al* (1981) using the same apparatus, these results are shown in Figure 1.6. Shown also are the higher energy measurements of Griffith *et al* (1979) and Coleman *et al* (1979), all sets of results are in agreement over the range at which they coincide. Also shown

are the available theoretical calculations at these energies. As expected these perturbative calculations agree better with experimental data towards higher energies. The calculations are the eikonal-Born series calculation of Byron (1978), the distorted wave second Born approximation (see section 2.2.1) calculation of Dewangan and Walters (1977) and the Bethe-Born calculation of Inokuti and McDowell (1974).

There have, of course, been many experiments to measure  $\sigma_T$  for positrons incident on other atoms and molecules and these have provided many an insight into the behaviour of positrons and, on comparison of corresponding data, electrons in collisions. Further details of these measurements and comparisons are given in the review papers of Griffith and Heyland (1978), Charlton (1985) and Kauppi and Stein (1990).

The first inelastic positron scattering cross-sections to be measured were excitation cross-sections. The experiments were made using systems already developed for measuring total cross-sections. This was because the time-of-flight methods that had been employed proved suitable for measuring excitation cross-sections by virtue of their capacity to distinguish between scattered positrons of different energies. They were thus capable of detecting positrons with the characteristic energy loss of those which had excited certain electronic transitions although the energy resolution was poor since recorded times-of-flight were dependent on the positrons' scattering angles as well as energies. The earliest measurement was by Coleman and Hutton (1980) who observed on their time-of-flight spectra positrons which had excited the  $1^1S-2^1S$  transition in He. The measured excitation cross-section is shown in Figure 1.7. Recently Diana *et al* (1989) have reported preliminary results for the excitation of  $2^1S$  in He using a lengthened form of the same apparatus which leads to an increased timing resolution. The measurements extend up to 55eV and they report yield results slightly higher than previously measured-an effect they ascribe to the inclusion of other transitions.

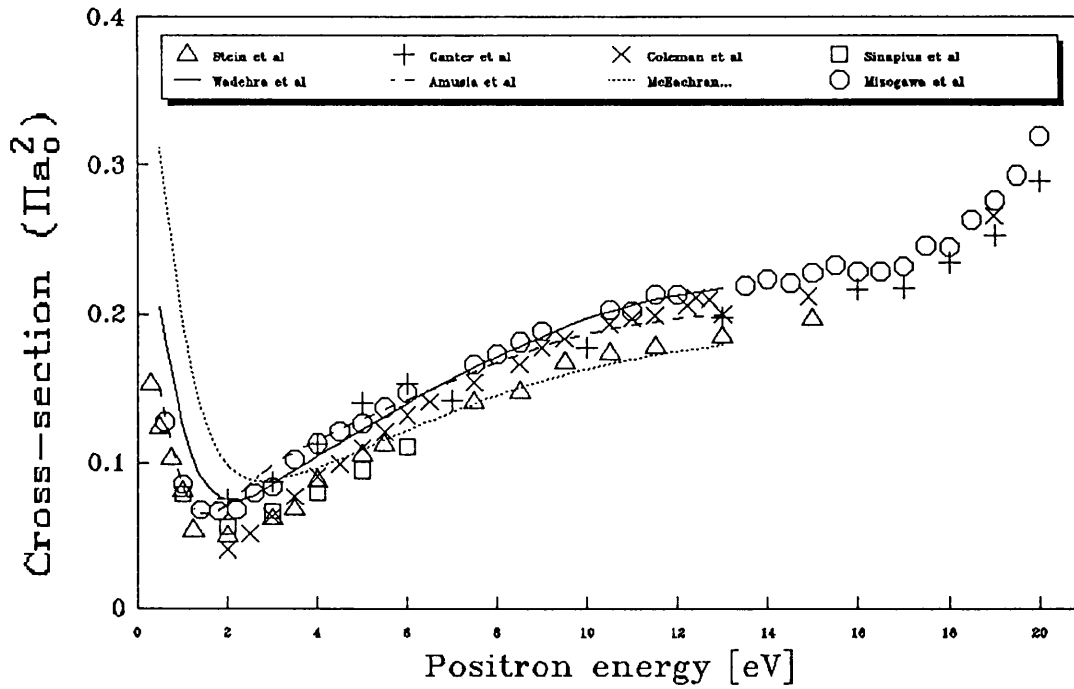


Fig 1.5 The total cross-section for positrons incident on Helium for energies below 20eV.

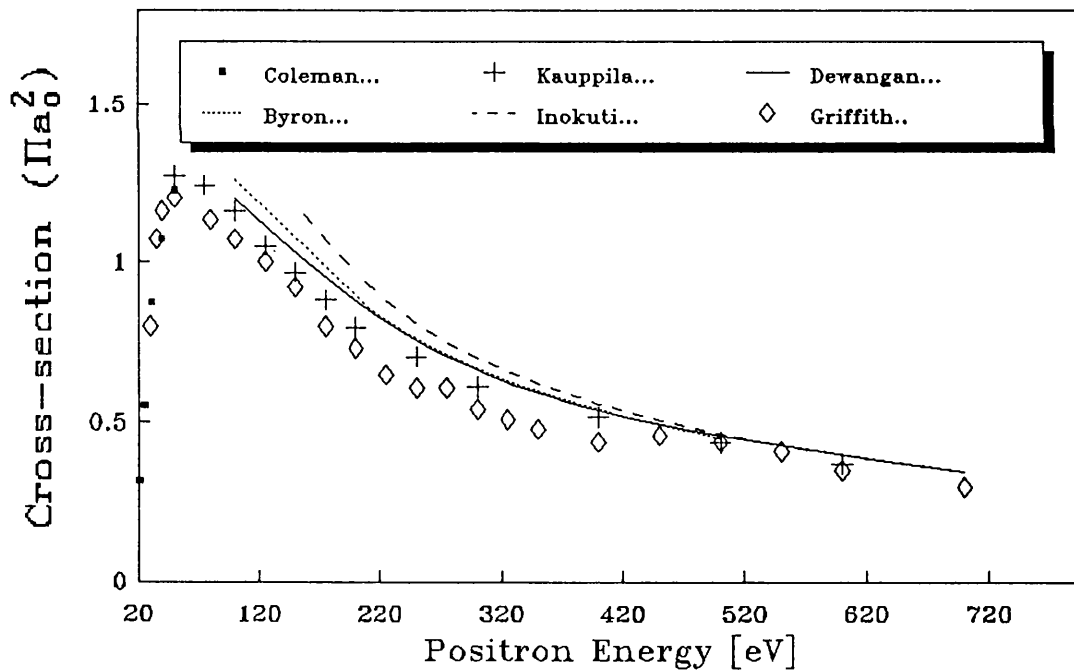


Fig 1.6 The total cross-section for positrons incident on Helium for energies above 20eV.

The other apparatus that has been used to measure positron excitation cross-sections is the Retarding Potential-Time of Flight (RP-TOF) system of Sueoka (1982) that is shown in Figure 1.18 and discussed below. To observe excitation it was modified to account for positrons which had scattered more than once and consequently had times-of-flight indistinguishable from those which had lost energy on excitation (Sueoka, 1989). Results have been reported for the lowest transition in He up to 120eV. Comparison is made with the summed theoretical result of Parcell *et al* (1983, 1987) whose calculations used a distorted wave approximation and reasonable agreement is obtained although the experimental results are generally higher.

Considerable interest has also been shown in positronium formation as this reaction occurs exclusively for positrons and can therefore yield information on positron scattering mechanisms. Initially, the positronium formation cross-section  $\sigma_{P_s}$  was determined below the excitation threshold by assuming the shape of the elastic cross-section and subtracting it from the total cross-section. Clearly though this procedure was unsatisfactory and direct measurements of  $\sigma_{P_s}$  were required. The first measurements for He were made by Charlton *et al* (1980) but only up to 12eV above threshold; they were subsequently extended to 150eV by Charlton *et al* (1983) and results are shown in Figure 1.8. The other sets of measurements of  $\sigma_{P_s}$  for He have been made by Fornari *et al* (1983) using a time-of-flight technique at low energies; Diana *et al* (1985a) with the same apparatus but a different technique and Fromme *et al* (1986). All these measurements were made on systems with which measurements of the total ionization cross-section,  $\sigma_i$  were made and the experiments are discussed in detail in section 1.4.

The results of all experiments, shown in Figure 1.8, show clearly the disagreement of the data of Charlton *et al* (1980, 1983) with other experimental data. The authors (Charlton, 1985) have suggested that this discrepancy may arise from quenching collisions of ortho-positronium on the cell walls or that positronium was

preferentially formed in the forward direction in their experiment. The latter point has gained credence following the study of Laricchia *et al* (1987) of Ps formation in positron scattering from He and Ar which revealed that up to 4% of Ps formed was emitted in a 6° cone in the forward direction. On comparison with theory the other experimental data for  $\sigma_{Ps}$  in He is seen to agree reasonably at low energies with the distorted wave calculations available (Khan and Ghosh, 1983, Khan *et al*, 1985 and Mandal *et al*, 1979) but this is not the case at higher energies.

Apart from general information about the nature of the interaction the only new knowledge that can be gleaned from total cross-sections concerns the relative significance of their contributory components. If the possibility of annihilation is neglected, which - as was explained earlier - is quite valid at the energies under discussion, one can write for the total cross-section for positron scattering,  $\sigma_T$

$$\sigma_T = \sigma_{el} + \sum_{n=2}^{\infty} \sigma(nLS) + \sigma_i + \sigma_{Ps} \quad (1.9)$$

where  $\sigma_T$  and  $\sigma_{Ps}$  are as defined,  $\sigma_i$  is the total ionization cross-section (see section 1.5) and  $\sigma(nLS)$  is the angle-integrated cross-section for excitation of the state specified by quantum numbers  $n$ ,  $L$  and  $S$ . Ever since the earliest measurements of  $\sigma_T$  attempts have been made to evaluate one or more of the quantities on the left hand side of equation (1.9) (e.g. Griffith *et al*, 1979) but only recently have these become reasonably accurate after measurements and calculations of most of these quantities have become available. In view of the measurements discussed above and in the next section, together with the uncertainty regarding the measurements of the excitation cross-section, Campeanu *et al* (1987a) have attempted to partition the total cross-section for He so that the unmeasured quantities  $\sigma_{el}$  and  $\sigma(nLS)$  can be determined from the measured ones. They do this as follows:

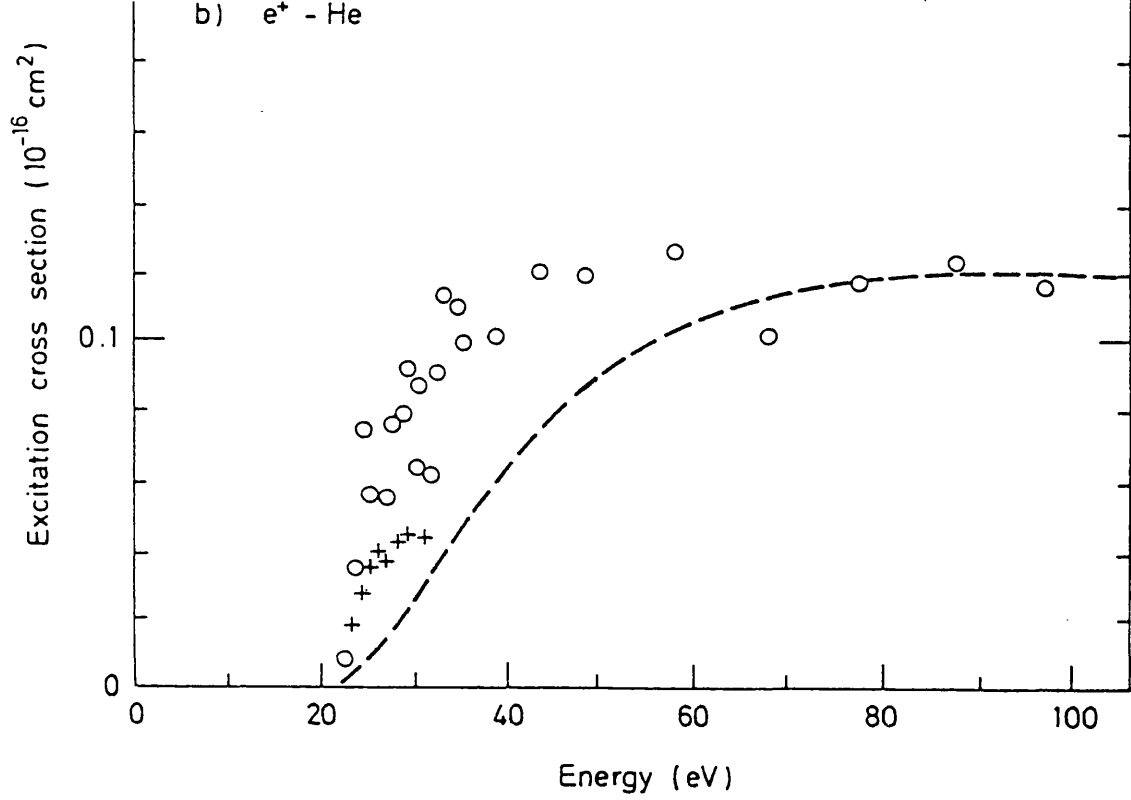


Fig 1.7 The excitation cross-section of positrons incident on Helium.

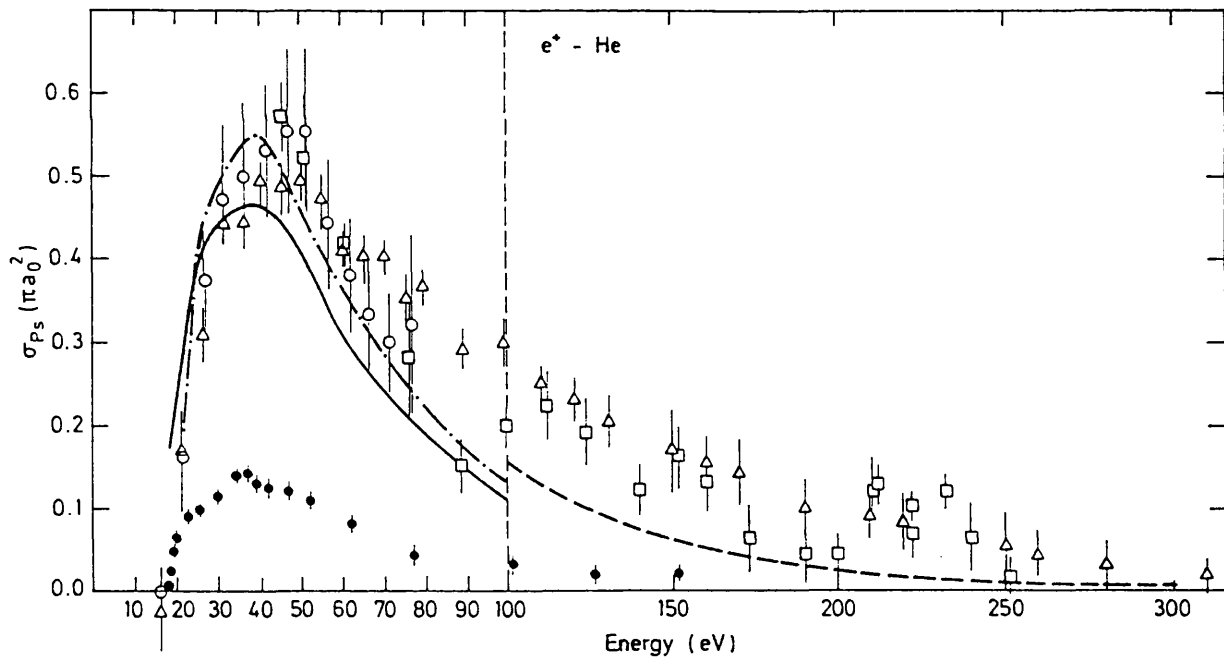


Fig 1.8 The positronium formation cross-section for positrons incident on helium.

$$\sigma_T - \sigma_i - \sigma_{Ps} - \sigma_{el} + \sum_{n=2}^{\infty} \sigma(nLS) - \sigma_{noion} \quad (1.10)$$

where  $\sigma_{no\ ion}$  is the total cross-section for those channels in which an ion is not produced. Since measurements of  $\sigma_T$ ,  $\sigma_i$  and  $\sigma_{Ps}$  were available, the sum of  $\sigma_{el}$  and  $\sigma(nLS)$  could be deduced. Values of  $\sigma(nLS)$  had been calculated by Parcell *et al* (1983, 1987) up to  $n=2$  so  $\sigma_{el}$  could be calculated from these enabling the authors to study its behaviour near the threshold for inelastic processes - one of their stated aims. The resulting data is shown in Figure 1.9, the selected cross-sections having been measured previously by Stein *et al* (1978) and Fromme *et al* (1986).

A cusp in  $\sigma_{no\ ion}$  at the threshold can be seen - this could only be due to structure in  $\sigma_{el}$  as it is the only contributing cross-section at this point. The existence of such a cusp in  $\sigma_{el}$  had previously been predicted by Brown and Humberston (1985). For electrons, a cusp in  $\sigma_{el}$  at the threshold for inelastic processes is predicted as a result of flux conservation (Mott and Massey, 1965): since the inelastic channel will have infinite slope at the threshold, the elastic channel would correspondingly decrease sharply immediately above threshold thus giving rise to a cusp structure. In positron impact the first inelastic channel is that for positronium formation,  $\sigma_{Ps}$  rises sharply from threshold and it has been proposed that a cusp in  $\sigma_{el}$  could result.

The lines marked H and L in Figure 1.9 are the high and low limits of the theoretical values of  $\sigma_{no\ ion}$ , these are seen to lie either side of the line  $\sigma_{no\ ion}$  which is determined from experimental values, in fact the L line agrees with experiment within error bars above 75eV showing the usefulness of the distorted wave approximation for calculating excitation cross-sections at these energies. At lower energies both the available measurements of the excitation cross-section and this partitioning study suggest that theory is inadequate.

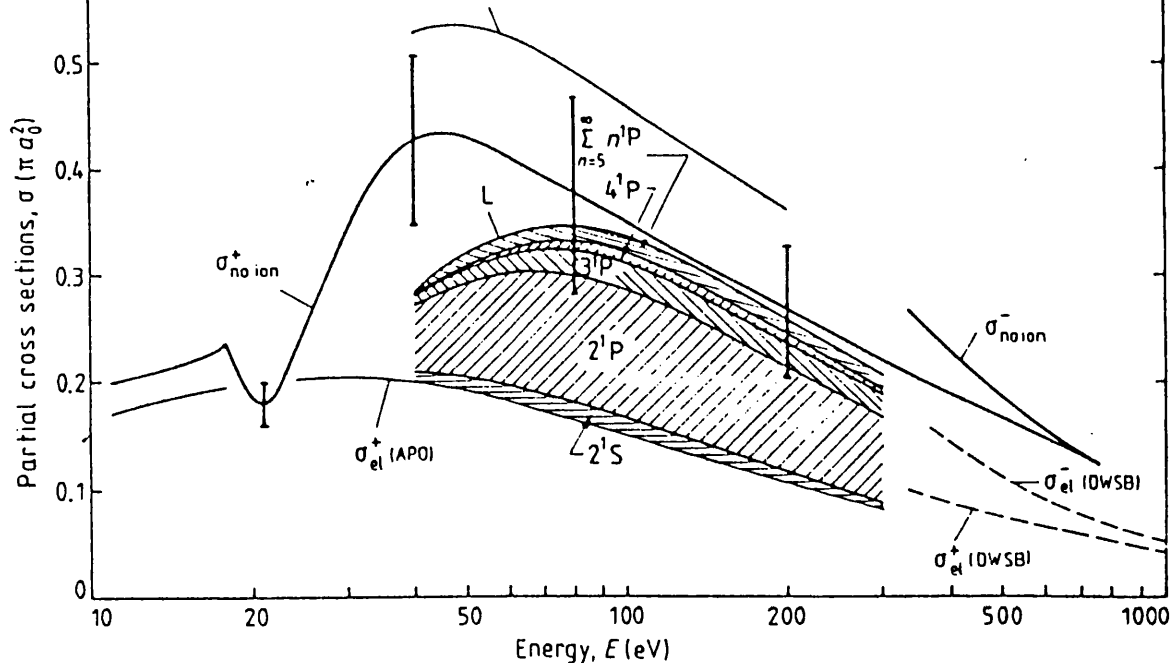


**Fig 1.9** The total cross-section excluding ionization and Ps formation for positrons incident on helium showing contributions from individual channels (Campeanu *et al*, 1987).

Atomic hydrogen is one of the most interesting atoms to consider theoretically because of its simplicity but, to date, experimental data is very limited. A detailed discussion of calculations of  $\sigma_i$  for atomic hydrogen is given in Chapter 2 as these are relevant to the experimental work that will subsequently be described. There now follows a brief overview of theoretical results for the other cross-sections for positrons scattering off atomic hydrogen.

Below the threshold for inelastic processes (less than 6.8eV, the lowest energy at which Ps can form)  $\sigma_{el}$  has been calculated exactly by Bhatia *et al* (1971, 1974) using a variational calculation based on the work of Gailitis (1965). These results can then be used as a benchmark by which to assess the accuracy of other, more approximate, methods. Most authors who have published elastic cross-sections above the inelastic threshold have favourably compared their below-threshold results with those of Bhatia *et al* (1971, 1974). Calculations have been made by Byron *et al* (1985) using

the Unitarized Eikonal-Born Series; Makowski *et al* (1986) with an iterative method for representing scattering matrices and a second-order optical potential; Gien (1977) using a modified Glauber method (discussed in Chapter 2); Winick and Reinhardt (1978) using the moment T-matrix approach; Humberston (1984) using the Kohn variational method and, most recently, Higgins *et al* (1990) with an R-matrix calculation. All these calculations are shown in Figure 1.10 which displays the good level of agreement between the different methods. A great deal of theoretical attention has been given to Ps formation in  $e^+$ -H collisions again because this is the simplest rearrangement collision in which a positron can participate. Figures 1.11 (a) and (b) show the low and high energy behaviour of the calculated values of  $\sigma_{Ps}$ . The low energy calculations shown have been made by Brown and Humberston (1985): Kohn variational; Mandal and Guha (1979): first Born approximation including exchange, denoted FOEA; Drachman *et al* (1976): a second Born approximation using a coupled static approximation for  $L \leq 1$  and Born terms for greater  $L$ ; Mandal *et al* (1979): a distorted wave calculation and finally, an R-matrix calculation by Higgins and Burke (1991). The variational calculation of Brown and Humberston agrees quite well with Drachman *et al*'s results suggesting the accuracy of the latter calculation over a broad energy range. The higher energy results of Drachman *et al* (1976) have been plotted in Figure 1.11 (b), this diagram shows the intermediate energy region where the above calculations of Mandal and Guha (1979) and Mandal *et al* (1979) are expected to be more accurate, and indeed good agreement with other results is seen. Also shown are the calculations of Basu and Ghosh (1988) SBA and BG, these are second Born approximation, and second Born with a coupled state first term respectively. From intermediate energies onwards these display significant discrepancies with Drachman *et al*'s results. The other results shown are the Glauber approximation results (see section 2.2.2) of Tripathi *et al* (1989), these are at their most accurate at higher energies and, as expected, are in good agreement with those of Drachman *et al* (1976).

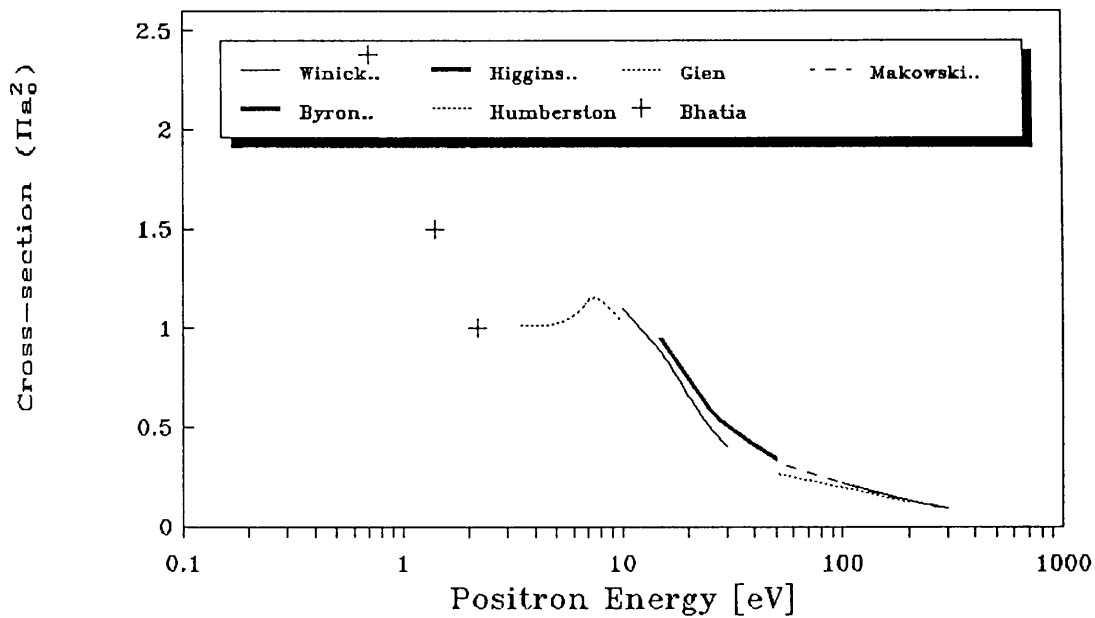


**Fig 1.10** The calculated elastic cross-section of positrons incident on atomic hydrogen.

Apart from ionization the remaining inelastic channel, excitation, has also received some theoretical attention. Calculated cross-sections for excitations from the ground state to the 2s and 2p levels are shown in Figure 1.12 (a) and (b) respectively. The calculations shown are those of Morgan (1982), Bransden *et al* (1985), Byron *et al* (1985), Srivastava *et al* (1987) and Walters (1988). On both diagrams there is good agreement between the results of Morgan, Walters and Bransden *et al*, this is to be expected as each calculation employed a six-state close coupling approximation although the latter two attempt to account for other states via the second Born approximation and polarization respectively. The concurrence of the final results shows the minor rôle played by the other states in this interaction.

Following the procedure of Campeanu *et al* (1987a) discussed above to partition the total cross-section of He one can use equation (1.9) in a similar way for H. The least well determined inelastic cross-section for atomic hydrogen is the total ionization

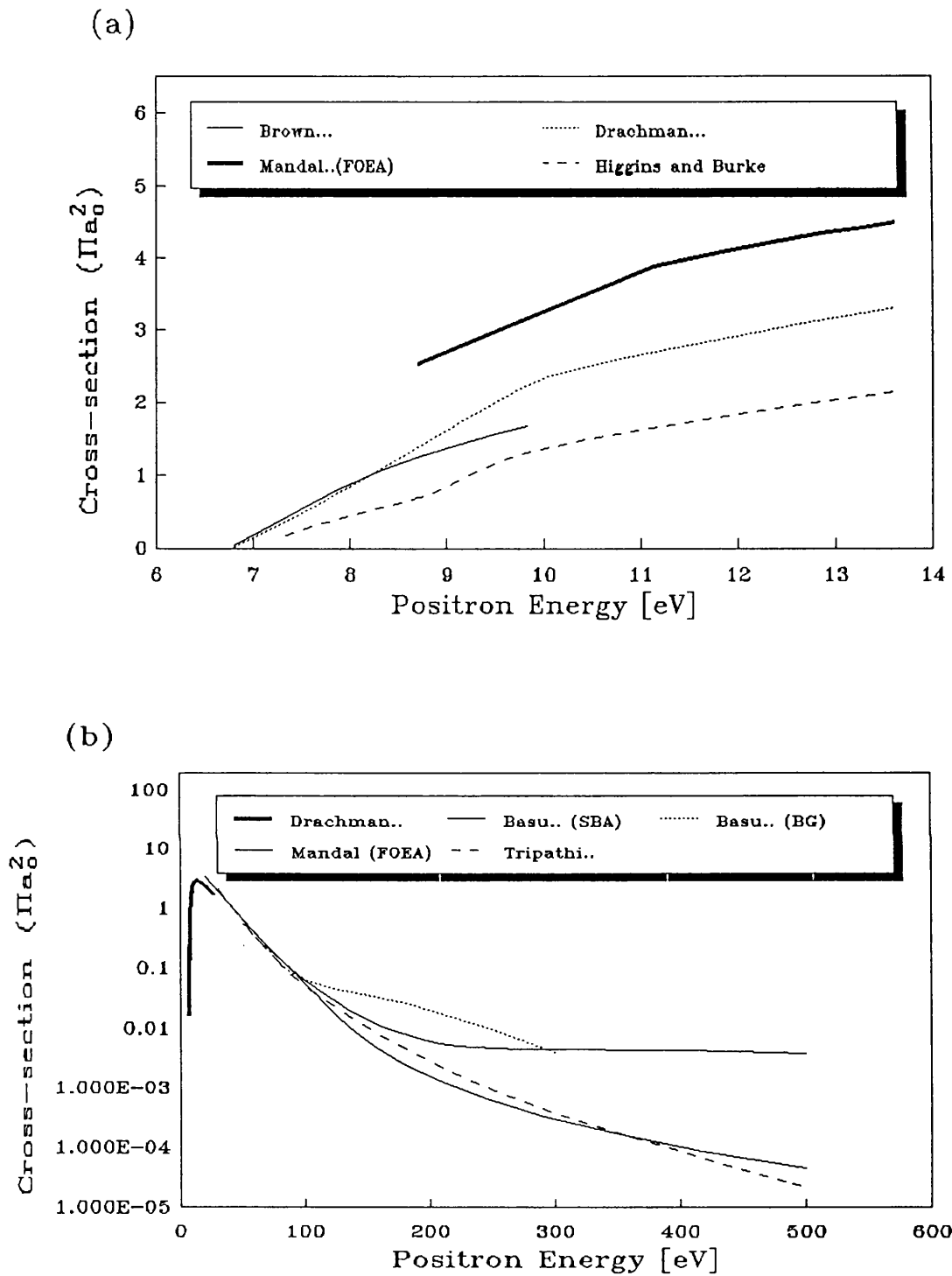
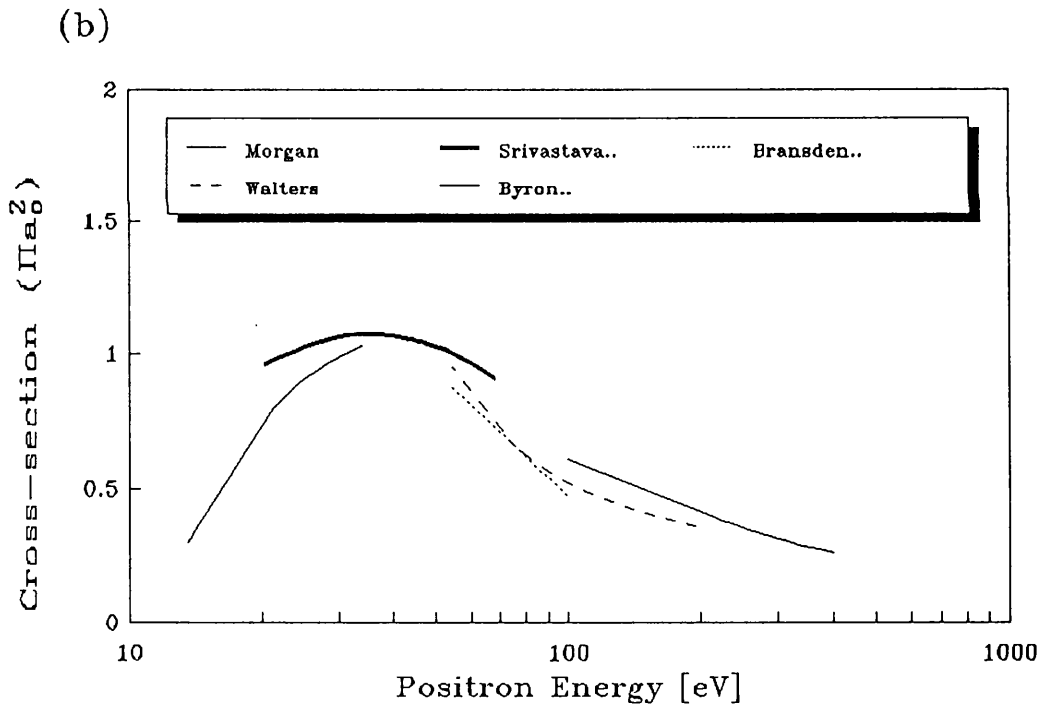
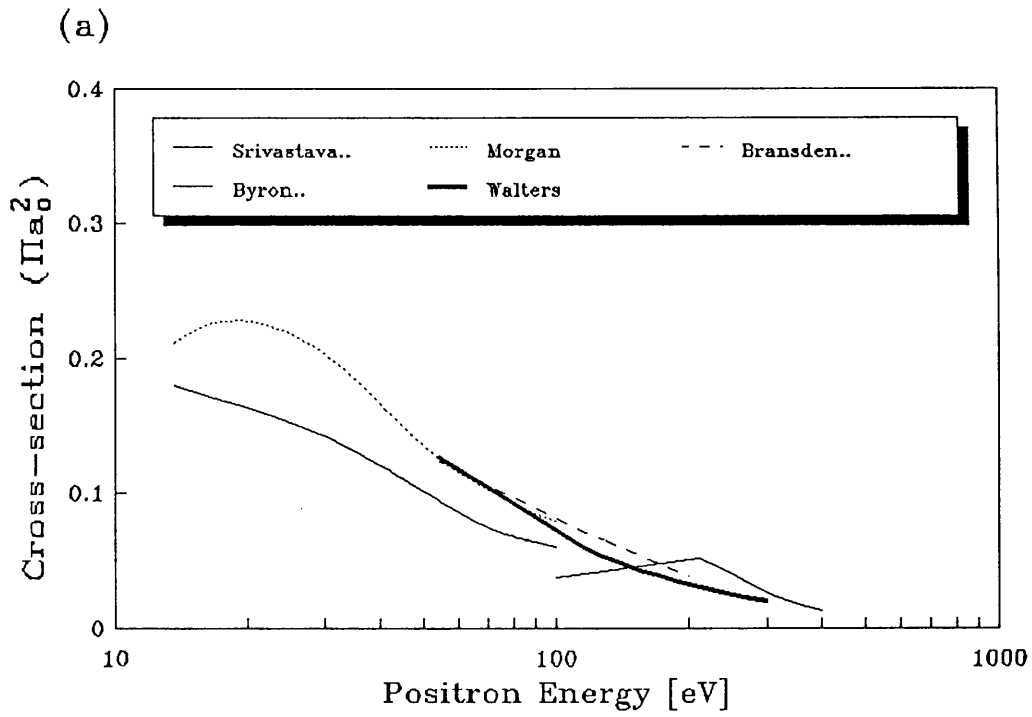


Fig 1.11 The positronium formation cross-section of positrons incident on atomic hydrogen (a) up to 14eV, (b) at higher energies.



**Fig 1.12** The cross-sections for excitation of atomic hydrogen by positron impact from its ground state into (a) the 2S level and (b) the 2P level.

cross-section, this will be discussed in detail in Chapter 2. However, one can estimate it by considering all the other cross-sections as follows. For each of the above cross-sections, the sets of calculated values which are believed to be most accurate and appear to be consistent over different energy ranges are combined. These are plotted in Figure 1.13; the calculations used were those of Bhatia *et al* (1971, 1974), Brown and Humberston (1985), Higgins *et al* (1990) and Makowski *et al* (1986) for  $\sigma_{ei}$ ; Drachman *et al* (1976) and Basu and Ghosh (1988) for  $\sigma_{Ps}$  and the 2s and 2p excitation cross-sections of Morgan (1982), Walters (1988), Srivastava (1988) and Byron (1981). By summing these cross-sections a cross-section for all channels bar ionization is obtained, this is labelled  $\sigma_{t-ion}$  in Figure 1.13. Also shown in Figure 1.13 is the total cross-section those authors who calculated the elastic cross-section evaluated from their elastic phase-shifts using the optical theorem. If one then subtracts  $\sigma_{t-ion}$  from this calculated total cross-section the total ionization cross-section can be estimated. This can be seen clearly by rearranging equation (1.9). A comparison of the ionization cross-section determined in this way with experimental measurements and with the best direct calculation of  $\sigma_{ion}$  to date (Campeanu, 1990 - see section 2.2.2) gives an indication of the accuracy of the various calculations of inelastic cross-sections. Such a comparison is made in Figure 1.14 and the accuracy of these calculations is clearly called into question at intermediate energies.

## 1.5 The Measurement of Impact Ionization Cross-Sections

In the last decade it has become increasingly apparent that studying the ionization of atoms by positron impact can yield valuable information on the interactions of light charged particles and on the mechanism of ionization itself. Further insights into the respective rôles of mass and charge are gained by comparing the ionizing collisions of the singly charged particles and antiparticles  $e^+$ ,  $e^-$ ,  $p$  and  $p^-$  (e.g. the reviews by Charlton, 1990 and Schultz *et al*, 1991). These considerations have prompted the measurement of several single and double ionization cross-sections

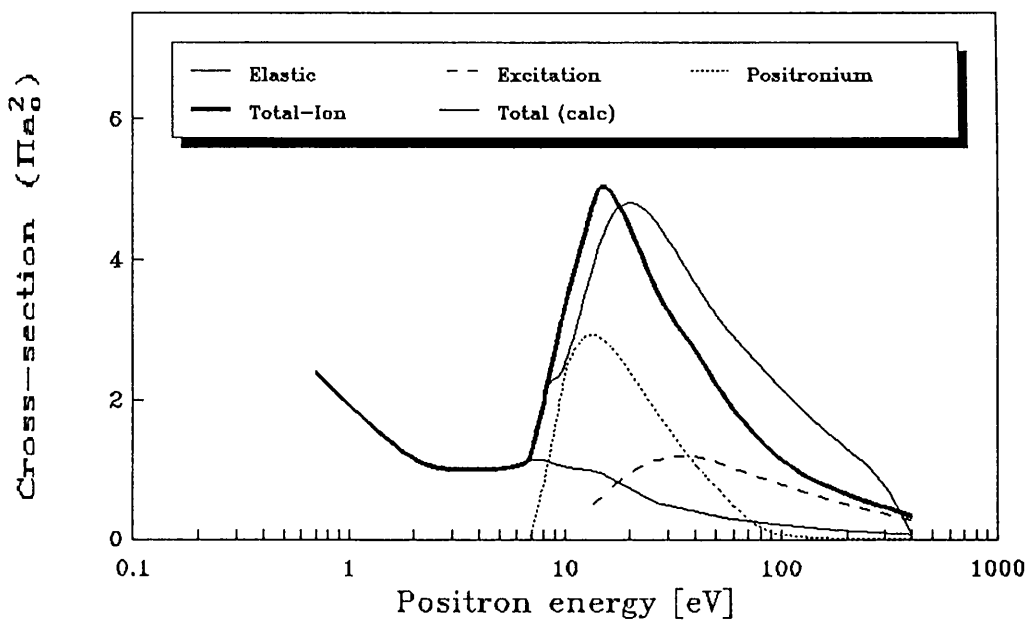


Fig 1.13 Calculated elastic, excitation and positronium formation cross-sections for  $e^+$ -H scattering and their sum (denoted Total-Ion) Also shown is the calculated total cross-section.

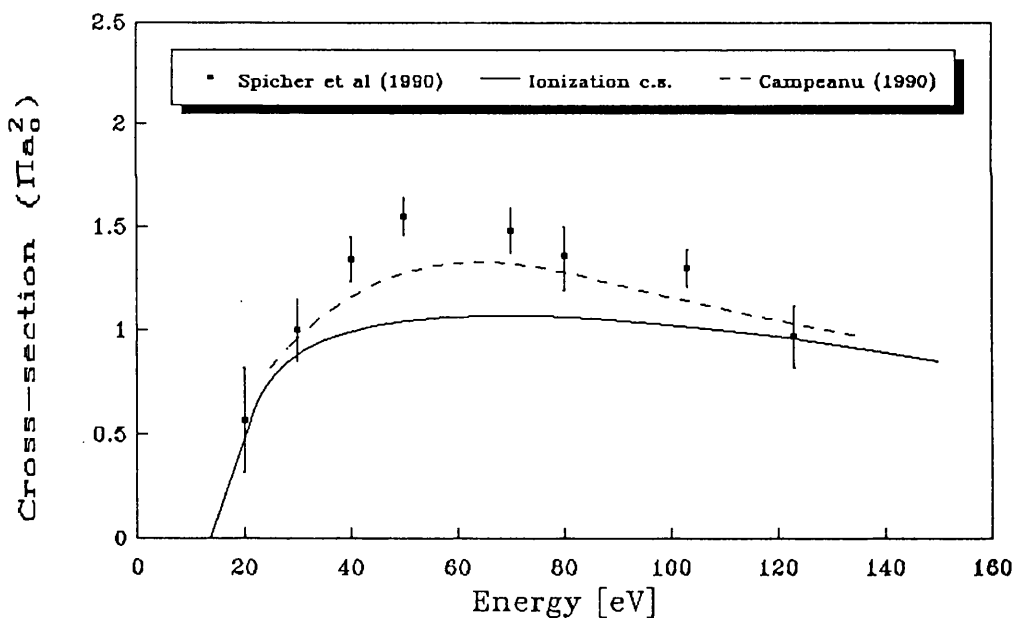
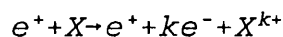


Fig 1.14 The positron impact ionization cross-section of atomic hydrogen determined from partitioning the total cross-section. Directly calculated and measured results are shown for comparison.

with positrons which will be reviewed in this section.

The reaction which will be discussed here can be written



where X is the target atom or molecule. k denotes the degree of ionization of X: single or double. The cross-section for this reaction can then be calculated from

$$\frac{I_i(E)}{I_p(E)} = \rho l \sum_k k \sigma_k(E) = \rho l \sigma_i(E) \quad (1.11)$$

where  $I_i(E)$  is the ion current;  $I_p(E)$  is the projectile current, in this case, positrons;  $\rho$  is the number density of the target gas and  $l$  is the path length of the positrons through the gas. The total ionization cross-section  $\sigma_i$  is here expressed as the sum of the individual cross-sections for ionization of  $n$  electrons,  $\sigma_k$ .

Broadly speaking, experimental work on this reaction can be divided into two groups- those which have employed gas scattering cells and those of the crossed-beam type. These will now be discussed in detail.

### 1.5.1 Scattering Cell Experiments

The combined cross-section for excitation and ionization of He, Ne and Ar was measured by Coleman *et al* (1982) and the ionization cross-sections determined therefrom are shown in Figures 1.15-1.17. The first direct determination of a positron ionization cross-section though was by Sueoka *et al* (1982) who used the RP-TOF system shown in Figure 1.18 to measure that of He. By retarding positrons of a given energy before they reached the detector those which have ionized atoms were distinguished from those which had excited them. Using the same method the

ionization cross-sections of Ne and Ar were also measured by Mori and Sueoka (1984). However these results were prone to errors arising from the multiple scattering of positrons as discussed above for excitation so the experiment was repeated with a different apparatus (Sueoka, 1989). These later results are shown in Figures 1.15-1.17.

Using the apparatus with which they determined positronium formation cross-sections (Fornari *et al*, 1983 and Diana *et al*, 1985a ) Diana *et al* (1985b, 1989) have measured the ionization cross-section for He, their later work was performed with a longer beam giving improved timing resolution. The apparatus shown in Figure 1.19 was filled with gas and a positron beam passed axially through it. The number of positrons undergoing any scattering process, F is deduced by counting those which scatter out of the primary beam and suffer a reduction in their transverse velocity and the number which form ions, f is calculated from the observed electron count-rates with and without gas present and with and without the positron beam.  $\sigma_{ion}$  is then determined from

$$\sigma_{ion} = \frac{f\sigma_{tot}}{F} \quad (1.10)$$

Ionization cross-sections have also been measured by Fromme *et al* (1986, 1988) for He and H<sub>2</sub>, these are also shown in Figures 1.15 and 1.20. The apparatus used is that shown in Figure 1.21. The combined cross-section for ionization and positronium formation was determined by detecting all ions produced. By recording the ions' times-of-flight starting from the detection of a positron the number of ions resulting from impact ionization was derived, in this way the cross-section for ionization could be measured individually and  $\sigma_{Ps}$  separated from the sum  $\sigma_{ion} + \sigma_{Ps}$ ; the  $\sigma_{Ps}$  values are discussed above.

The most recent measurements of positron ionization cross-sections have been by

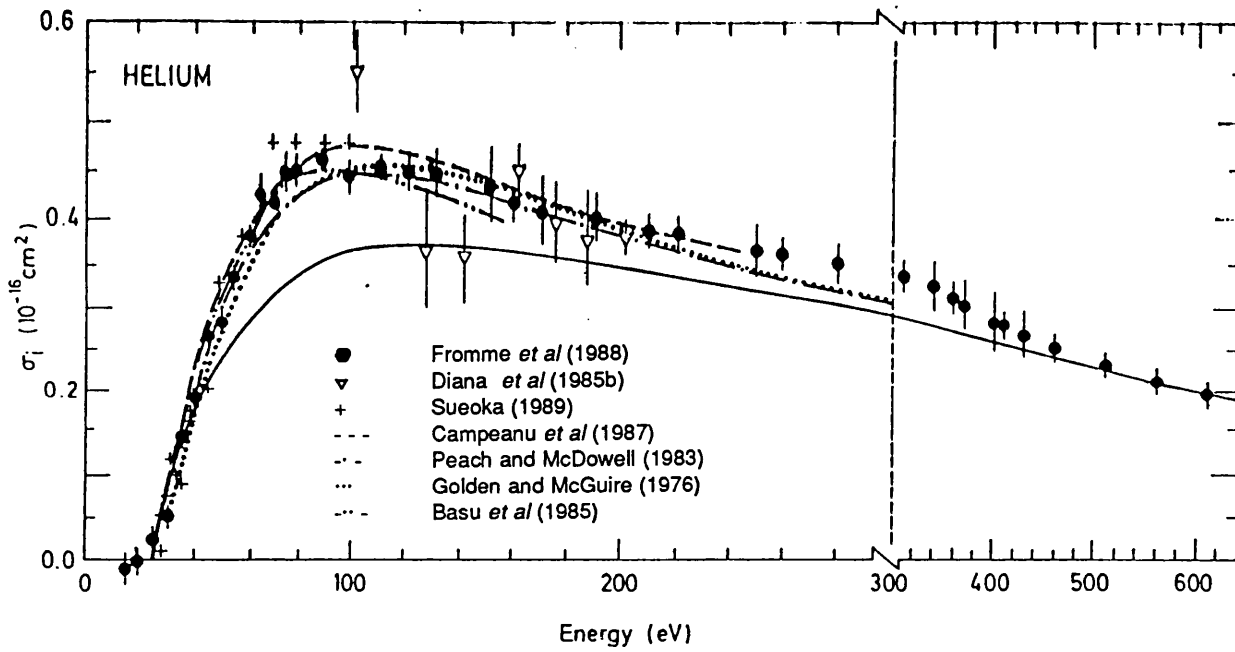


Fig 1.15 The positron impact ionization cross-section of He.

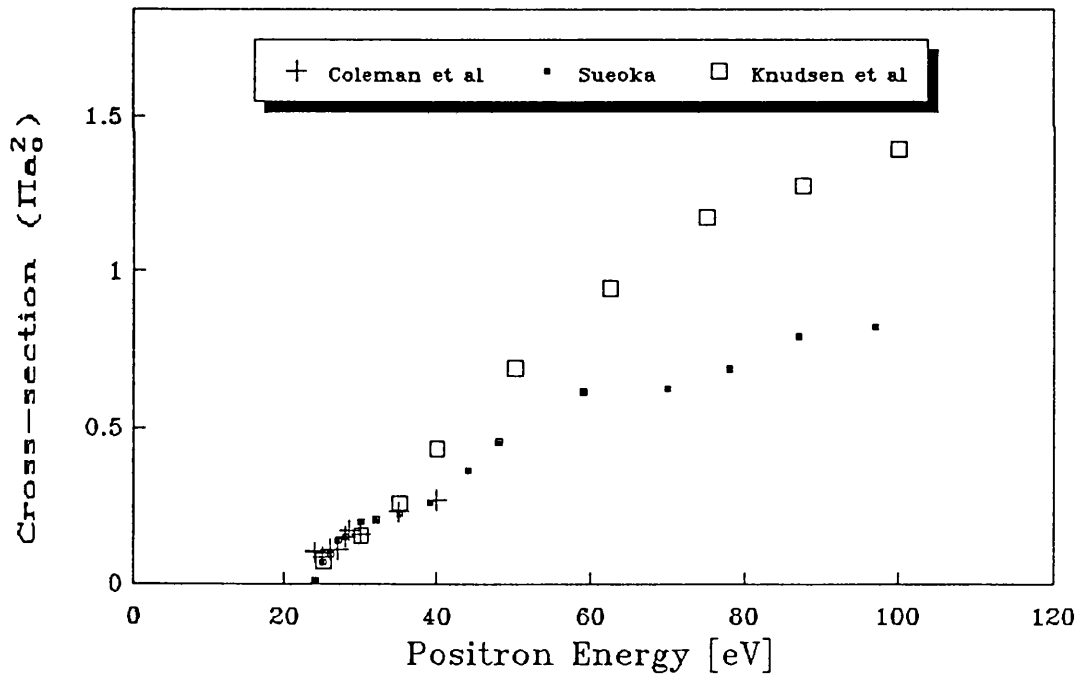


Fig 1.16 The positron impact ionization cross-section of Ne.

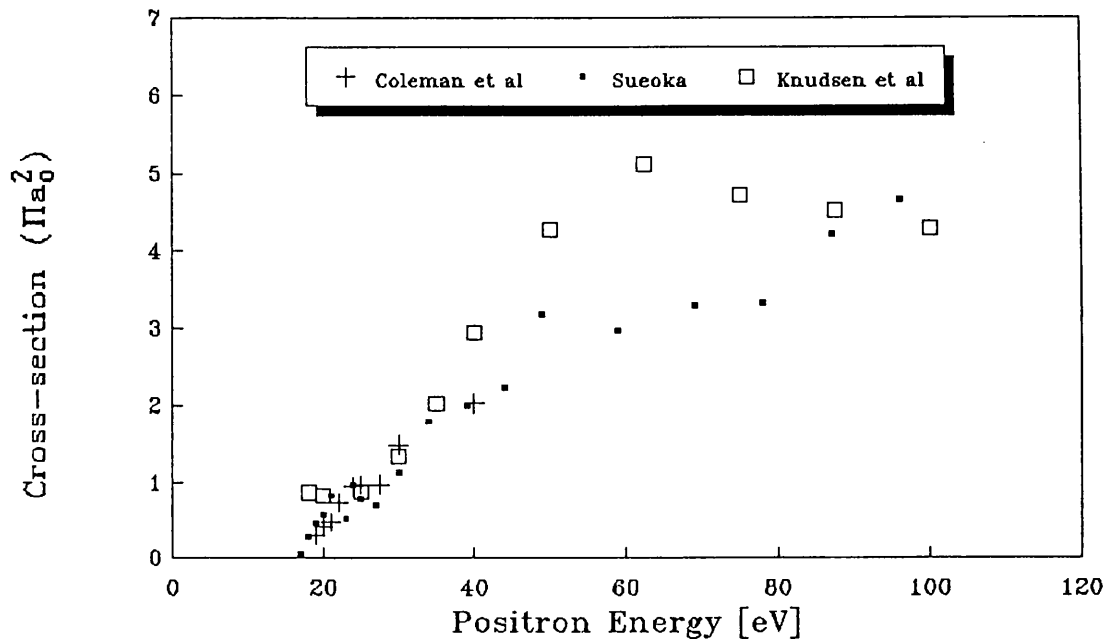


Fig 1.17 The positron impact ionization cross-section of Ar.

Knudsen *et al* (1990) who used the apparatus shown in Figure 1.22. This beam system, with slight modifications, had already been used to measure the single and double ionization cross-sections for electron, proton and antiproton impact (Brun-Nielsen, 1990, Charlton 1988, 1989, Haugen *et al*, 1982, and Andersen *et al*, 1986, 1987 and 1990 respectively).

Charlton *et al* (1988, 1989) have also measured the double ionization cross-section of positrons incident on noble gas atoms with this apparatus. This was as part of a programme of research to investigate the rôles of mass and charge in the dynamics of ionization by comparing the single and double ionization cross-sections of the matter-antimatter pairs electrons and positrons and protons and antiprotons. Figure 1.23 shows the ratio of double to single ionization cross-sections for all particles incident on He. All four data sets tend to the same value at high velocity as the effects of different masses and charge signs disappear but the convergence of the

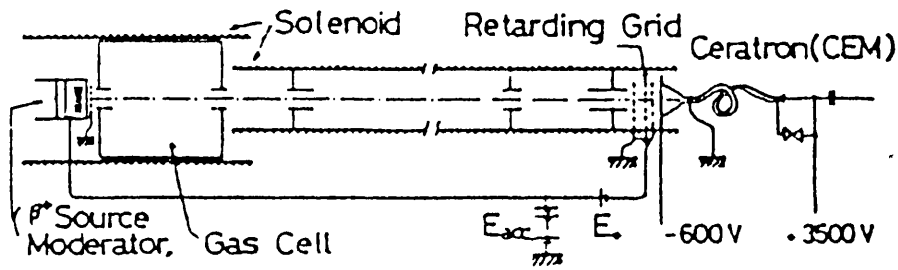


Fig 1.18 The RP-TOF apparatus used by Sueoka and Mori (1984) to measure the positron impact ionization cross-sections of He, Ne and Ar.

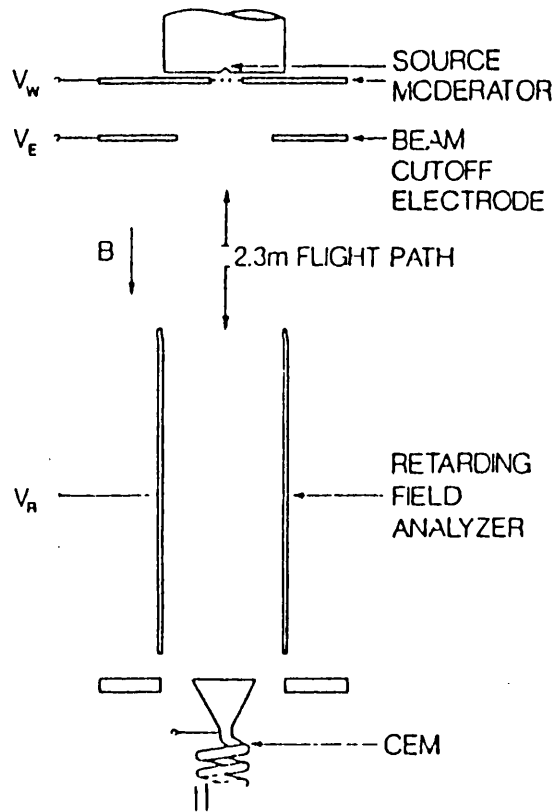


Fig 1.19 The apparatus used by Diana et al (1985) to measure the positron impact ionization cross-section of He.

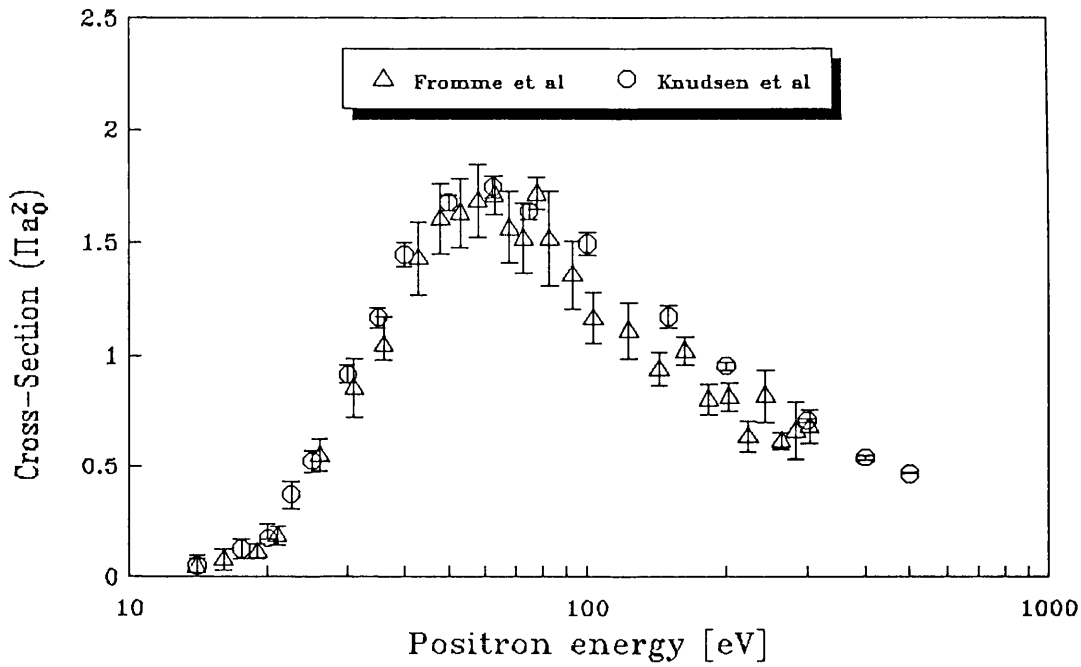


Fig 1.20 The positron impact ionization cross-section of molecular hydrogen.

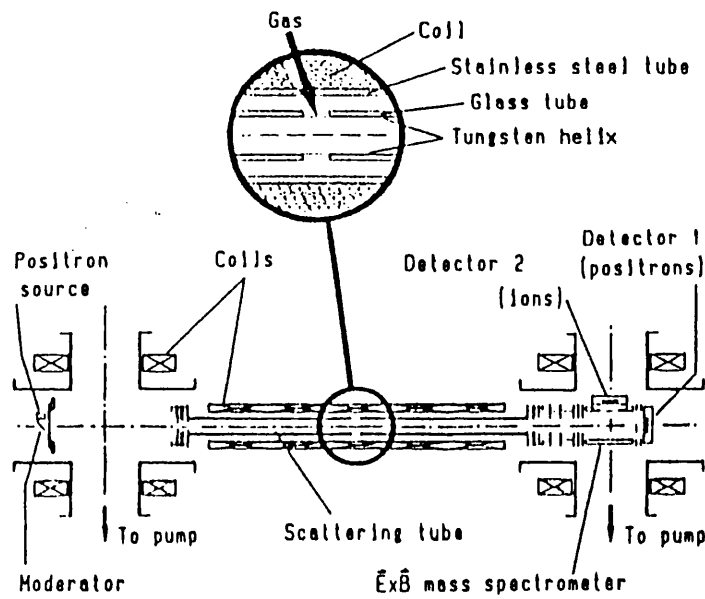


Fig 1.21 The apparatus used by Fromme et al (1986, 1988) to measure the positron impact ionization cross-sections of He and H<sub>2</sub>.

positron and proton data and, separately, the electron and antiproton data shows the dominance of charge effects at intermediate velocities. At low velocity the lower kinetic energy possessed by the lighter particles causes a decrease in their ratios relative to the heavier projectiles. Modifications made to the apparatus when measuring the positron single ionization cross-section will be highlighted below.

The positron beam was derived from a  $^{22}\text{Na}$  source-W mesh moderator arrangement and guided by a magnetic field. Electrostatically biased tubes were employed to remove high energy electrons from the primary beam and to repel positrons which were backscattered from the gas so that they would be detected. Scattering takes place in a gas cell and positrons then travel to a multi-channel plate detector. Ion extraction and detection is performed by applying an electric field across the gas cell which serves to sweep the ions out of the cell through an aperture in its side wall after which they are focussed onto a Ceratron detector. In the single ionization studies of Knudsen *et al* (1990) this field was pulsed because the electric field across the cell would deflect the positrons in the beam. This was not a significant problem in the previous experiments with heavier projectile particles or when looking at multiply charged ions due to their higher energies. A  $\pm 100\text{V}$  pulse was applied to the two sides of the cell on the detection of a positron by the MCP detector, the intensity of the beam ( $\sim 10^4 \text{ e}^+ \text{ s}^{-1}$ ) was such that pulses of 1-3  $\mu\text{s}$  duration could be applied without affecting the beam. The onset time of the voltage pulse was such that ions would not drift so far before it was applied that they will no longer pass through the aperture to the detector. The time delay between the detection of a positron and an ion was then recorded and an effective ionic time-of-flight spectrum was recorded from which the total ionization cross-section was deduced. Measurements were made for He, Ne, Ar and  $\text{H}_2$  and these are shown in Figures 1.15-1.17 and 1.20.

An illustrative comparison with theoretical results has been made for  $\text{e}^+$ -He ionization (see Figure 1.15). It can be seen that excellent agreement with experiment

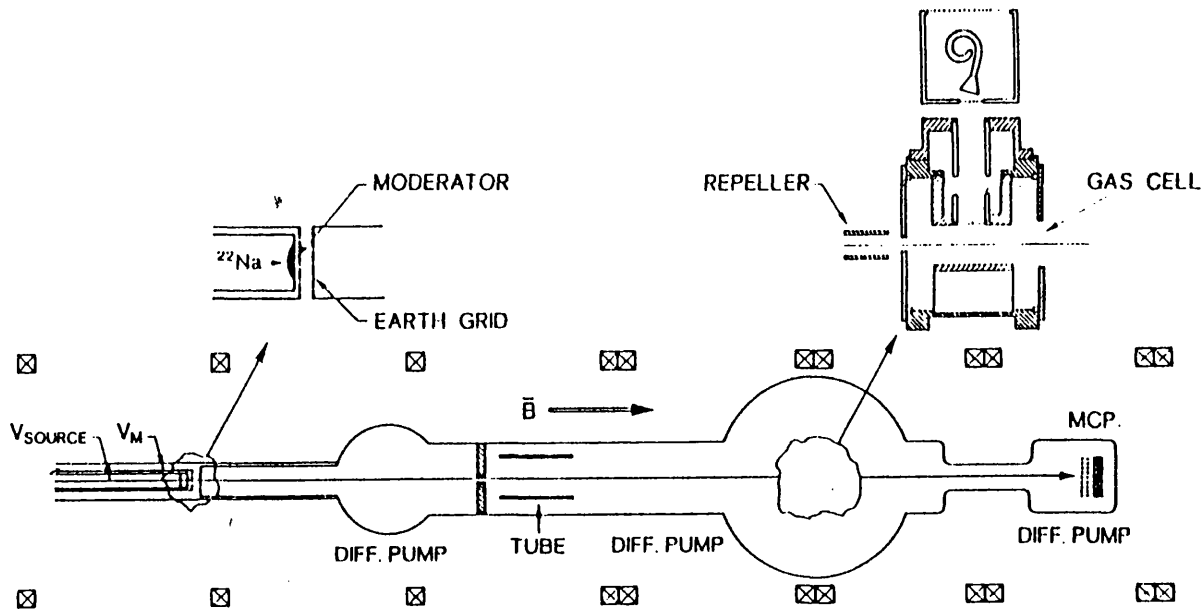


Fig 1.22 The apparatus used by Knudsen et al (1990) to measure the positron impact ionization cross-sections of He, Ne, Ar and  $\text{H}_2$ .

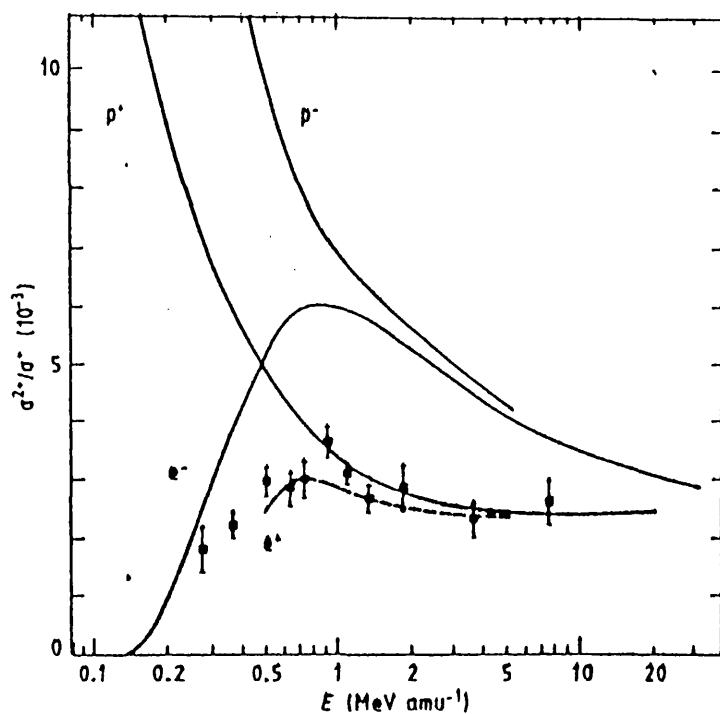


Fig 1.23 The ratio of double-to-single ionization cross-sections of He for  $e^-$ ,  $e^+$ ,  $p$  and  $\bar{p}$  (from Charlton et al, 1988, 1989 and Andersen et al, 1987).

is achieved for the CTMC results of Peach and McDowell (1983) and Schultz and Olson (1988) and the distorted wave calculations of Basu *et al* (1985) and Campeanu *et al* (1987b).

### 1.5.2 Crossed-Beam Experiments

This method was developed to measure scattering cross-sections for atomic species which were unstable at room temperature such as atomic hydrogen. It was first developed by Funk (1930) to study the ionization of sodium vapour from a furnace. A block diagram of a typical crossed-beam experiment is shown in Figure 1.24. It consists of two beams—one of projectile particles and one of target atoms intersecting each other perpendicularly. One or more of the scattering products are then detected after leaving the interaction region. A significant development was made by Boyd and Green (1958) in that they modulated the target beam and detected the ionization products in phase with the modulation, in this way they could exclude the contribution to their data arising from ionization of the background gas. This was particularly important with the low experimental count-rates that were encountered when using a diffuse target.

The calculation of the ionization cross-section from such experiments is modified slightly from the form outlined in equation (1.11), it is given by (from Kieffer and Dunn, 1966)

$$\frac{I_i(E)}{I_p(E)} = \sigma_i(E) R \left[ \frac{(v_p^2 + v_t^2)^{\frac{1}{2}}}{v_t v_p} \right] F \quad (1.12)$$

where  $v_p$  and  $v_t$  are the velocities of the projectile and target particles respectively which are assumed to be perpendicular.  $R$  is the intensity of the beam of target particles and  $F$  is a geometrical factor describing the overlap of the two beams over

the interaction region and is given by

$$F = \frac{\int j_p(z) j_t(z) dz}{\int j_t(z) dz \int j_p(z) dz} \quad (1.13)$$

where  $j_p(z)$  and  $j_t(z)$  are the spatial distributions of the projectile and the target over the region of overlap of the beams,  $z$  is the distance along the axis perpendicular to both beams. The difficulty in calculating  $\sigma_i$  from equation (1.13) arises from problems in determining  $F$ , it is also common in crossed-beam experiments not to measure  $R$  directly thus creating further complications. Methods by which this has been averted are discussed below in the context of individual experiments.

The first measurement of the electron impact ionization cross-section for atomic hydrogen was by Fite and Brackmann (1958). The method which they used was essentially that developed by Boyd and Green (1958) in which the atomic beam was modulated to remove the spurious counts from ionization of the background gas. The apparatus is shown in Figure 1.25. Molecular hydrogen was dissociated in a W furnace from which a mixed atomic and molecular beam was derived. This was then crossed with an electron beam formed in an electron gun. The target beam then entered a curved electrostatic mass spectrometer which was pulsed at the beam modulation frequency so  $H_2^+$  ions from the background gas could be accounted for.  $H^+$  ions were then distinguished from  $H_2^+$  ions using the mass spectrometer. Two types of cross-section were measured: these were termed relative and absolute. For the relative cross-sections experimental data was normalized to cross-sections calculated with the Born approximation at high energies and the low energy results were then evaluated. The absolute cross-sections were determined by knowing the dissociation fraction of the gas precisely through measuring the ion currents with the furnace on and off and then normalizing to previously measured  $H_2$  cross-sections. The normalization procedures employed here obviated the need to calculate the

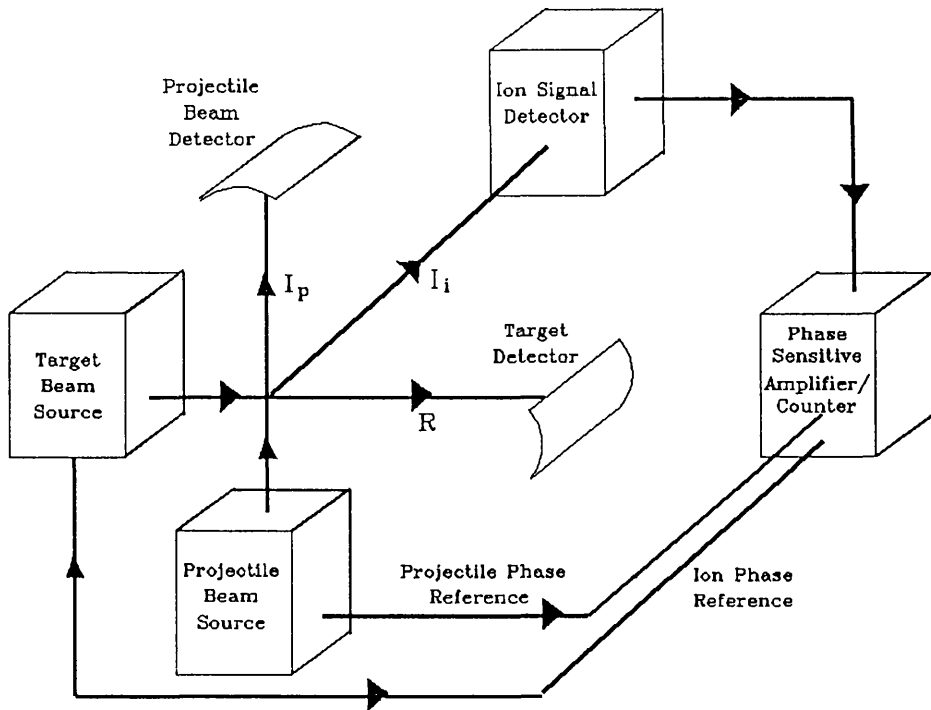


Fig 1.24 A block diagram of a typical crossed-beam experiment to measure the ionization cross-sections of gases showing the quantities in equations (1.16) and (1.17).

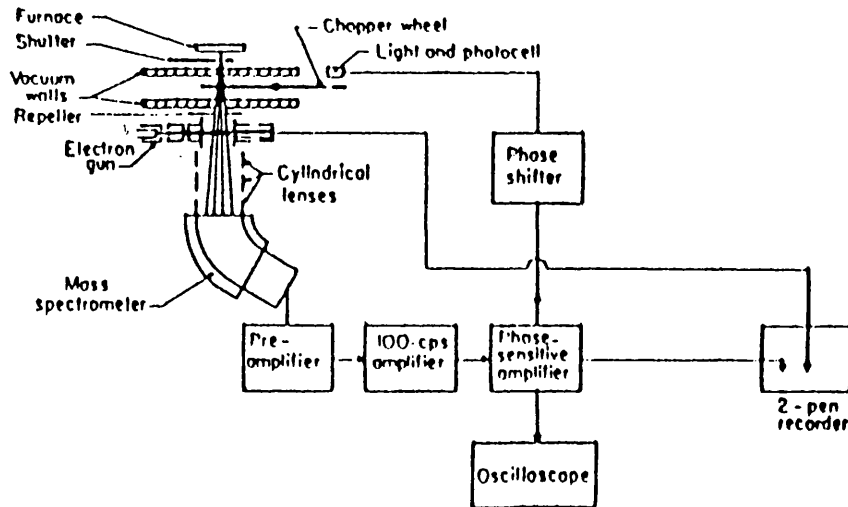


Fig 1.25 A schematic diagram of the apparatus used by Fite and Brackmann (1958) to measure the electron impact ionization cross-section of atomic hydrogen.

overlap factor,  $F$  given in equation (1.13), since it was assumed to be equal for both  $H$  and  $H_2$ . Figure 1.26 shows the good agreement that was found between both these sets of results.

In a similar experiment, using the apparatus of Boyd and Green (1958) in which atomic hydrogen was produced by dissociation in a radio-frequency discharge, the electron impact ionization cross-section of  $H$  was measured by Boksenberg (1961). Again these results were normalized to Born approximation data at high energies and lower energy cross-sections were interpolated from these. Figure 1.26 shows the agreement that was obtained with the previous results, the small discrepancy probably arises from the different efficiencies of collection of thermal ions in these experiments. Rothe *et al* (1962) also measured the ionization cross-section of atomic hydrogen. Molecular hydrogen was dissociated in a radio-frequency discharge and ion collection was by means of a mass spectrometer which was again modulated. Absolute cross-sections were obtained by measuring the dissociation fraction and normalizing to  $H_2$  results, these are also shown in Figure 1.26. This data had to be corrected for  $H^+$  ions arising from dissociative ionization of  $H_2$  since the experimental geometry allowed these to be collected efficiently. A more recent measurement of the electron impact ionization cross-section of atomic hydrogen was made by Shah *et al* (1987). The system shown in Figure 1.27 was used.  $H$  atoms were produced in a  $W$  furnace and were crossed by a beam of electrons from an electron gun. The main difference in this experiment from earlier work is that the electron beam is now pulsed. Ions were extracted from the interaction region electrostatically and perpendicularly to the two beams with the extraction field being applied immediately after the passage of a pulse of electrons through the interaction region. Atomic and molecular ions were then distinguished by their different times of flight in an electric field to a detector, i.e. by their charge to mass ratios. The pulsed field ensured that no field effects were present to influence the scattering process or to change the overlap of the beams in any unquantifiable way. Since the system was originally developed for proton scattering experiments the substitution of a proton

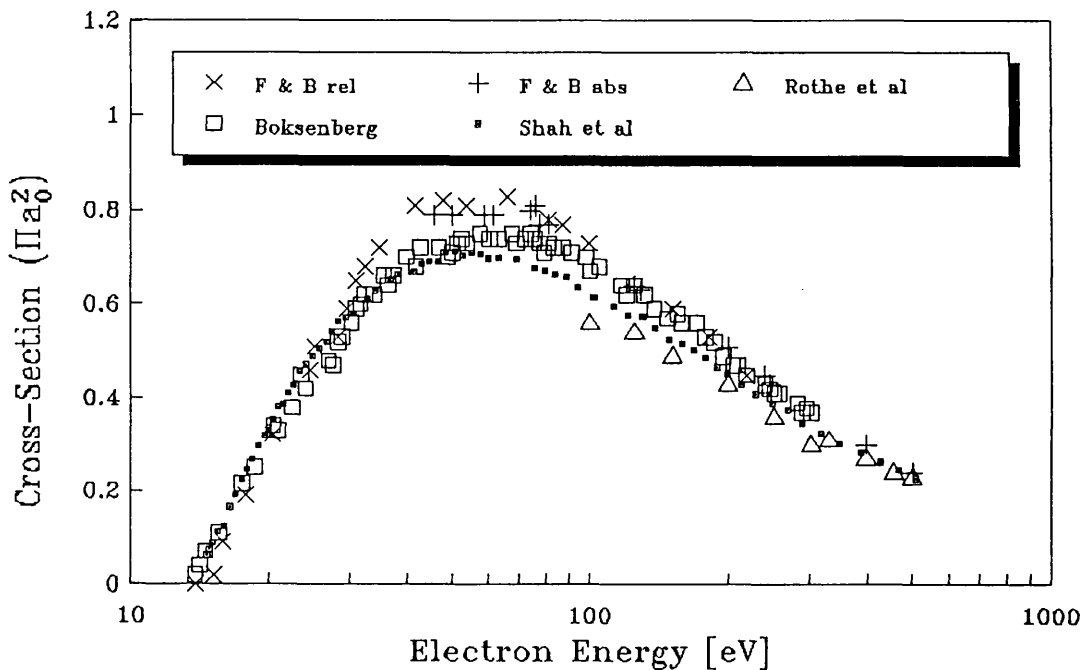


Fig 1.26 The measured electron impact ionization cross-sections of atomic hydrogen.

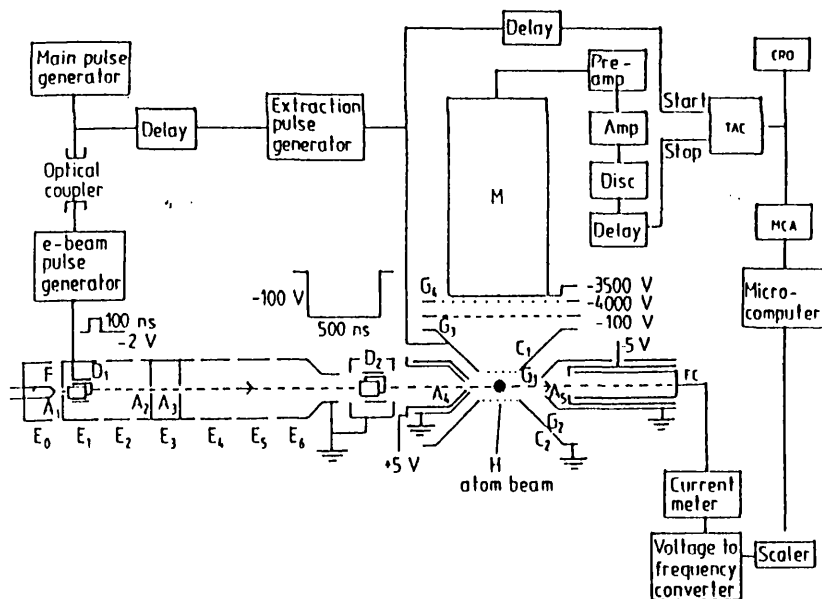
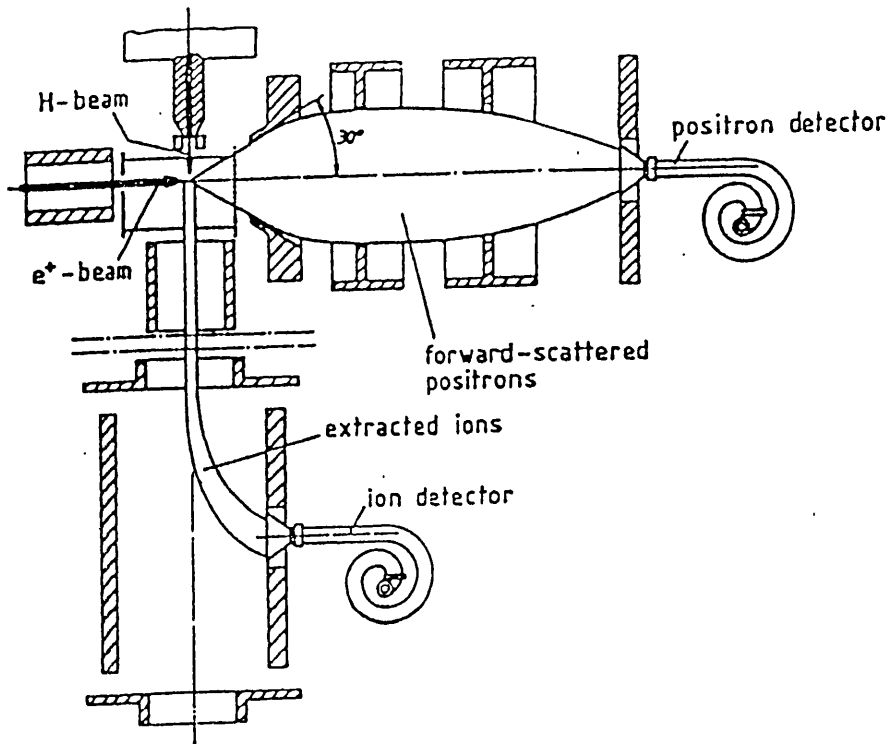


Fig 1.27 A schematic diagram of the apparatus used by Shah et al (1987) to measure the electron impact ionization cross-section of atomic hydrogen.

beam for the electron beam presented no great experimental difficulties and the electron results were therefore normalized to proton data using previously measured proton ionization cross-sections. The results are also shown in Figure 1.26.

Remarkable agreement is found for all sets of data although the most recently measured cross-sections (Shah *et al*, 1987) are believed to be the most accurate because of the extensive precautions that were taken to minimize systematic effects. The only crossed-beam experiment to measure the ionization cross-section of an unstable species on positron impact has been performed recently by Spicher *et al* (1990). To measure the ionization cross-section of positrons incident on atomic hydrogen the experimental apparatus shown in Figure 1.28. was used. A beam of positrons was produced by moderating fast  $\beta^+$  emitted from a  $^{22}\text{Na}$  radioactive source with W mesh. The positrons are deflected through  $90^\circ$  in an electrostatic analyzer and are then transported by electrostatic lenses to the interaction region. Here, they cross a beam of atomic and molecular hydrogen effusing from a capillary at the end of discharge tube. The plasma in which molecular hydrogen is dissociated is sustained by the input of radio-frequency power. Such a source of atomic hydrogen was developed by Slevin and Stirling (1981) and will be described fully in section 3.3.2. Positrons which are scattered by the gas up to angles of  $30^\circ$  are focussed and detected with a channeltron. Ions are allowed to drift slightly in the gas beam and are then extracted electrostatically on an axis perpendicular to the gas and deflected through  $90^\circ$  to another channeltron detector. Atomic and molecular ions are distinguished by their times of flight to this detector with the starting pulse being derived from the detection of a positron. The ion detector is not on a line-of-sight to the discharge tube as the contribution to the background in the time-of-flight spectrum from light would be too great. This has been further reduced by coating all reflective surfaces inside the system with carbon.

The reactions which produce ions are listed in Table 1.2. Since the object was to measure  $\sigma_i$  all the other listed processes had to be accounted for or eliminated. All



**Fig 1.28** A diagram of the apparatus used by Spicher *et al* (1990) to measure the positron impact ionization cross-section.

those involving the formation of Positronium,  $\sigma_{Ps}(H)$ ,  $\sigma_{Ps}(H_2)$  and  $\sigma_{Ps}(H_{2,diss})$  produce ions that are not correlated with a positron and are not detected as the timing sequence is not initiated. As explained above  $H^+$  and  $H_2^+$  are distinguishable by their times of flight. The other process that can occur is dissociative ionization. The authors note that protons produced in this way are more energetic than those from single atom ionization and would not be collected with this arrangement-this was then verified experimentally.

Since detection probabilities and densities in the interaction region are not known only relative cross-sections, as defined above, could be measured. The experiment could be repeated with electrons as projectiles by reversing the polarities of the source and moderator and of the transport system and then forming a beam from the

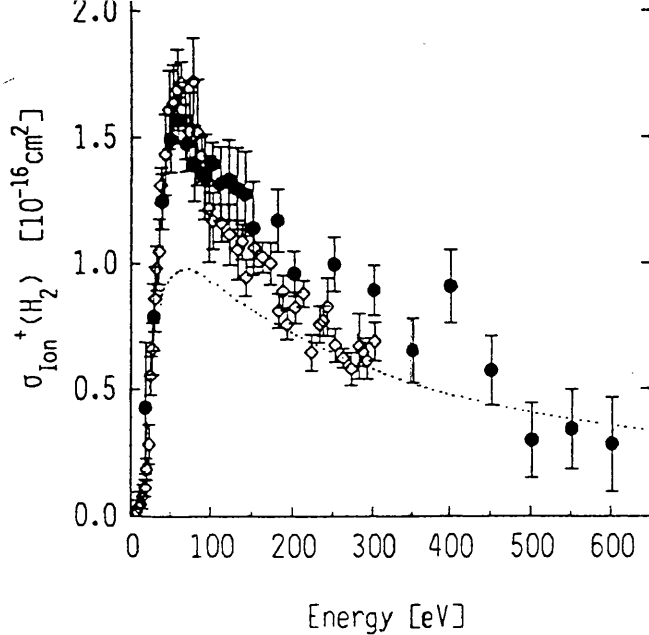


Fig 1.29 (a) The positron ionization cross-sections measured by Spicher *et al* (1990) for molecular hydrogen: ●, with the results of Fromme *et al* (1988) (◊) and, for electrons (•••) Rapp and Englander-Golden (1965).

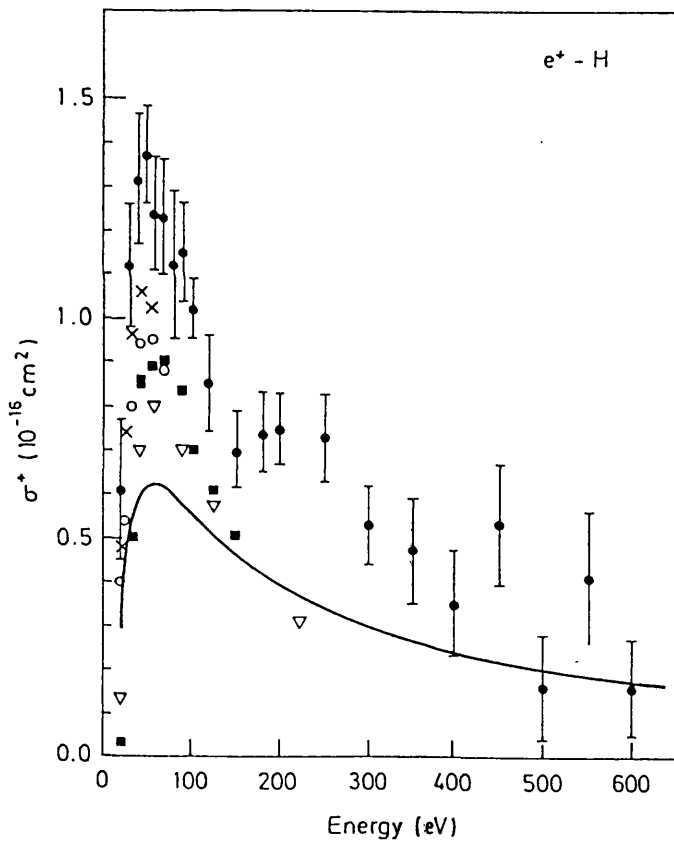


Fig 1.29 (b) The positron ionization cross-section of Spicher *et al* (1990) for atomic hydrogen: ●, with the theoretical results of Ghosh *et al* (1985) (x), Wetmore and Olson (1986) (■), Ohsaki *et al* (1985) (▽) and Mukherjee *et al* (1989) (○) and, for electrons (—) Shah *et al* (1987).

secondary electrons produced when  $\beta^+$  particles strike the moderator. Data obtained with electrons was then normalized to previously measured cross-sections and the normalization factors thus deduced were applied to positron results yielding the cross-sections shown in Figure 1.29 (a) and (b).

To assess the validity of their normalization procedure one must consider their measured impact ionization cross-sections of  $H_2$ , these are shown in Figure 1.29. Reasonable agreement is obtained with previous data taken by the same group on a different apparatus (Fromme *et al*, 1988) except at energies above about 150eV where the newer results seem to be slightly higher. As is shown in the following discussion this may be a consequence of the limited angular acceptance of the beam detector.

In applying the same normalization procedure to electrons and positrons the angular distribution of the scattered projectiles are assumed to be identical for both particles. It is claimed that this is valid over the energy range where the normalization is done (200-600eV) as the first Born approximation which does not differentiate between particles of different charge-sign is thought to apply. It will be demonstrated in section 2.3.1.1 that this is not the case.

The slight discrepancy between the measured electron data and previous experimental results in the energy range 50-100eV shown in Figure 1.29 may indicate that the electron cross-section is underestimated at high energies in the H data. A possible explanation for the observed results is that erroneously low results were normalized to accurate data at high energies resulting in the low energy values being shifted above this data. As a result of normalizing in the same way for both incident particles the positron data is then too high at higher energy hence the discrepancy between the different results seen in Figure 1.29.

$e^+ + H \rightarrow Ps + H^+$	$\sigma_{Ps}(H)$
$e^+ + H \rightarrow e^+ + e^- + H^+$	$\sigma_i(H)$
$e^+ + H_2 \rightarrow Ps + H_2^+$	$\sigma_{Ps}(H_2)$
$e^+ + H_2 \rightarrow e^+ + e^- + H_2^+$	$\sigma_i(H_2)$
$e^+ + H_2 \rightarrow Ps + H + H^+$	$\sigma_{Ps}(H_2, \text{diss})$
$e^+ + H_2 \rightarrow e^+ + e^- + H + H^+$	$\sigma_i(H_2, \text{diss})$

**Table 1.2** A table showing the possible reactions in  $e^+$ -H scattering which give rise to ions and the notation that is used for the cross-section of each.

Separate normalization was made for H and  $H_2$  to remove the factor R in equation (1.12) since the relative densities of the two target species were not known. The other unknown - F, the overlap factor given in equation (1.13) - was also eliminated in the normalization process but in repeating the normalization for positron data it is assumed that the positron and electron beams have identical distributions,  $j_p(z)$ . This may not be the case since Spicher *et al* (1990) do not specify beam intensities this possible source of error is not quantifiable. Given these considerations it is therefore clear that further study of the  $e^+$ -H system is warranted.

## 1.6 Motivation for this Work

Being the antimatter equivalent of electrons the interactions of positrons with atoms and molecules can be most informative in understanding the dynamics of inelastic collisions. This comes from the difference in charge-sign between these particles. The interactions of the particles with the atomic or molecular potentials thus differ in that they are attractive and repulsive for, respectively, electrons and positrons. The polarization interaction is attractive for both so at lower energies, when polarization of the target is significant, the electron cross-section tends to be larger (Campeanu *et al*, 1987a). Departures from this are valuable sources of information in that they

shed light on the influence of the projectiles' properties on reactions.

A case in point is ionization at higher energies where the positron cross-section exceeds that for electrons up to the point at which they converge according to the Born approximation. It has been postulated that this is due to the positive positron presenting an attractive potential which produces a region of reduced binding to the atom (Schultz *et al*, 1991). The ionization of hydrogen is thus of great interest as it is the simplest atom and interactions with it are three-body problems for which confident theoretical predictions can be made. In this way physical models and approximations based on them can be tested for their accuracy in depicting actual processes.

The only experimental work on the  $e^+$ -H system to date has been described above (Spicher *et al*, 1990) and its possible sources of inaccuracy have been outlined. The experiment that will be discussed in the following three chapters addresses the same interaction but is inherently different in that what may be limitations to the earlier work are not considerations here.

Also discussed is a complementary experiment in which the final state interaction between a scattered positron and an ionized electron in  $e^+$ -Ar collisions is studied. Although strong interactions have been predicted and observed in ionization by other positively charged particles different calculations conflict as to its significance in positron collisions. The experiment that will be described in Chapter 5 has yielded preliminary results which may resolve this disagreement.

The aim of the two pieces of experimental work that will be described in detail in the following chapters is therefore to add to an increasing body of knowledge concerning the exact nature of three body interactions between light particles. This will aid our understanding of some of the most fundamental processes in physics.

## CHAPTER 2

# THE THEORETICAL CALCULATION OF THE TOTAL POSITRON IMPACT IONIZATION CROSS-SECTION OF ATOMIC HYDROGEN

### 2.1 Introduction

In this chapter the general theories, both classical and quantum mechanical, which have been applied to impact ionization by charged particles will be reviewed. Special emphasis will be given to their use in calculating the total ionization cross-section of positrons incident on atomic hydrogen. Comparison with experimental data is made to determine the accuracy of the calculations and the validity of any approximations made.

Atomic units will be used throughout, i.e.  $e = \hbar = 1$ . Cross-sections will be expressed in  $\pi a_0^2$  where  $a_0$  is the Bohr radius. Energy will be quoted in electron-volts (eV).

### 2.2 Classical Calculations

The first calculation of impact ionization cross-sections was by Thomson (1912). This treatment was classical in that all the particles involved were considered to be obeying the Newtonian laws of motion. Thomson simplified the problem by neglecting the interactions of particles other than the projectile and the atomic electron. This binary encounter approximation therefore reduces impact ionization to a two body Coulomb scattering problem for which the Rutherford formula is valid.

A further approximation Thomson made was to assume that the atomic electron was initially at rest. This leads to the following expression for the total electron impact ionization cross-section :

$$\sigma_{ion} = \frac{4}{E_I E_e} \left( 1 - \frac{E_I}{E_e} \right) \quad (2.1)$$

where  $E_I$  is the ionization energy and  $E_e$  is the energy of the incident electron. Figure 2.1 shows the inaccuracy of results calculated with (2.1) at all energies. At low and intermediate energies this arises from Thomson's assumption that the atomic electron is initially stationary (cf. the Born approximation, see section 2.3.1.1). At high incident electron energies it is due to the incorrect asymptotic energy dependence of (2.1). Bethe (1930) considered the asymptotic limit of the Born approximation in Coulomb scattering and obtained the following exact expression:

$$\lim_{E_e \rightarrow \infty} \sigma_{ion} \sim \frac{\ln E_e}{E_e} + \frac{1}{E_e} \quad (2.2)$$

Clearly Thomson's expression does not have this logarithmic form. Gryzinski (1959) sought to improve Thomson's theory by assuming a particular initial velocity for the atomic electron, isotropically distributed for a large number of atoms. The erroneous simplification in this analysis of replacing the relative velocity of the incident and atomic electrons by its average value  $\bar{v}$  was removed by Stabler (1964) who thus obtained for the ionization of atomic hydrogen

$$\sigma_{ion} = \begin{cases} \frac{8}{3\sqrt{E_I E_e}} \left[ \frac{(E_e - 1)^3}{E_A} \right]^{\frac{1}{2}} \pi a_0^2 & E_I \leq E_e \leq E_A + I \\ \frac{4}{E_I E_e} \left[ 1 + \frac{2E_A}{3E_I} - \frac{E_I}{(E_e - E_A)} \right] \pi a_0^2 & E_e \geq E_A + I \end{cases} \quad (2.3)$$

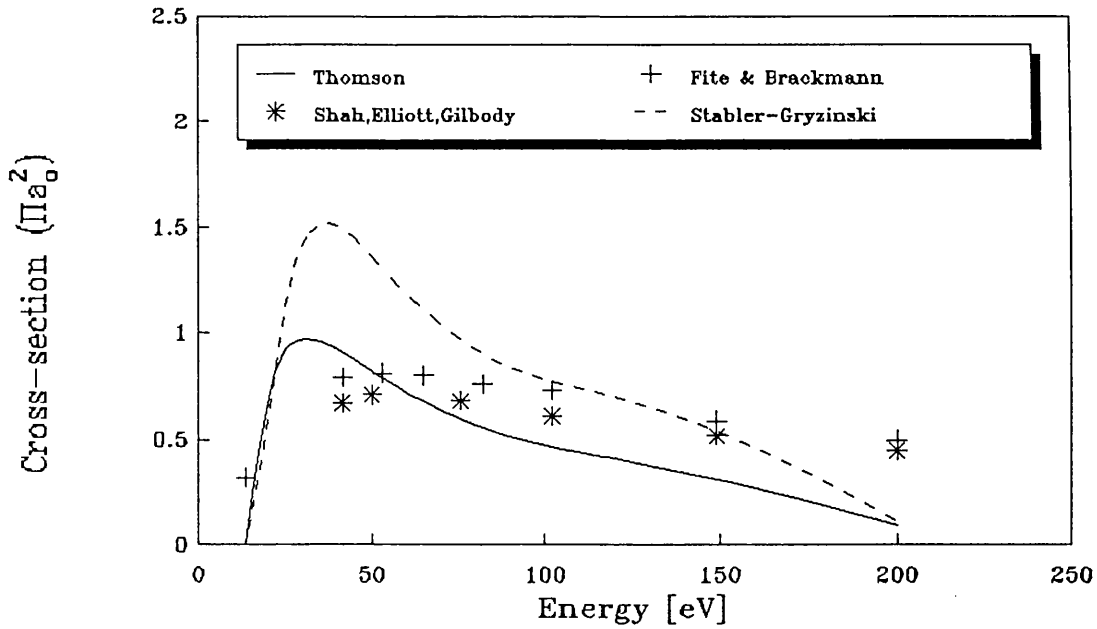


**Fig 2.1** Electron impact ionization cross-sections of atomic hydrogen calculated using the Binary Encounter Approximation.

Figure 2.1 shows clearly that this work is no improvement on Thomson's casting doubt on the accuracy of the assumed form of the atomic electron velocity distribution. Subsequently Gryzinski (1965) has achieved better agreement with experimental results by considering a semi-empirical distribution of the form

$$f(v) = \left(\frac{\bar{v}}{v}\right)^3 e^{-\frac{\bar{v}}{v}} \quad (2.4)$$

This gives the required asymptotic logarithmic dependence but with the incorrect coefficient for the logarithmic term. Kingston (1964) has further advanced this development of the binary encounter approximation by using the quantum distribution of velocities for electrons in atomic hydrogen derived by Fock (1935)

$$\frac{4\pi}{n^2} \sum_{l, m} |\phi_{nlm}(\mathbf{p})|^2 v^2 dv = \frac{32 v_n^5 v^2 dv}{\pi (v^2 + v_n^2)^4} \quad (2.5)$$

for the momentum wave functions with principal quantum number  $n$  and angular momentum quantum numbers  $l$  and  $m$ . The atomic velocity,  $v_n$  is

$$v_n = \frac{e^2}{n\hbar} \quad (2.6)$$

Even with this exact formulation for the velocity distribution the binary encounter approximation still lacks sufficient precision due to its very two-body nature. This limitation prompted Abrines and Percival (1966a) to discard this approximation and integrate the classical equations of motion exactly. They showed (concurrently with Mapleton, 1966) that a distribution of velocities with an identical form to (2.5) could be derived from the classical microcanonical distribution (Landau and Lifshitz, 1958) for a system of particles each with total energy  $-E_0$  in the phase space defined by the position vector  $\mathbf{r}$  and momentum vector  $\mathbf{p}$  which is expressed

$$\rho(\mathbf{r}, \mathbf{p}) = \delta(H + E_0) \quad (2.7)$$

where  $H$  is the classical Hamiltonian which can be written for a particle in the Coulomb field of a charge  $Z$  as

$$H = \frac{1}{2} \frac{p^2}{m} - \frac{Z}{r} \quad (2.8)$$

It was also shown that this distribution was uniform in the square of the angular momentum given by

$$l^2 = (\mathbf{r} \times \mathbf{p})^2 \quad (2.9)$$

between its limits of zero, which in classical mechanics corresponds to the harmonic motion of the atomic electron in a straight line, through elliptical orbits of decreasing eccentricity to its maximum value which gives a circular orbit. Random sampling over this distribution was used to obtain the initial position and momentum co-ordinates for the atomic electron.

From (2.8) the Hamiltonian for the three body system shown in Figure 2.2 can be written

$$H = \frac{1}{2} \left[ \frac{1}{m_A} + \frac{1}{m_B} \right] (p_1^2 + p_2^2 + p_3^2) + \frac{1}{2} \left[ \frac{1}{m_A} + \frac{1}{m_B + m_C} \right] (p_4^2 + p_5^2 + p_6^2) + \frac{Z_A Z_B}{R_{AB}} + \frac{Z_B Z_C}{R_{BC}} + \frac{Z_C Z_A}{R_{CA}} \quad (2.10)$$

where the subscripts (1,2,3) denote the Cartesian co-ordinates of projectile C with respect to B and (4,5,6) are the Cartesian co-ordinates of A with respect to the centre of mass of the atomic system (B,C). Following from (2.10) one can write Hamilton's equations for this system as

$$\begin{aligned} \frac{\partial \dot{q}_j}{\partial t} &= \left[ \frac{1}{m_B} + \frac{1}{m_C} \right] p_j \\ \frac{\partial \dot{q}_{j+3}}{\partial t} &= \left[ \frac{1}{m_A} + \frac{1}{m_B + m_C} \right] p_{j+3} \\ \frac{\partial p_j}{\partial t} &= \frac{Z_A Z_B}{R_{BC}^3} \frac{m_C}{m_B + m_C} \left[ \frac{m_C}{m_B + m_C} q_j + q_{j+3} \right] + \frac{Z_B Z_C}{R_{AB}^3} q_j \\ &\quad + \frac{Z_C Z_A}{R_{CA}^3} \frac{m_B}{m_B + m_C} \left[ \frac{m_B}{m_B + m_C} q_j - q_{j+3} \right] \\ \frac{\partial p_{j+3}}{\partial t} &= \frac{Z_A Z_B}{R_{AB}^3} \left[ \frac{m_C}{m_B + m_C} q_j + q_{j+3} \right] - \frac{Z_A Z_B}{R_{CA}^3} \left[ \frac{m_B}{m_B + m_C} q_j - q_{j+3} \right] \end{aligned} \quad (2.11)$$

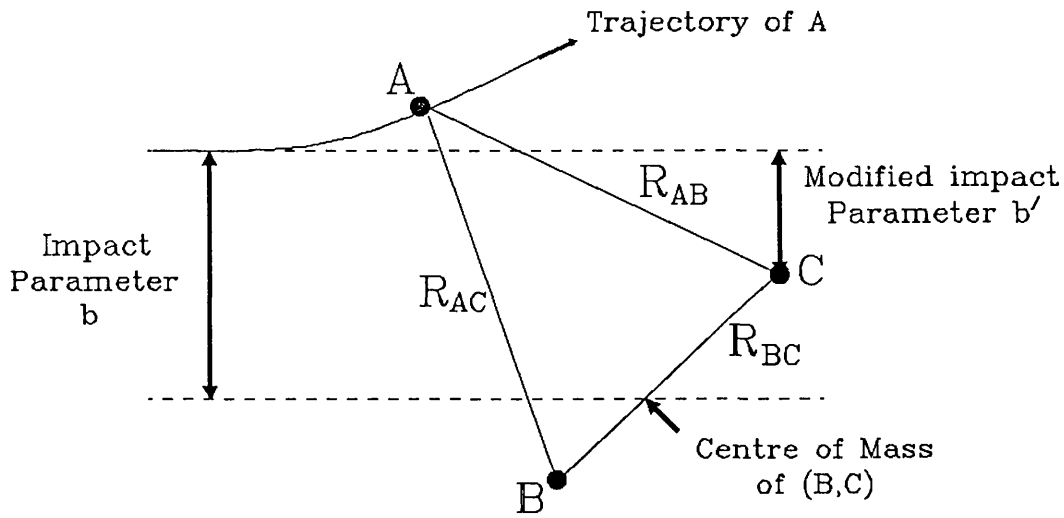


Fig 2.2 A diagram showing the notation that is employed in the discussion of classical calculations in the text.

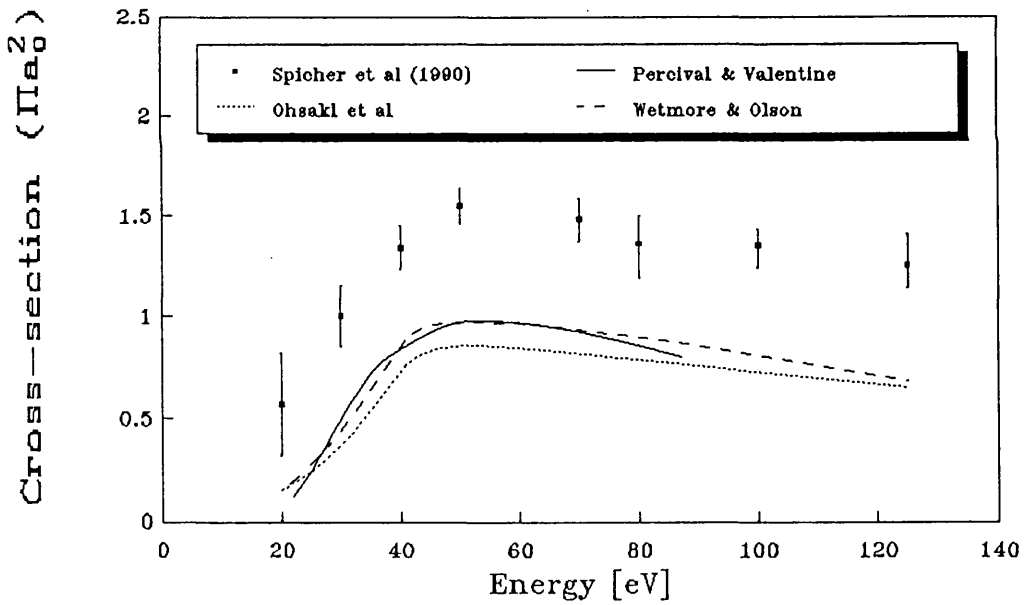


Fig 2.3 Positron impact ionization cross-sections of atomic hydrogen calculated using the Classical Trajectory Monte Carlo (CTMC) method.

In their method, Abrines and Percival solve these equations for proton impact ionization of atomic hydrogen for a random sample of the square of the modified impact parameter  $b'$  (shown in Figure 2.2) from a distribution uniform up to a limit  $b_{\max}$ . Beyond this limit the cross-section for the relevant process is negligible.

After collision the relative positions of the three particles reveal which of the possible reactions occurred: elastic scattering, ionization or charge exchange. For  $N$  collisions the cross-section for process  $x$  is given by

$$\sigma_x = \frac{N_x}{N} \pi b_{\max}^2 \quad (2.12)$$

where  $N_x$  is the number of collisions that involved process  $x$ .

The encouraging similarity of the results of these calculations to experimental data led Percival and Valentine (1967) to apply the same method to positron impact ionization yielding the results shown in Figure 2.3. Their disagreement with the measured cross-sections cannot be ascribed to the simplification of considering the modified impact parameter  $b'$  rather than the conventional impact parameter  $b$  shown in Figure 2.2. This simplification, intended to ease the calculation, essentially reduces the problem to a two-body collision and one would therefore expect it to be less accurate at low energies. Due to this, the same calculation repeated without simplification by Ohsaki *et al* (1985) and Wetmore and Olson (1986) gives results with slightly different energy dependencies below 50eV (see Figure 2.3). These later calculations agree to within reported statistical errors but differ considerably from experimental data.

It is interesting to note the reasonably good agreement of cross-sections calculated with this method for electron and proton impact ionization of atomic hydrogen (see

Rudge, 1968 and Abrines and Percival, 1966b), in contrast to the positron case. This can be explained by an inherent limitation of calculations in the classical domain. Classical mechanics can be considered to be the limit of quantum mechanics as  $\hbar \rightarrow 0$ . This removal of Heisenberg's uncertainty principle leads to a limit on the validity of classical mechanics which can be expressed for particles of momentum  $p$  being scattered through an angle  $\theta$  (from Bransden and Joachain, 1983, pp534)

$$\theta \geq \theta_c = \frac{\hbar}{p} \quad (2.13)$$

Below the critical angle  $\theta_c$ , the validity of a classical calculation is thus precluded.  $\theta_c$  will be small for relatively massive projectiles such as protons and one would expect classical mechanics to yield reasonably accurate results even at low energies - this is indeed observed to be the case for ionization of atomic hydrogen. For lighter particles though  $\theta_c$  is large enough for classical mechanics to fail to describe the motion of a significant number of scattered projectiles. This explains the inaccuracy of the calculated ionization cross-sections for both electrons and positrons below  $\sim 60\text{eV}$ . At higher energies the CTMC method suffers from predicting the incorrect asymptotic energy dependence as did the binary encounter approximation. This is by virtue of their being purely classical treatments which neglect long distance interactions between the three charged particles. The fact that the electron data exhibits good agreement with experimental results at high energies implies that this interaction may be quite weak in this case. This would not seem to be the case for protons and positrons.

### 2.3 Quantum Mechanical Calculations

As for all other scattering processes the total cross-section for ionization is evaluated

quantum mechanically by solving Schrödinger's equation

$$H\Psi(\mathbf{r}_1, \mathbf{r}_2) - E\Psi(\mathbf{r}_1, \mathbf{r}_2) \quad (2.14)$$

for the wave function  $\Psi(\mathbf{r}_1, \mathbf{r}_2)$  where H is the total Hamiltonian given by

$$H = -\frac{\hbar^2}{2m_1} \nabla_{\mathbf{r}_1}^2 - \frac{\hbar^2}{2m_2} \nabla_{\mathbf{r}_2}^2 - \frac{1}{r_1} - \frac{1}{r_2} - \frac{1}{|\mathbf{r}_1 - \mathbf{r}_2|} \quad (2.15)$$

with the notation of Figure 2.4, and the total energy E is

$$E = \frac{1}{2}k_i^2 - E_I + \frac{1}{2}k_f^2 + \frac{1}{2}k_e^2 \quad (2.16)$$

where  $k_i$ ,  $k_f$  and  $k_e$  are, respectively, the momenta of the projectile before collision and after collision and the momentum of the ionized electron as shown in Figure 2.4.

The total ionization cross-section is given by:

$$\sigma_{ion} = \int d\hat{k}_f d\hat{k}_e \frac{k_f}{k_e} |f_{ion}|^2 \quad (2.17)$$

where the ionization amplitude is

$$f_{ion} = (2\pi)^{-\frac{5}{2}} \langle \Psi(\mathbf{r}_1, \mathbf{r}_2) | H - E | \phi(\mathbf{r}_2) F(\mathbf{r}_1) \rangle \quad (2.18)$$

with  $\phi(\mathbf{r}_2)$  and  $F(\mathbf{r}_1)$  being the wave functions of the target atom and the incident particle respectively.

To reduce the complexity of quantum mechanical calculations approximations can be made for  $\Psi(\mathbf{r}_1, \mathbf{r}_2)$  and  $F(\mathbf{r}_1)$ . These will now be discussed in order of increasing

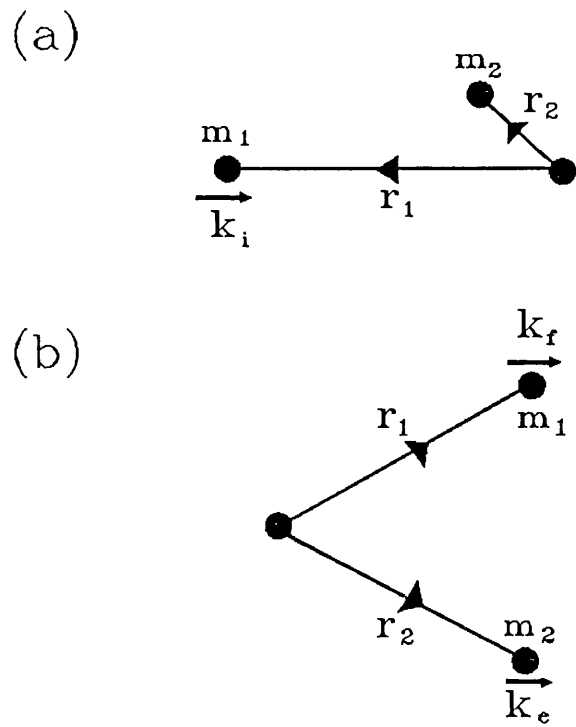


**Fig 2.4** The notation used in the present discussion of quantum mechanical systems for (a) the pre- and (b) post-collision systems.

refinement for both electron impact ionization which is the context in which they were first developed and positron impact ionization to which they can be applied with or without modification. The calculated cross-sections are then compared with the available experimental data to assess the accuracy of the calculation.

### 2.3.1 High Energy Approximations

#### 2.3.1.1 The Born Approximation

This is the simplest and therefore one of the most widely used approximations to the wave function  $\psi(\mathbf{r}_1, \mathbf{r}_2)$ . The approximation lies in expanding the wave function in powers of the interaction potential  $U(\mathbf{r})$ . Consider a solution of Schrödinger's equation, the Lippmann-Schwinger equation

$$\psi_{k_i}(\mathbf{r}) - \phi_{k_i}(\mathbf{r}) + \int G_0^{(+)}(\mathbf{r}, \mathbf{r}') U(\mathbf{r}') \psi_{k_i}(\mathbf{r}') d\mathbf{r}' \quad (2.19)$$

where  $G_0^{(+)}(\mathbf{r}, \mathbf{r}')$  is the outgoing Green's function, and  $\phi_{k_i}(\mathbf{r})$  is the incident plane wave.

If this is solved by iteration one obtains the sequence of functions

$$\begin{aligned} \psi_0(\mathbf{r}) - \phi_{k_i}(\mathbf{r}) \\ \psi_1(\mathbf{r}) - \phi_{k_i}(\mathbf{r}) + \int G_0^{(+)}(\mathbf{r}, \mathbf{r}') U(\mathbf{r}') \phi_{k_i}(\mathbf{r}') d\mathbf{r}' \\ \vdots \\ \psi_n(\mathbf{r}) - \phi_{k_i}(\mathbf{r}) + \int G_0^{(+)}(\mathbf{r}, \mathbf{r}') U(\mathbf{r}') \psi_{n-1}(\mathbf{r}') d\mathbf{r}' \end{aligned} \quad (2.20)$$

which can be substituted for  $\psi(\mathbf{r}_1, \mathbf{r}_2)$  in the integral expression for the scattering amplitude (2.18) to give the functions

$$\begin{aligned} f_{B1} - -2\pi^2 \langle \phi_{k_f} | U | \phi_{k_i} \rangle \\ f_{B2} - -2\pi^2 \langle \phi_{k_f} | U | \psi_1 \rangle \\ \vdots \\ \vdots \end{aligned} \quad (2.21)$$

which are truncations to one and two terms respectively of the Born series for the scattering amplitude. The simplicity of the first term,  $f_{B1}$  has led to its wide use as an expression for the scattering amplitude. This is the first Born approximation as originally derived by Born (1926). The limit of its validity can be assessed by considering the convergence of the Born series, this depends on the strength of the scattering potential  $U$  and the time  $a/v$  the incident particle of velocity  $v$  spends within the potential. Rapid convergence requires "weak" scattering i.e. the passage time of the particle must be much less than the time  $\hbar/U$  required for the potential to significantly influence the particle:

$$\frac{Ua}{\hbar v} \ll 1 \quad (2.22)$$

For electron or positron scattering off a screened Coulomb potential of atomic dimensions the Born approximation is therefore valid only for incident particles with a kinetic energy greater than  $\sim 500\text{eV}$ .

All the theoretical treatments of impact ionization which have employed the first Born approximation have considered electrons as the incident particle. From (2.18) it is clear that the Born scattering amplitude will have a different sign (when the sign of the potential is reversed) for positron impact ionization but the cross-section  $\sigma_{\text{ion}}$  given by (2.17) will be identical since it depends on the square of the amplitude. However, in an attempt to refine the Born approximation most authors who have used it in electron impact ionization have also included the possibility of exchange between the incident and atomic electrons in their calculations. The exact form of their expressions for the ionization amplitude must therefore be considered before their numerical results can be used for positron impact ionization.

Exchange effects in ionization were first considered in the derivation of the asymptotic forms of the wave function by Peterkop (1960) and Rudge and Seaton (1964). These are

$$\begin{aligned} \lim_{r_1 \rightarrow \infty} \psi(r_1, r_2) &\sim e^{ik_i \cdot r_1} \phi_0(r_2) + \frac{1}{r_1} \sum_a \phi_a(r_2) f_a(\hat{r}_1) e^{ik_a r_1} \\ &\quad + \frac{1}{r_1} \int \phi(k_f, r_2) e^{ik_f r_1} f(k_f, k_0) dk_f \\ \lim_{r_2 \rightarrow \infty} \psi(r_1, r_2) &\sim \frac{1}{r_2} \sum_a \phi_a(r_2) g_a(\hat{r}_2) e^{ik_a r_2} + \frac{1}{r_2} \int \phi(k_f, r_1) e^{ik_f r_2} g(k_f, k_0) dk_f \end{aligned} \quad (2.23)$$

These expressions allow for excitation to a bound state  $a$  of the atom as well as ionization into the continuum. The amplitudes  $f(\mathbf{k}_f, \mathbf{k}_e)$  and  $g(\mathbf{k}_f, \mathbf{k}_e)$  are known as the "direct" and "exchange" ionization amplitudes respectively and it has been shown by Peterkop (1961) that

$$f(\mathbf{k}_f, \mathbf{k}_e) = g(\mathbf{k}_e, \mathbf{k}_f) \quad (2.24)$$

The scattering amplitude from which the cross-section is calculated then reduces from

$$|f_{ion}|^2 = |f(\mathbf{k}_f, \mathbf{k}_e)|^2 + |g(\mathbf{k}_f, \mathbf{k}_e)|^2 + \text{Re}[f(\mathbf{k}_f, \mathbf{k}_e) g^*(\mathbf{k}_f, \mathbf{k}_e)] \quad (2.25)$$

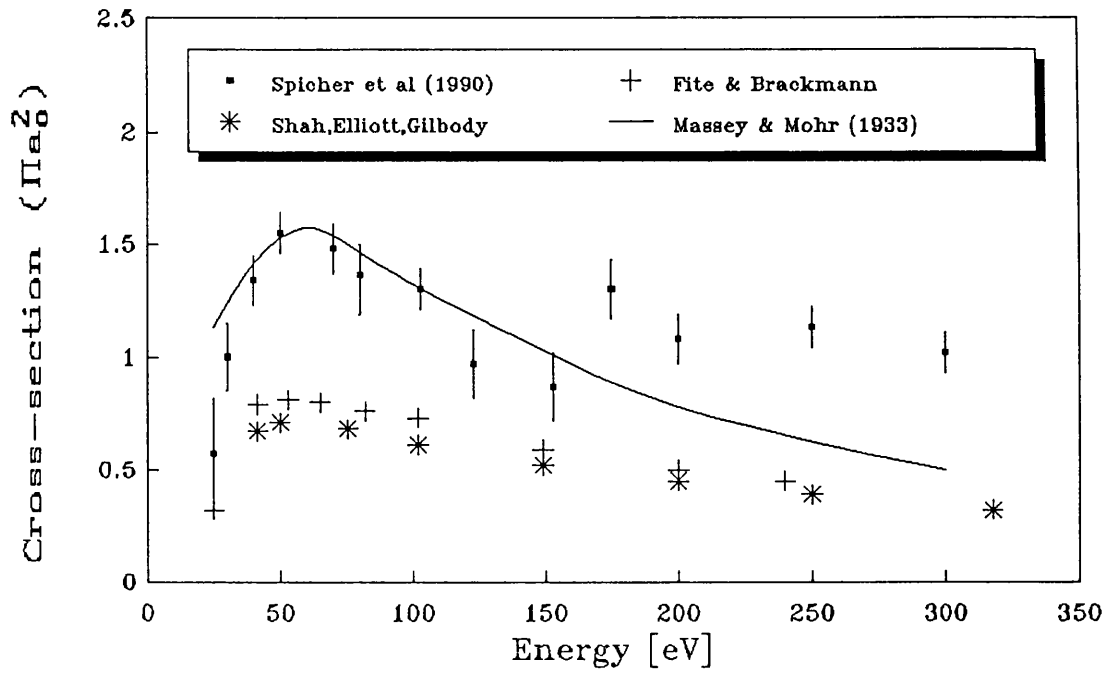
to

$$|f_{ion}|^2 = |f(\mathbf{k}_f, \mathbf{k}_e)|^2 + |f(\mathbf{k}_e, \mathbf{k}_f)|^2 + \text{Re}[f(\mathbf{k}_f, \mathbf{k}_e) f^*(\mathbf{k}_e, \mathbf{k}_f)] \quad (2.26)$$

The cross-section is obtained by integrating this over  $k_f$ ,  $k_e$  and  $k_f^2$ . To obtain results which can also be considered as positron impact ionization cross-sections one must neglect exchange i.e. the exchange amplitude and interference terms in (2.25). Rudge (1968) has pointed out that many authors only leave out the interference term in (2.25) and to correctly neglect exchange they must then only integrate to  $E/2$  as the first two terms in (2.25) are equal and the integral is symmetric with respect to substituting  $k_f^2$  for  $k_e^2$ . Thus, for a calculation to be suitable for the case of positrons being incident on a target it must neglect the interference term and integrate to  $E$  since there is no exchange amplitude when the projectile is distinguishable from the atomic electron. This discussion will therefore be restricted to calculations which have the following form for the ionization cross-section

$$\sigma_{ion} = \int_0^E \frac{k_e k_f}{\pi k_i^2} d(\frac{1}{2} k_e^2) \int |f(\mathbf{k}_f, \mathbf{k}_e)|^2 d\hat{\mathbf{k}}_f d\hat{\mathbf{k}}_e \quad (2.27)$$

(a)



(b)

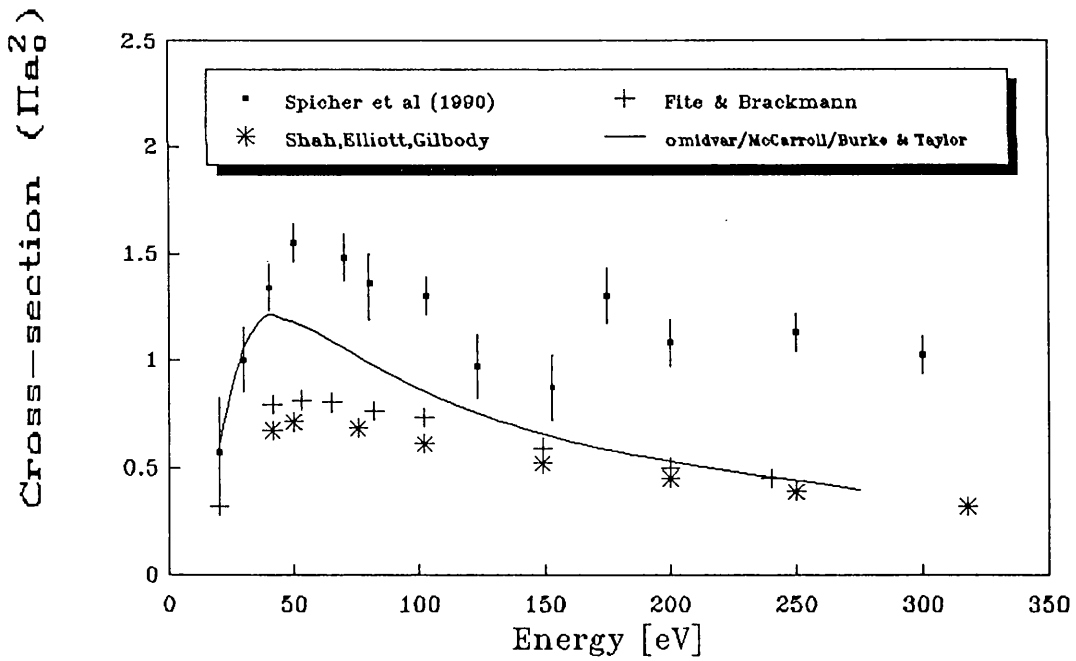


**Fig 2.5** Electron impact ionization cross-sections calculated using the first Born approximation which are suitable for consideration in positron scattering (see text).

The first attempt to calculate the electron impact ionization cross-section of atomic hydrogen using the first Born approximation was by Massey and Mohr (1933) who used the following form for the ionization amplitude

$$f_{ion} = \langle \phi_0 e^{i\mathbf{k}_i \cdot \mathbf{r}_1} | U | \phi_k e^{i\mathbf{k}_f \cdot \mathbf{r}_1} \rangle \quad (2.28)$$

where  $\phi_0$  is the target ground state wave function and  $\phi_k$  is an exact wave function for the electron in the Coulomb field of the  $H^+$  ion derived by Sommerfeld (1931). These authors then integrated (2.27) numerically to obtain the total ionization cross-section  $\sigma_{ion}$ . McCarroll (1957) and Omidvar (1965) have since repeated this calculation with greater accuracy. Burke and Taylor (1965) adopted a slightly different approach in that they took  $\phi_k$  in (2.28) to be a superposition of a Coulomb modified plane wave and an outgoing distorted spherical wave. They then considered a partial wave analysis of  $\phi_k$  and summed the contributions to the cross-section from different angular momenta to get the total cross-section. All these theoretical results are shown in Figure 2.5 (a) and (b) together with the measured electron impact ionization cross-sections of Fite and Brackmann (1958) and Shah *et al* (1987) and the measured positron impact ionization cross-section of Spicher *et al* (1990). It is clear that the most recent theoretical calculations based on the Born approximation are in agreement but are significantly different to the results of Massey and Mohr thus casting some doubt on the accuracy of this earlier work. Within the range of validity of the approximation - above 500eV - the later results are also in accordance with the experimental data for both electrons and positrons. At lower incident energies though, one can see that the positron data doesn't converge with the Born approximation until a much higher energy than the electron data: this may indicate that a stronger interaction exists in positron scattering than in the electron case.

### 2.3.2.2 The Glauber Approximation

This is based on a method of approximation developed in optics and first employed in quantum theory by Moliere (1947). It was extended to high energy scattering off

atoms by Glauber (1959). One can write for the Hamiltonian,  $H$  in Schrödinger's equation (2.14)

$$H = -\frac{1}{2}\nabla_1^2 + h(r_2) - \frac{1}{r_1} + \frac{1}{|\mathbf{r}_1 - \mathbf{r}_2|} \quad (2.29)$$

where

$$h(r_2) = -\frac{1}{2}\nabla_2^2 - \frac{1}{r_2} - W \quad (2.30)$$

is the two-body Coulomb Hamiltonian for energy  $W$ . Glauber then takes the following form for the solution

$$\psi = e^{ik_i z} \phi \quad (2.31)$$

where  $\phi$  is a function which varies slowly over a particle wavelength. Approximating to first order Schrödinger's equation then takes the form

$$ik_i \frac{\partial \phi}{\partial z} = (h + V) \phi \quad (2.32)$$

where

$$V = -\frac{1}{r_1} + \frac{1}{|\mathbf{r}_1 - \mathbf{r}_2|} \quad (2.33)$$

A further approximation is to disregard  $h$  which represents the energy of the ejected electron in ionizing collisions i.e. it is assumed that these electrons have very little kinetic energy. The solution of (2.32) is then

$$\phi(z) = \exp\left(-\frac{i}{k_i} \int_{-\infty}^z V(z') dz'\right) \quad (2.34)$$

and  $\psi(\mathbf{r}_1, \mathbf{r}_2)$  is now given by

$$\psi(\mathbf{r}_1, \mathbf{r}_2) = \phi(\mathbf{r}_2) e^{ik_1 z_1} e^{-\frac{i}{k_1} \int_{-\infty}^{z_1} V(\mathbf{r}_2, \mathbf{b} + \hat{k}_1 z') dz'} \quad (2.35)$$

where the following substitution has been made

$$\mathbf{r}_1 = \mathbf{b} + \hat{k}_1 z_1 \quad (2.36)$$

with  $\mathbf{b}$  being the impact parameter. From the integral expression (2.18) one obtains for the Glauber scattering amplitude after McGuire *et al* (1973)

$$f_G = \frac{ik_1}{2\pi} \int d^2\mathbf{b} e^{i\mathbf{q} \cdot \mathbf{b}} \langle \chi(\mathbf{r}_2) | (1 - e^{-\frac{i}{k_0} \int_{-\infty}^{\infty} V(\mathbf{r}_1, \mathbf{r}_2) dz} | \phi_0(\mathbf{r}_2) \rangle \quad (2.37)$$

where  $\mathbf{q} = \mathbf{k}_i - \mathbf{k}_f$  is the momentum transfer,  $\phi_0(\mathbf{r}_2)$  is the ground state hydrogenic wave function and  $\chi(\mathbf{r}_2)$  is the radial Coulomb wave function for an electron in the field of the  $H^+$  ion which satisfies

$$\left[ \frac{d^2}{dr_2^2} - \frac{l(l+1)}{r_2^2} + k_e^2 - \frac{2m_e m_p}{\hbar^2 (m_e + m_p)} \frac{e^2}{r_2} \right] \chi(\mathbf{r}_2) = 0 \quad (2.38)$$

The ionization cross-section is then calculated from (2.17)

To satisfy the approximations made in this method two conditions must be met. The energy of the incident particle must greatly exceed the magnitude of the scattering potential to justify the neglect of  $h(\mathbf{r}_2)$ . Also the particle wavelength must be smaller than the range  $a$  of the potential in order to approximate to first order in (2.32) (Glauber, 1959). These conditions can also be written:

$$\frac{V}{E} \ll 1 \quad ka \gg 1 \quad (2.39)$$

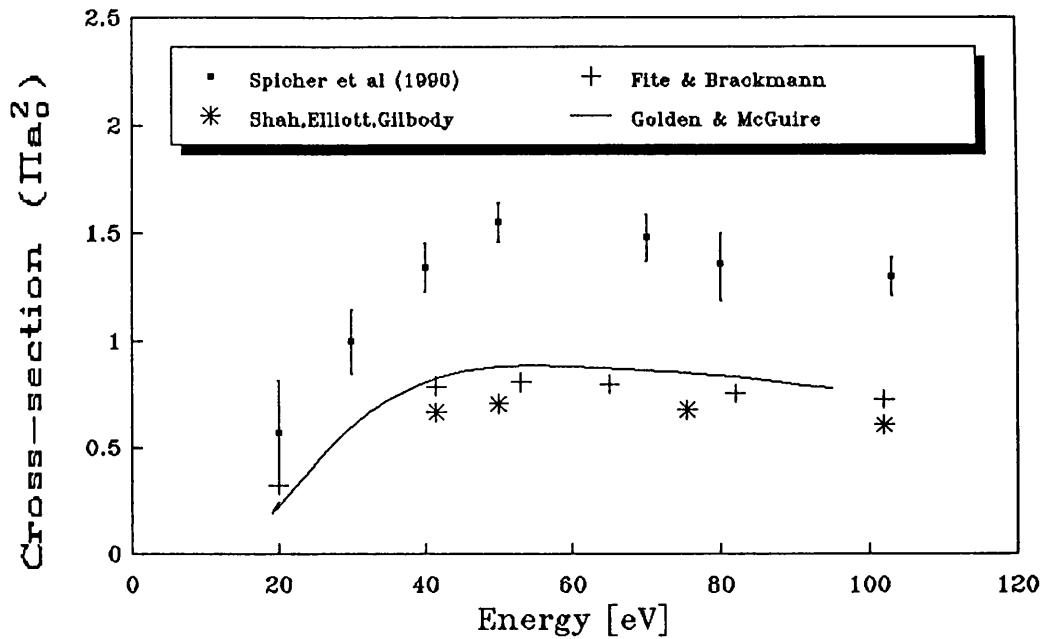


**Fig 2.6** The electron impact ionization cross-section of atomic hydrogen calculated using the Glauber approximation but allowing for the possibility of exchange.

For electron or positron scattering off a screened Coulomb potential of atomic dimensions these require that the kinetic energy of the incident particle be above about 30eV.

Golden and McGuire (1974) have calculated the electron impact ionization cross-section using a Glauber amplitude in which they expand  $\chi(\mathbf{r}_2)$  in partial waves to facilitate the analytic derivation of an expression for the ionization amplitude. Again, given the potential dependence of  $f_G$ , the calculated cross-section is equally applicable for positron or electron impact ionization.

Plotted in Figure 2.6 are the Glauber-Exchange results of Golden and McGuire in which electron exchange is included by considering an ionization amplitude of the

form (2.25) in which both  $f(\mathbf{k}_p, \mathbf{k}_e)$  and  $g(\mathbf{k}_p, \mathbf{k}_e)$  are calculated by the Glauber method. The experimentally determined cross-sections of Fite and Brackmann (1958) and Shah *et al* (1987) for electrons and of Spicher *et al* (1990) for positrons have been shown for comparison. It is clear from the diagram that the Glauber-Exchange calculation gives reasonable agreement with the experimental electron data in the energy range over which the approximation is valid. However, the basic Glauber results, excluding exchange, differ considerably from the positron data, being smaller at all energies. This discrepancy could well be explained by the assumption that the ejected electron has little relative momentum compared to the ion being erroneous. If this were the case the electron would completely screen the bare ionic nucleus from the positron and would not interact with the positron either. Recent theoretical work (Campeanu, 1990 - see section 2.3.2) indicates that this is not correct and thus casts doubt on the suitability of the Glauber approximation for calculations on positron impact ionization of atomic hydrogen.

### 2.3.2 Distorted Wave Calculations

It is apparent from the preceding discussion that there are serious deficiencies in the high energy approximations at the incident energies where the total ionization cross-section shows most structure (below  $\sim 150\text{eV}$ ). Thus in order to simulate the collision dynamics accurately more complex models for the potential in which the particles move have been tested. In this section these calculations will be reviewed with occasional reference to systems other than  $e^+ - \text{H}$  if it aids the elucidation of the underlying principles.

Since, after ionization, the scattered positron and the ionized electron will be moving in the Coulomb field of the remaining proton one can represent the final state wave function  $\Psi(\mathbf{r}_1, \mathbf{r}_2)$  as a product of two Coulomb waves each associated with one of the

outgoing particles:

$$\Psi(\mathbf{r}_1, \mathbf{r}_2) = \chi_{k_e}(Z, \mathbf{r}_2) \chi_{k_f}(Z, \mathbf{r}_1) \quad (2.40)$$

where the Coulomb waves satisfy equations of the form

$$\left[ \nabla^2 + k^2 - \frac{\beta}{r} \right] \chi(\mathbf{r}) = 0 \quad (2.41)$$

where

$$\beta = \frac{2\mu Ze^2}{\hbar} \quad (2.42)$$

with Z being the nuclear charge of the ion. The ionization amplitude used in (2.17) is then, from (2.18)

$$f_{ion} = (2\pi)^{-\frac{5}{2}} \left\langle \chi_{k_f}(Z, \mathbf{r}_1) \chi_{k_e}(Z, \mathbf{r}_2) \left| \frac{1}{|\mathbf{r}_2 - \mathbf{r}_1|} \right| \Phi_0(\mathbf{r}_2) F(\mathbf{r}_1) \right\rangle \quad (2.43)$$

where the wave function for the incident positron  $F(\mathbf{r}_1)$  has a radial part which satisfies a one-dimensional form of Schrödinger's equation (2.14)

$$\left[ \frac{d^2}{dr_1^2} + k_i^2 - \frac{l(l+1)}{r_1^2} - V(r_1) \right] u_l(k_i, r) = 0 \quad (2.44)$$

where  $V(r_1)$  is the target potential.

It can be seen from equations (2.40) (2.41) and (2.44) that neglecting the interaction potential (i.e putting  $Z=0$ ) reduces to the first Born approximation (FBA, see section 2.2.1). Ghosh *et al* (1985) repeated the work of Geltman and Hidalgo (1974) in considering a simple modification of this but for incident positrons rather than electrons. This involved making  $Z=1$  in the expression for  $\chi_k$  thus representing the scattered positron moving in the full Coulomb field of the ion. It is referred to in the literature as the double Coulomb approximation (DCA). Ghosh and co-workers then improved on these simple approximations by allowing for polarization of the

target atom by the incoming positron the possible importance of which was pointed out by Mott and Massey (1965). This, the polarized orbital method of Temkin and Lamkin (1961) involved making the following substitution for  $V(\mathbf{r}_1)$  in (2.44)

$$V(\mathbf{r}_1) = V_S + V_{POL} \quad (2.45)$$

where  $V_S$  is the repulsive static potential and  $V_{pol}$  is the polarization potential derived by Temkin and Lamkin (1961) using the dipole approximation

$$V_{POL} = \frac{2}{r_1} - \frac{2}{|\mathbf{r}_1 - \mathbf{r}_2|} \approx \frac{2r_2}{r_1^2} \mathbf{r}_1 \cdot \mathbf{r}_2 \quad (2.46)$$

In this way polarization is treated as a perturbation to the static potential. The subsequent approximations are DW1 which is equivalent to FBA but with the alternative form for  $V(\mathbf{r}_1)$ , similarly DW2 corresponds to DCA. After partial wave analysis of  $f_{ion}$  the total ionization cross-section is then calculated from (2.17). As a check on their method Ghosh *et al* (1985) compared their FBA results to those of Burke and Taylor (1965) and found them in agreement to within 1%.

Figure 2.7 shows the cross-sections calculated with each of the models of Ghosh *et al* (1985) and, for comparison, the experimental data of Spicher *et al* (1990). Significant differences exist between the theoretical and experimental data at all energies. Inaccuracies will certainly arise in models FBA and DW1 since it is assumed that the ionized electron always screens the positron from the ionic Coulomb potential, regardless of which outgoing particle is furthest from the ion - they are clearly unphysical when  $k_e^2 > k_f^2$ . Conversely, in DCA and DW2 it is assumed that neither particle is ever even partially screened from the ionic charge. It does not appear that inclusion of polarization in the incident channel has a great effect on the calculated cross-section suggesting that this is not as significant a consideration in the  $e^+ - H$  system as the deficiencies in the approximations. An attempt to refine these approximations in positron impact ionization of helium, to

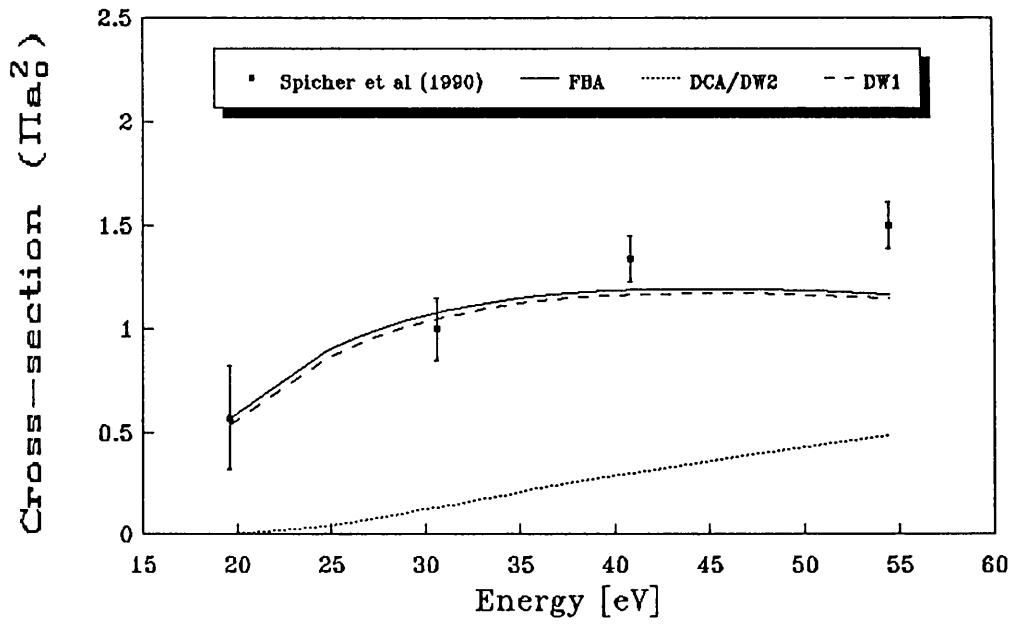


Fig 2.7 The positron impact ionization cross-section calculated using the indicated models (see text) by Ghosh *et al* (1985).

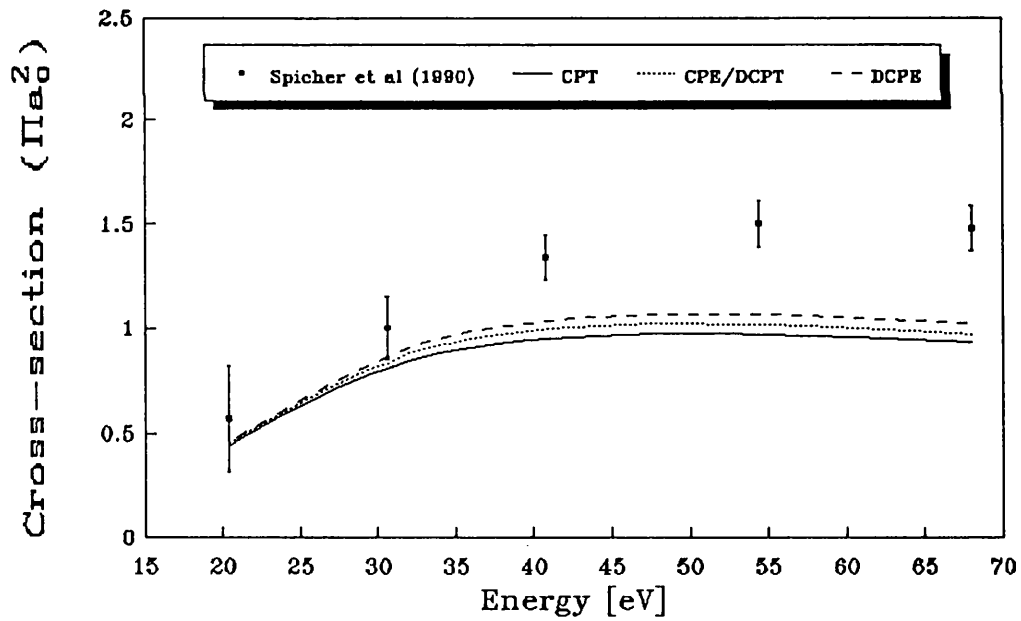


Fig 2.8 The positron impact ionization cross-section of atomic hydrogen calculated using different models (for details see text) by Mukherjee *et al* (1989).

which they had also been applied (Basu *et al*, 1985) was made by Campeanu *et al* (1987). Their models CPA and CCA correspond to DW1 and DW2 of Ghosh *et al* (1985) apart from the following form for  $V_{pol}$  in (2.45) (Schrader, 1979)

$$V_{POL} = \begin{cases} \frac{-\alpha}{2r_0^4} & r_1 \leq r_0 \\ \frac{-\alpha}{2r_1^4} & r_1 > r_0 \end{cases} \quad (2.47)$$

where  $\alpha$  is the dipole polarizability of helium and  $r_0$  is a cut-off parameter ( $r_0 = 1.774a_0$  was assumed, after Schrader, 1979). To prevent the occurrence of the unphysical situation discussed earlier, the CPT model limits the integration in (2.43) to  $k_e^2 \leq k_f^2$  but is otherwise equivalent to CPA. The CPE model integrates fully over  $dk_e$  but, in the region  $k_e^2 \geq k_f^2$ , considers the ejected electron to be moving in the "double" Coulomb potential of the ion together with the positron, which is in the unscreened ionic field. For He these latter two models provided excellent agreement with the experimental data of Fromme *et al* (1986) - see section 1.5.1 for experimental details.

Mukherjee *et al* (1989) extended this work to positron impact ionization of atomic hydrogen but based their CPT and CPE models on the DW1 model of Ghosh *et al* (1985) rather than the CPA model of Campeanu *et al* i.e. they took the Temkin-Lamkin form (2.46) for the dipole polarization potential. They also consider the effects of the distortion due to dipole polarization on the final state wave functions: the DCPT model differs only from CPT in that the scattered positron wave function  $\chi_{kf}$  is calculated using the potential  $V(r_1)$  from (2.46) and DCPE differs from CPE in using the potential (2.46) to calculate the wave function of the ionized electron  $\chi_{ke}$  in the momentum range  $k_e^2 < k_f^2$ . In DCPT the scattered positron is considered to be moving in the polarized potential of the hydrogen atom, this is a reasonable assumption for high  $k_f$  since the proton-electron separation,  $r_2$  will then be small compared to the positron distance,  $r_1$  and the potential of the proton and electron

will be similar to that of polarized atomic hydrogen. The DCPE model has the ionized electron, for  $k_c^2 < k_f^2$ , moving in the polarized atomic potential.

For each model Mukherjee *et al* then solved the differential equations for the wave functions in (2.43) and then, for up to 12 partial wave components in the initial state, and 5 in the final state, integrated  $f_{ion}$  over the energy ranges specified above to get the cross-section. The results for each model are plotted in Figure 2.8 together with the experimental data of Spicher *et al* (1990). All models again display marked differences with the measured cross-section. It is clear that the inclusion of polarization effects in the final state is relatively unimportant when one considers the magnitude of the discrepancy between experimental and theoretical data. It also appears from comparison of Figures 2.7 and 2.8 that this representation of charge screening effects in the final state is not sufficient to account for the discrepancy since the simpler models of Ghosh *et al* (1985) yield results that are actually closer to the observed ones than do the more physical models of Mukherjee *et al* (1989).

Campeanu (1990) attempts to further refine the DCPE model of Mukherjee *et al* by taking for the polarization potential  $V_{POL}$  in (2.45) the full expansion of the Coulomb form in (2.46) in inverse powers of  $r_1$ , the positron-proton separation. This is given by Dalgarno and Lynn (1958) as

$$V_{POL} = -\frac{2}{r_1} \sum_{n=1}^{\infty} \left( \frac{r_2}{r_1} \right)^n P_n(\cos \theta_{12}) \quad (2.48)$$

when  $r_2 < r_1$ . Also considered in this work is the DCPE model of Mukherjee *et al* using Schrader's form (equations (2.47) with  $r_0 = 2.399a_0$ ) of  $V_{POL}$ . The results of both these models are very similar to those of Mukherjee *et al* with the Temkin-Lamkin form of  $V_{POL}$  (2.46), as can be seen from Figure 2.9. It is clear, therefore, that neither polarization of the atomic orbital in the initial state nor a similar effect on the unbound proton-electron system in the final state has a profound influence on the dynamics of positron impact ionization of atomic hydrogen, and accordingly

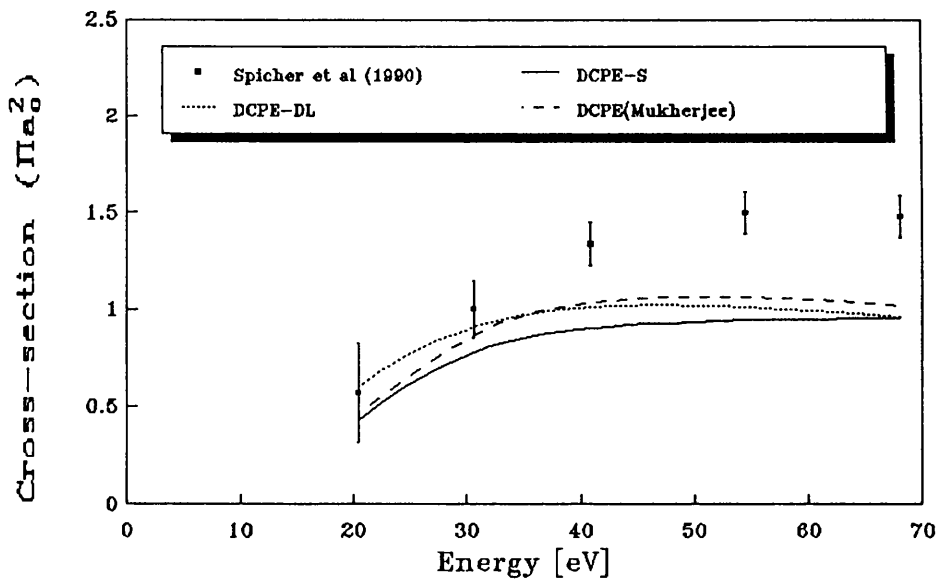


**Fig 2.9** The results of distorted wave calculations of the positron impact ionization cross-section of atomic hydrogen using different forms of the polarization potential  $V_{POL}$ , see text for details.

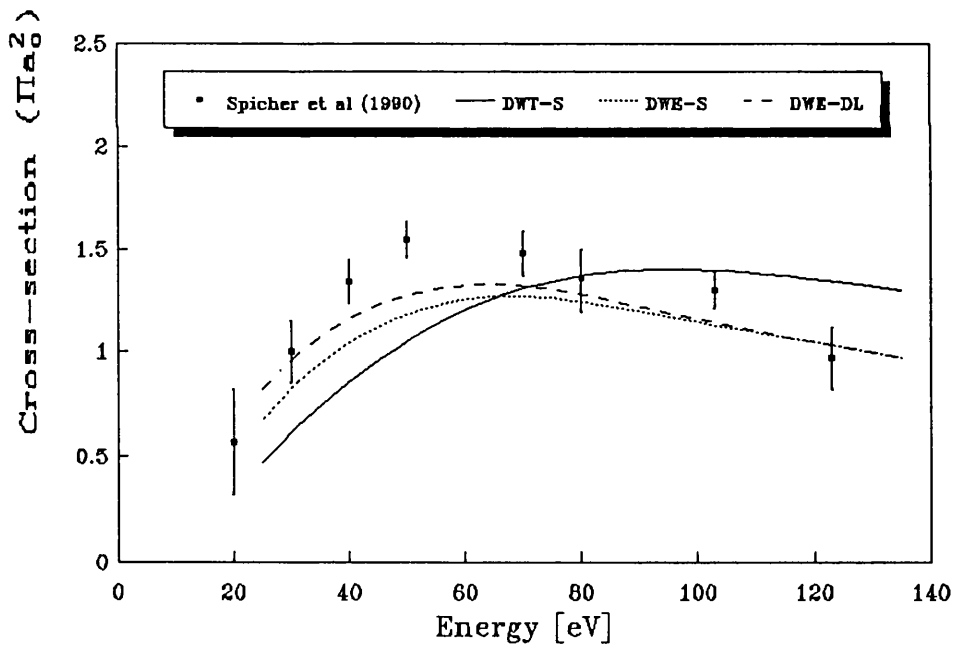


**Fig 2.10** The positron impact ionization cross-section of atomic hydrogen calculated using different models incorporating final state correlation by Campeanu (1990).

does not affect the value of the total ionization cross-section significantly.

Following similar work by Rudge and Seaton (1965) who consider the interaction between the two final state electrons in electron impact ionization of atomic hydrogen, Campeanu has attempted to include the effects of correlation between the scattered positron and ionized electron in the DCPE model. An indication of the possible importance of this effect can be seen in the results of Rudge and Seaton. Using a simple plane incident wave reasonable agreement with experimental data at low energies is obtained by inclusion of final state correlation. They consider each outgoing electron to be in the Coulomb potential of an effective charge given by

$$Z_j = 1 - \frac{k_j}{|\mathbf{k}_f - \mathbf{k}_e|} \quad j = e, f \quad (2.49)$$

This accounts for the partial screening of the ionic charge by the slower of the outgoing particles and the Coulomb interaction between the particles. Ghosh *et al* (1984) used a similar model to calculate the triple differential cross-section for positron impact ionization of atomic hydrogen and obtained results qualitatively different from their FBA and DCA models (see above). This prompted Campeanu (1990) to incorporate correlation effects into the much more refined DCPE model by calculating both final state wave Coulomb wave functions,  $\chi_{ke}$  and  $\chi_{kf}$  using ionic charges given by (2.49) for all energies of the ejected electron. The ionization amplitude  $f_{\text{ion}}$  is calculated from (2.43) as prescribed by this model for both the Schrader (2.47) and Dalgarno-Lynn (2.48) forms of the polarization potential. The cross-sections obtained after partial wave decomposition and subsequent integration of  $f_{\text{ion}}$  in (2.17) are shown in Figure 2.10 together with the experimental results of Spicher *et al* (1990). These theoretical results show reasonable agreement with experimental data - a marked improvement on other models which signifies the strength of the correlation between the scattered positron and the ionized electron.

It appears, therefore, that the DCPE model using the Dalgarno-Lynn polarization

potential (2.48) and allowing for a final state interaction between the outgoing particles via expression (2.49) provides a more complete representation of positron impact ionization of atomic hydrogen than has been achieved previously.

## 2.4 Summary

The development of a mathematical model which can accurately predict observables such as the impact ionization cross-section yields valuable information about the dynamics of the system in question. From the attempts to form such a model for positron impact ionization of atomic hydrogen one can reach several conclusions about the nature of the interaction:

- Long-range polarization of the atomic orbital by the incident positron and the analogous final state case for the unbound electron and proton is insignificant compared to the three body Coulomb interaction.
- The attractive nature of the positron-electron interaction leads to a correlation between the particles for a long distance beyond the collision region.

To ensure that the collision dynamics in positron impact ionization of atomic hydrogen are fully understood it is therefore important to measure the total ionization cross-section accurately. The completeness of our understanding of this problem can then be determined.

## CHAPTER 3

# THE DETERMINATION OF THE TOTAL POSITRON IMPACT IONIZATION CROSS-SECTION OF ATOMIC HYDROGEN-EXPERIMENT

### 3.1 General Layout and Principles of Operation

The total ionization cross-section of positrons incident on hydrogen atoms is to be measured here in a crossed-beam experiment of the type described earlier (see section 1.5.2). A magnetically transported mono-energetic positron beam crosses a highly dissociated jet of hydrogen gas effusing from a radio-frequency powered atomic hydrogen source normally to the axis of symmetry of the diverging atomic beam.

On the detection of a positron after its traversal of the scattering region an electric field perpendicular to the axes of both the positron beam and the atomic source is applied momentarily across this region. It serves to extract positive ions created on positron impact ionization thus enabling their detection. The time of flight of ions to the detector in this applied field identifies ions of different charge-to-mass ratios.

Three separate pieces of experimental apparatus-the positron beam, the atomic hydrogen source and the ion extraction system-have therefore been interfaced to facilitate the measurement of the total positron impact ionization cross-section of atomic hydrogen. Each of these will now be discussed in detail as will the procedures utilized for the collection and analysis of experimental data.

### 3.2 Slow Positron Production and Transport

As discussed earlier (section 1.3) slow positrons are obtained by moderating the

energies of fast  $\beta^+$  particles emitted in the decay of certain radio-nuclides. In this experiment a  $^{22}\text{Na}$   $\beta^+$ -source supplied by Amersham International was used. Its activity at the time the experiment was performed was  $800\mu\text{Ci}$ . It takes the form of a 4mm diameter deposit of  $^{22}\text{Na}$  on a platinum disc 4mm thick with a diameter of 18mm sealed with a  $10\mu\text{m}$  titanium window. A central M2 threaded hole in the platinum disc enabled it to be mounted onto a brass plug externally threaded with a diameter of 20mm. This plug is then to be screwed into a cylindrical PTFE block (as shown in Figure 3.1) which is mounted via two threaded stainless steel rods onto a 70mm diameter stainless steel flange. A PTFE washer with an internal diameter of 10mm isolates the source from two brass washers of similar dimensions between which the moderator is held, these again are held in place by the two threaded rods. The moderator consists of four superimposed 15mm square annealed pieces of 60% transmission W mesh - the number, determined empirically by Zafar (1990), which gives the optimum slow positron yield. The annealing procedure involves heating the pieces of mesh resistively in a W foil oven in a vacuum of  $\sim 5 \times 10^{-2}$  Torr. Heating is done in bursts of approximately 5 seconds so as to avoid evaporating any contaminants present on the electrode assembly. This also ensures that the pressure does not increase above  $10^{-1}$  Torr so there is no possibility of electrical breakdown occurring. Annealing is deemed to be complete when a temperature of  $2000^\circ\text{C}$  can be reached without a significant pressure increase occurring. The brass washers holding the moderator are isolated by a PTFE washer from another pair of brass washers which hold another 60% transmission W mesh. Earthing this mesh and holding the moderator at a positive potential  $V_{\text{mod}}$  relative to it leads to the extraction of slow positrons with kinetic energy  $E$  given by

$$E = eV_{\text{mod}} + \Delta E \quad (3.1)$$

where  $\Delta E$  is the energy with which a positron leaves the moderator.  $\Delta E$  can have any value between zero and the positron work function  $\Phi_+$  and is dependent on the extent of inelastic processes the positron undergoes at the surface of the moderator. The energy spread of the positron beam is thus determined by  $\Phi_+$  which for clean W is approximately 2.8eV (Jacobsen *et al*, 1990). To maximize the yield of slow positrons the source and brass plug are biased to a slightly more positive potential than the

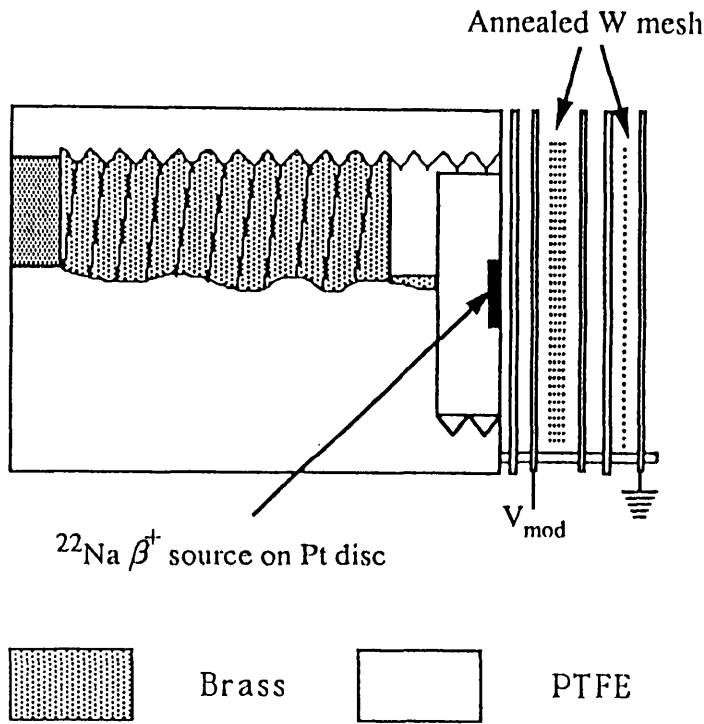


Fig 3.1 A cut-away diagram of the source/moderator holder showing the brass plug on which the source is held and the W moderator meshes.

moderator - this will cause backscattered positrons to return through the moderator. The source-moderator assembly is bolted onto a 125mm long stainless steel tube of internal diameter 37mm which is bolted via a 114mm adaptor flange onto a 300mm long stainless steel tube of internal diameter 50mm. The small dimensions of the vacuum system where the source and moderator are housed allows for the adequate Pb shielding of annihilation  $\gamma$ -rays from this region.

Beam guidance is by means of an axial magnetic field. This is produced by a series of Helmholtz coils of mean diameter 26.5cm which ensure the uniformity of the field as shown in Figure 3.2, and is 40Gauss at the source-moderator end increasing to 50 Gauss along the beam-line. The field increase after the moderator reduces the transverse spatial spread of the beam. Another consequence of using a mesh moderator is that many fast  $\beta^+$  particles will be transmitted or will be scattered off the mesh

wires into the beam. These and their associated annihilation  $\gamma$ -rays must be separated from the slow positrons hence the use of the stainless steel and Pb plugs shown in Figure 3.2. The diversion of slow positrons of the required energy through the aperture in the Pb is achieved with parallel electrostatic plates situated 0.7m from the source. Such plates provide an electric field perpendicular to the axial magnetic field and the resulting force on a charged particle between them will deflect the particle a distance proportional to the magnitude of its component of velocity parallel to the magnetic field. In this way a mono-energetic slow positron beam is obtained. Planar  $E \times B$  plates have been widely used for this purpose (e.g. Mills, 1980) but, following Hutchins *et al* (1986) who demonstrated the distortion in beam cross-section that occurs on deflection with planar plates, part-cylindrical plates have been employed in this experiment. These plates, 0.3m long with radii 58mm and 83mm, are held at approximately numerically equal positive and negative potentials respectively. This ensures that the positron beam moves in a region of zero potential and thus acquires no additional kinetic energy during its traversal of the plates. The  $E \times B$  plates and subsequent Pb plug are both placed axially in a 500m long brass tube of internal diameter 95mm. It was anticipated that the extensive aperturing of the beam discussed above would impede the flow of gas along the beam line during pumping from atmospheric pressure so an Edwards E02 oil vapour diffusion pump coupled to an Edwards ED35 rotary pump was situated approximately halfway along the beam-line. This was attached to a stainless steel four-way of internal diameter 50mm and length 203mm along the beam axis which was placed between the stainless steel and brass tubes mentioned above.

The axes of the beam, the atomic hydrogen source and the ion extraction system intersect 1.35m from the end of the source-moderator assembly. To locate the beam centrally on this point of intersection and to limit its width an 8mm aperture is placed 30mm before this, the centre of the scattering region. Initial beam alignment is made with another, removable, 8mm aperture situated a similar distance after this point. It is placed in the beam axis by moving the linear manipulator on which it is mounted in and out. As this aperture might restrict the maximum angle at which particles can scatter and still be detected it is removed before commencing an experimental

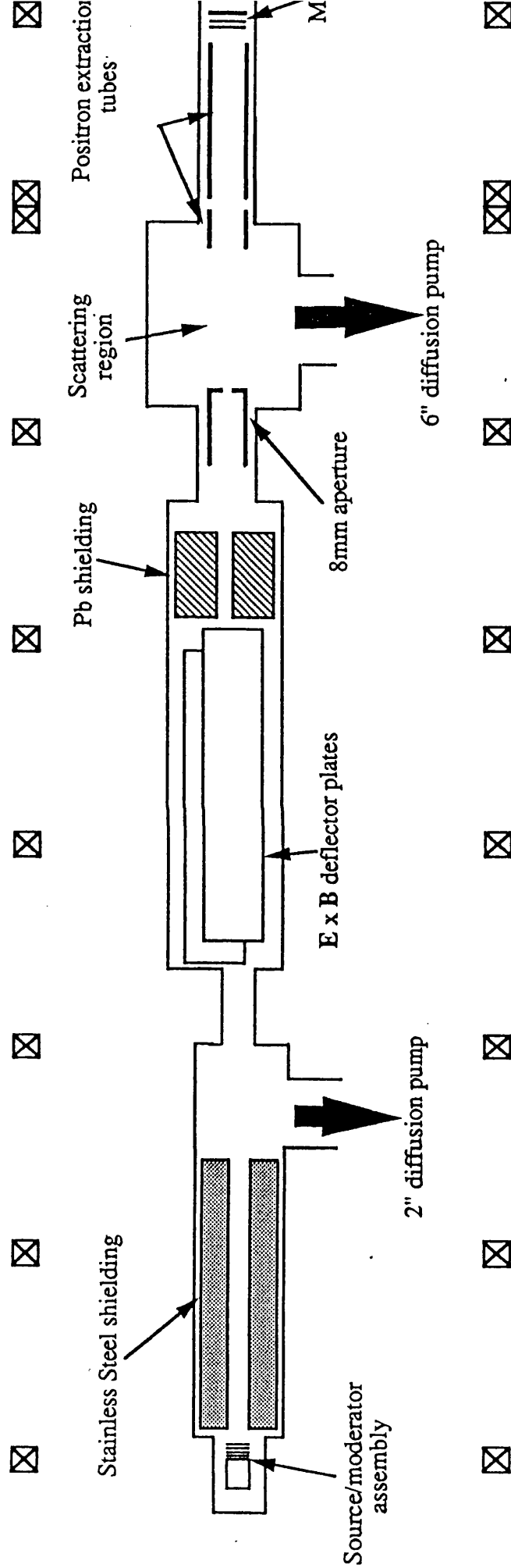


Fig 3.2 A schematic diagram of the evacuated positron beam system

measurement. The chamber in which the interaction takes place is a 152mm cubic Al block machined to an internal diameter of 127mm. Its dimensions preclude placing the coils adjacent to it at the required Helmholtz separation. However, the consequent weakening of the magnetic field is avoided by placing two coils immediately after the chamber - this ensures that the field is uniform throughout the scattering region with the resulting retention in the beam of positrons scattered through angles of up to  $2\pi$  at certain incident energies. This is demonstrated in a plot of the calculated acceptance angle as a function of positron energy shown in Figure 3.3. For a given transverse momentum transfer on collision this is defined as the maximum angle a particle can scatter at and still move in a path with a helical radius small enough to allow it to impinge on the detector. Details of the method by which it is calculated are given in section 5.3.1. The maximum radius for the helical paths of positrons was taken to be 4mm, the distance between the edge of the region of overlap of beam and gas and an ion extraction plate (see section 3.4). Obviously not all positrons will scatter from this part of the interaction region so the acceptance angle plotted in Figure 3.3 is an underestimate for most scattered positrons.

With no gas input through the atomic hydrogen source a pressure of  $<5 \times 10^{-6}$  Torr is maintained in the scattering region with an Edwards E06 oil vapour diffusion pump, coupled to an Edwards ED500 rotary pump, attached to the base of the scattering chamber. This pressure is measured with a Vacuum Generators IGC11 naked Bayard-Alpert ionization gauge-if this measures a pressure higher than  $\sim 10^{-5}$  Torr all detector potential supplies are switched off automatically to protect the detectors. The pressures in the backing lines of both diffusion pumps are monitored with Pirani pressure gauges and if either exceeds approximately 0.1 Torr the diffusion pumps are shut off and magnetic valves on the backing lines close to prevent oil backstreaming into the system.

Positron detection is by means of two Varian VUW8920ZS microchannel plates which

provide a signal through the multiplication of secondary electrons liberated by positron impact and collected on an earthed Cu screen - these are shown schematically in Figure 3.4. They are 50mm discs of 0.42mm thickness made of Pb glass and consisting of an array of 9.8 $\mu$ m diameter cylindrical channels coated internally with a semiconducting material capable of high secondary electron emission. To ensure that an incident positron does strike the inner surface of a channel the channels are inclined at 40° to the normal to the plate surface. The reported gain of one such plate with a potential difference of 1kV across it to accelerate the secondary electrons is  $\sim 4 \times 10^4$ . The potentials applied to the plates are shown in Figure 3.4, -2.2kV is applied to the front so that all positrons, including those which have lost energy, are detected with the same efficiency. With this configuration  $\sim 10$ mV pulses were obtained, the gain being maximized by orienting the plates at 180° to each other so that positive ions created at the rear plate output do not reach the front plate - the so-called chevron arrangement. The plates are situated 0.45m from the centre of the scattering region in a ceramic washer of internal diameter 50mm and thickness 3mm. They are held in place between two stainless steel washers of internal diameter 44mm by three leaf springs attached to one washer which rest on the outer non-detecting part of the front plate. This arrangement also provides noise-free electrical contacts to the back and front of the plates. Contact between the plates is by means of a thin insulating ceramic washer whose internal edge lies just outside the circumference of the plates' active area coated on either side with Cu up to a diameter of 50mm. Separate potentials can then be applied to the back surface of the front plate and the front surface of the back plate, in this experiment they are equal. This configuration allows the strip current through each plate to be monitored individually and swift remedial action to be taken if either exceeds  $\sim 25\mu$ A. Positron detection efficiency is increased by their acceleration by the two 90% transmission Cu meshes shown in Figure 3.4. This entire assembly is held by three M3 threaded stainless steel rods on a 152mm diameter Al flange. The flange is mounted on an Al tube of internal diameter 95mm which is connected by an Al adaptor flange onto a stainless steel T-piece of internal diameter 60mm which is fixed via a brass connecting tube (internal diameter 75mm) to the scattering chamber.

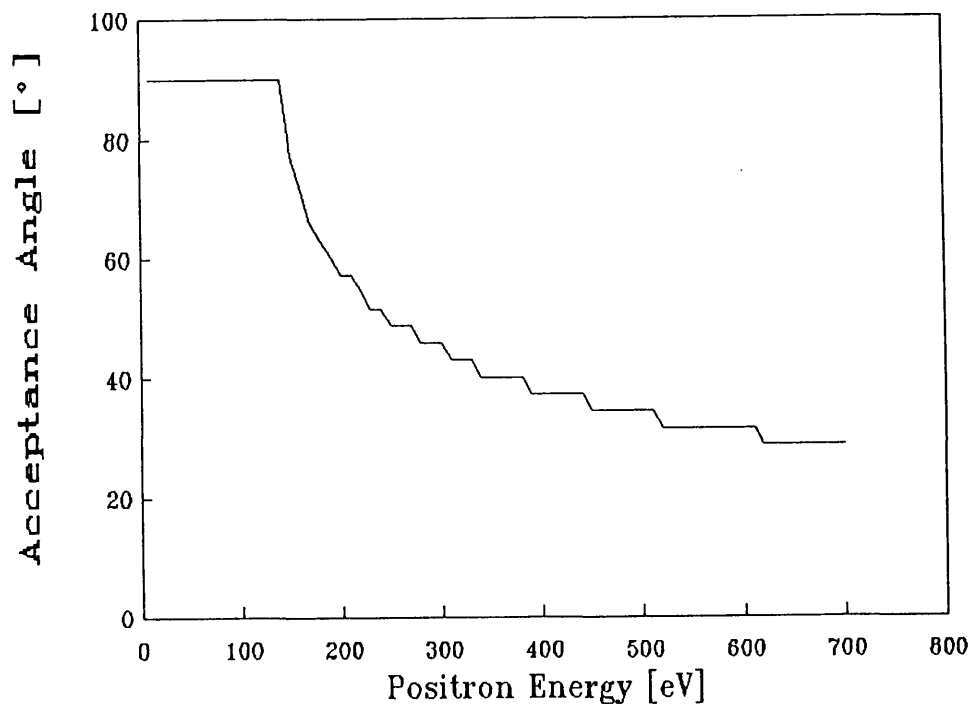


**Fig 3.3** The calculated acceptance angle at all positron energies in the 50 Gauss magnetic field.

The incorporation of electrically biased tubes in the beam line as shown in Figure 3.2 was as a result of measuring the positron impact ionization cross-section of molecular hydrogen ( $H_2$ ) to test for any sources of systematic error. The reasons for their use will be made clear in a detailed discussion of these measurements in Chapter 4.

### 3.3 The Atomic Hydrogen Source

Hydrogen atoms are obtained by dissociating  $H_2$  molecules in an R.F. discharge similar to one used by Slevin and Stirling (1981). Its design and operation are discussed in the relevant sub-section as are the supply and purification of molecular hydrogen.

#### 3.3.1 The Gas Handling System

To ensure the longevity and stability of the RF discharge the hydrogen gas must be of high purity and its rate of flow must be accurately controlled and monitored. These

conditions are best satisfied by having a hot palladium leak valve of the type described by Viennet *et al* (1973) between the gas cylinder and the vacuum system. It is well established that hydrogen can diffuse through a Pd-Ag lattice at a rate proportional to the temperature of the crystal (Wicke and Brodowsky, 1978). This occurs through the dissociative chemisorption of H<sub>2</sub> onto the Pd-Ag surface with subsequent migration through interstitial sites in the lattice. Since this process occurs exclusively with hydrogen and its isotopes any impurities present in the gas are removed at the gas-solid interface. In this experiment 99.95% pure molecular hydrogen at a pressure of  $\sim 5 \times 10^3$  Torr fills an 80mm long Pd-Ag tube of bore  $\sim 1$ mm closed at one end and joined at the other to a  $\frac{1}{4}$ " Pyrex-Kovar seal which is soldered to a 70mm stainless steel flange. This tube is resistively heated by passing a current of a few Amps to ground through it (Figure 3.5 (a)). The flange holding the Pd leak is mounted on a stainless steel four-way of internal diameter 37mm. Assuming that the temperature and pumping speed in this chamber remain constant then the rate of flow of H<sub>2</sub> from the Pd will be proportional to the pressure in the chamber. Figure 3.5 (b) shows the dependence of this pressure, measured with a Pirani gauge, on the current passing through the Pd-Ag tube.

Once in the vacuum system the purity of the gas is maintained by using only stainless

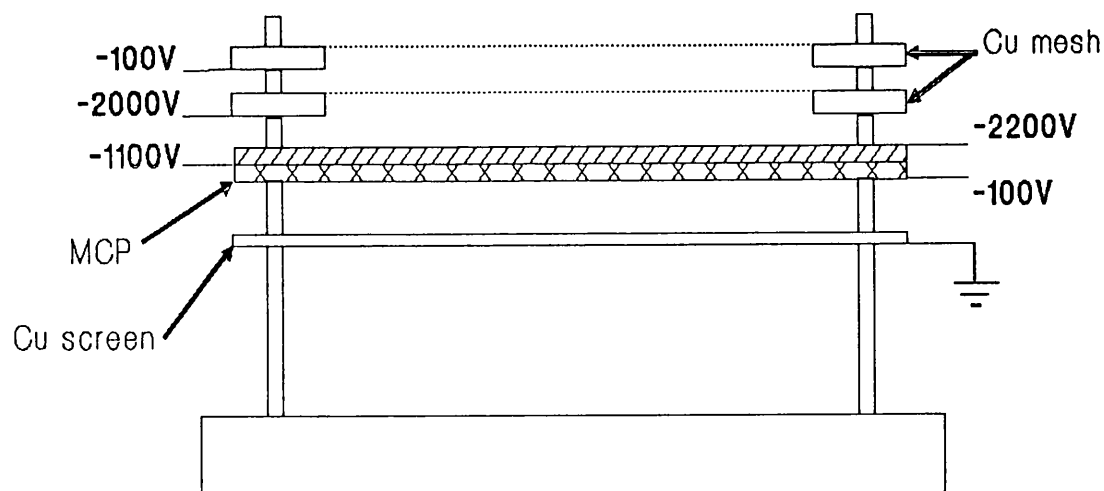
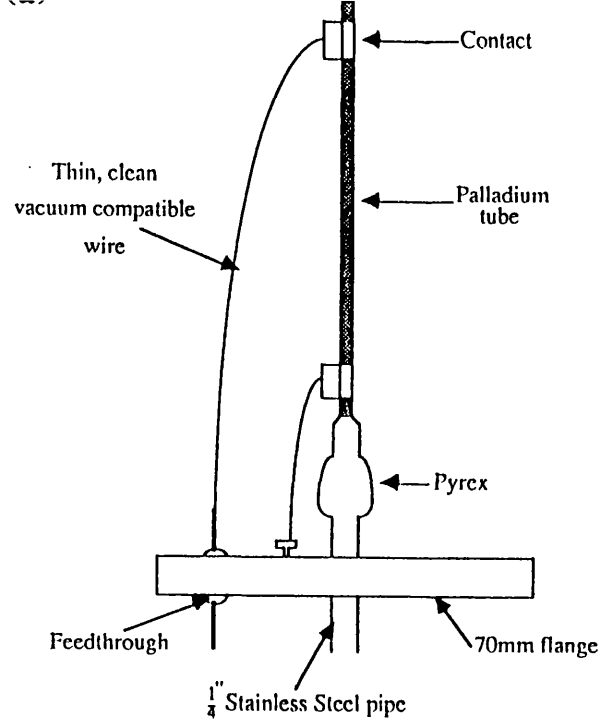
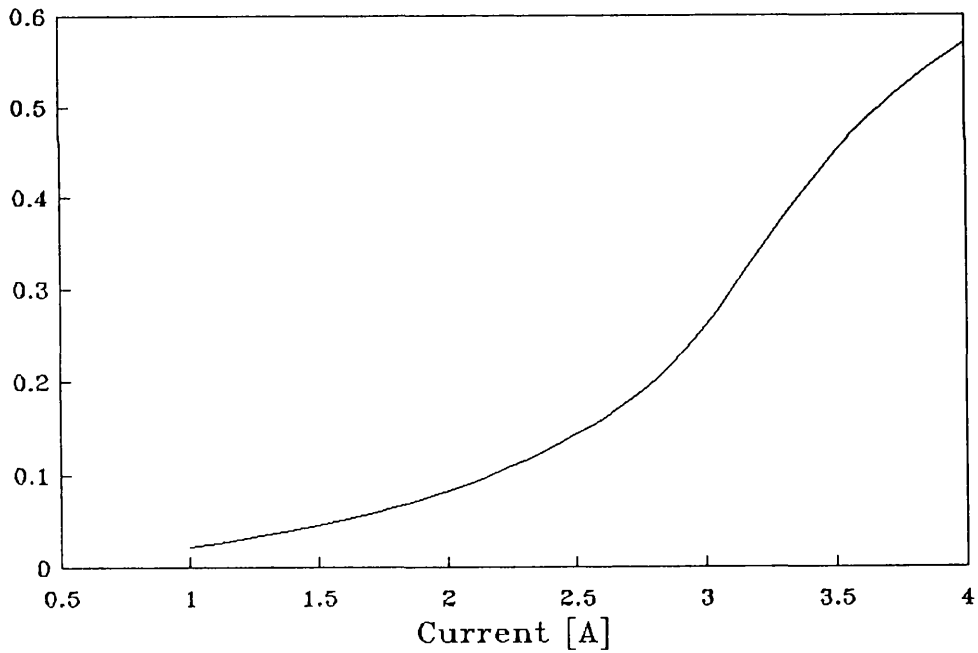


Fig 3.4 A schematic diagram of the microchannel plates used for positron detection in this experiment



(b)



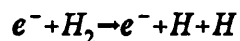
**Fig 3.5** (a) A schematic diagram of the Pd-Ag hydrogen gas leak valve.  
 (b) A graph showing the variation of hydrogen pressure in the gas handling system with current passing through the Pd-Ag leak valve.

steel tubes and fittings whose inner surfaces are thoroughly cleaned with solvent and dried before installation. When letting the system up to atmospheric pressure the condensation on all surfaces of water and of hydrocarbons from the vacuum pumps must be minimized. This is done by filling the system to one atmosphere with dry N<sub>2</sub> through a ¼" tube soldered to another 70mm flange on the four-way and then through the discharge tube. Thus it is ensured that this part of the vacuum system is always at an equal or higher pressure than the remainder of the system and therefore no backstreaming of impurities into this section of the apparatus occurs.

The gas handling system employed here therefore permits the regulation and monitoring of hydrogen flow at a level of accuracy sufficient for the prolonged operation of a stable gas discharge. It is also important to take the above precautions in maintaining the purity of the gas to maximize the degree of molecular dissociation in the discharge.

### 3.3.2 The Radio-Frequency Discharge

Hydrogen atoms can be produced on the dissociation of H<sub>2</sub> molecules on electron collision i.e. by the reaction



In a gas discharge this process can occur often enough for statistically accurate experiments to be performed with the extracted atoms in a reasonably short time. For this reason gas discharges powered by either continuous (e.g. Wood, 1920 and Schwab *et al*, 1987) or alternating (e.g Ding *et al*, 1977 and Spicher *et al*, 1990) electric fields have been employed in many experimental studies of atomic species. When, as in this experiment, the atomic hydrogen source is to be interfaced with a conventional magnetic transport positron beam system it has to fulfill certain requirements in its stability and produced atom concentration because of the moderate intensity of the e<sup>+</sup> beam. This, and design considerations, prompted the use here of a radio-frequency hydrogen discharge tube of the type described by Slevin and Stirling (1981). There

follows a brief description of the relevant atomic interactions that occur in a gas plasma in an alternating field and a more detailed discussion on the discharge tube employed in this experiment.

An electron in a vacuum will, on average, gain no energy from a high frequency alternating field. Also the maximum kinetic energy an electron will have during on oscillation of the field will be, typically, of the order of meV; which is obviously insufficient for any inelastic atomic processes to occur if a gas is present. The presence of a gas will however perturb the motion of an electron through collisions with molecules. Such damping of its oscillatory motion allows an electron to absorb a mean power from the field eventually enabling it to make inelastic collisions with gas molecules. Initially the most important process will be ionization since this produces ion pairs and electron multiplication takes place. When this is occurring at a rate far in excess of the rate of removal of electrons through ionic recombination, attachment or diffusion the conductivity of the gas will increase sharply and a net current will flow through it-the gas is said to have broken down. For molecular hydrogen the threshold energy for ionization is 15.6 eV. After breakdown there is a sufficient number density of electrons in the gas for other collisional inelastic processes to take place at a significant rate, these include molecular dissociation. In hydrogen there are two mechanisms by which this can occur, one is excitation to the repulsive  $^3\Sigma_u^+$  triplet state which will result in immediate dissociation into two neutral H atoms-this requires an incident electron energy of 8.8 eV. The main process is excitation to the stable  $^3\Sigma_g^+$  triplet state requiring electrons to have 11.8 eV energy, this then radiatively decays to  $^3\Sigma_u^+$  which again immediately dissociates. A continuum of radiation from this transition has been observed in hydrogen discharges.

The discharge tube used in this experiment is shown in Figure 3.6 and is 225mm long with a 20mm inside diameter. At either end there are 20mm long capillaries of 3mm bore to confine the discharge. There is a "kink" in the exit capillary which ensures that there is no direct path for atoms, particles or light out of the discharge tube. This kink is inside the water-cooled jacket to reduce the likelihood of H atoms impinging on its walls recombining. The tube is made of Pyrex and is cooled by the flow of water

through an external jacket. Cooling is necessary for two reasons: it prevents the tube overheating and cracking when the discharge is on and, as demonstrated by Wood and Wise (1962), the recombination of gaseous H atoms with those chemisorbed on a Pyrex surface is increasingly inhibited as the temperature of the surface is reduced. For safety purposes the flow of cooling water is incorporated into the protection circuitry of the experiment. This is done with an Edwards FS1 Flowtrol - if the flow rate falls below a certain level a bellows mechanism operates a relay which trips the power supplied to everything bar the two rotary pumps. Gas supply to and water flow through the discharge tube assembly is by means of stainless steel bellows soldered to glass-metal seals on each of three capillaries on the gas input end of the tube. These are joined by Swagelok connectors to plastic tubes (for the water) and a stainless steel tube for the gas which are in turn connected to a 200mm diameter stainless steel flange. The bellows and plastic tubing lend a degree of flexibility to the discharge tube assembly which was thought advisable from both the standpoints of the fragility of the Pyrex tube and the need to locate it accurately axially. This location was done with two pairs of arc-shaped Al pieces, each pair being held off an Al ring concentric with the discharge tube. By resting these Al pieces against the tube one could adjust its axial alignment by changing their positions relative to the rings. The two pairs of Al pieces are oriented so that two-dimensional adjustment of the tube's position is possible. The support rings are attached by M3 threaded rods to an Al plate machined to an internal diameter just greater than that of the discharge tube. This plate is held by three 400mm long M8 threaded rods off the 200mm flange to which the input tubes of the discharge tube are connected. With the mounting system used here the quick installation and removal of the discharge tube as well as its accurate positional alignment is therefore made possible.

Many authors have shown the importance of the cleanliness of the inner surfaces of gas discharge tubes (e.g. Wood, 1922). Minimizing the impurities on a Pyrex surface will lessen the rate of molecular recombination on that surface (Watkin, 1985) as well as the rate of removal of gas atoms in reactions with desorbed contaminants. In this experiment the discharge tube was cleaned as follows:

- 1) 5 washes with propan-2-ol

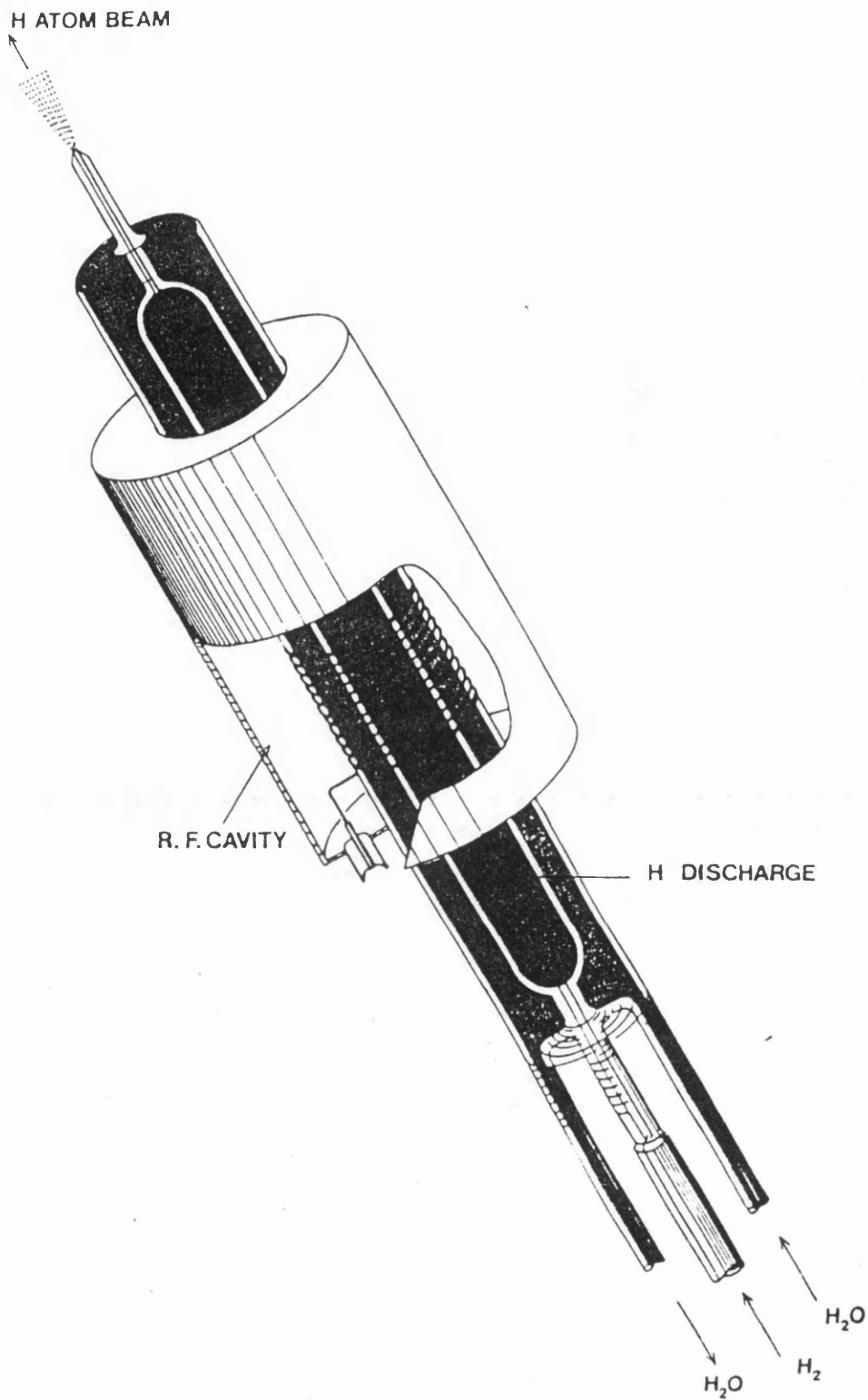


Fig 3.6 A schematic diagram of the radio-frequency discharge tube used in this experiment.

- 2) 10 washes with distilled water
- 3) 1 wash with 10% solution hydrofluoric acid (HF)-ensuring that it does not come into contact with the metal bellows
- 4) 10 washes with distilled water
- 5) 1 wash overnight with 20% solution ortho-phosphoric acid ( $H_3PO_4$ ) following the procedure of Donnelly (1991)
- 6) 10 washes with distilled water

The discharge tube was filled with solvent by mounting the tube vertically with the end of the exit nozzle in a trough containing the solvent and then drawing the solvent into the discharge tube with a Venturi pump attached to the gas input. After cleaning it was transferred as quickly as possible into the vacuum system, the precautions taken to maintain its cleanliness subsequently have been described in the previous section.

The entire assembly is held off one 200mm flange which is mounted on a stainless steel six-way cross of internal diameter 150mm, connected to this is a 165mm long stainless steel tube of the same internal diameter which is mounted on the scattering chamber via an adaptor flange. The end of the discharge tube is then ~5mm from the centre of the scattering region. Because of its proximity to the positron beam this end of the discharge tube has been coated with graphite and earthed to prevent possible charge-up by incident positrons.

The radio-frequency alternating electric field that is required to sustain the discharge is produced by an R.F. generator that is coupled to a cylindrical helical resonator of the type discussed by MacAlpine and Schildknecht (1959). The discharge tube passes axially through the resonator cavity (see Figure 3.7). The generator effectively consists of a heterodyne oscillator and a power amplifier. It produces a 35MHz output of up to 30W amplitude, variability of  $\pm 0.1$ MHz is provided for fine adjustment of the frequency. Its power output can be monitored directly with a meter as can the Voltage Standing Wave Ratio (VSWR) on the coaxial cable to the resonator. This is given by

$$VSWR = \frac{V_{for} + V_{ref}}{V_{for} - V_{ref}} \quad (3.2)$$

where  $V_{for}$  is the amplitude of the generator output and  $V_{ref}$  is the amplitude of the reflected wave. Reflection occurs as a result of an impedance mismatch with the resonator and  $V_{ref}$  will be dependent on the magnitude of this mismatch. The VSWR is therefore an indication of the power that is absorbed by the resonator and the gas plasma in the discharge tube which is a constituent part of it. Clearly the power input to the gas discharge must be maximized, this is achieved with a VSWR close to unity which is only attainable when reflection is minimized. Low reflection occurs when the resonator is tuned accurately to the output frequency of the oscillator. This resonator resembles an ordinary tuned circuit in that its operation can be described in terms of its distributed inductance, capacitance and resistance. As shown in Figure 3.7 it consists of a helical conductor (13 turns of 37mm diameter) inside a cylindrical OFHC Cu shield that is closed at both ends. The shield is 80mm in diameter and 100mm long, in each face there is a hole of a diameter just sufficient for the discharge tube to go through. It is held centrally in an Al cup of internal diameter 80mm by a PTFE locating ring, the cup being held on threaded rods screwed to the adaptor flange on the scattering chamber. McAlpine and Shildknecht demonstrated that the ratio of energy storage to energy dissipation, the Q-factor of the circuit, can be very high for such a compact system. The input power is coupled to the helical conductor by means of a tap coupling from a one-turn coil connected to a BNC connector mounted on the Cu shield. Rough frequency tuning can be done by adjusting the length of the helical conductor to minimize the reflected power input from a signal generator tuned to  $35 \pm 0.1$  MHz; more accurate tuning is done with the discharge tube in place by means of the trimming capacitor shown in Figure 3.7. A VSWR of  $\sim 1.7$  was achieved following this impedance matching process indicating that about 75% of the input power was being absorbed; this enabled the continuous running of the discharge with a generator power as low as 12W (for a gas pressure of 0.6 Torr in the gas handling system). Typical operational values for the power and pressure were 15W and 0.5 Torr respectively. Power transmission was by means of a  $50\Omega$  coaxial cable, the vacuum

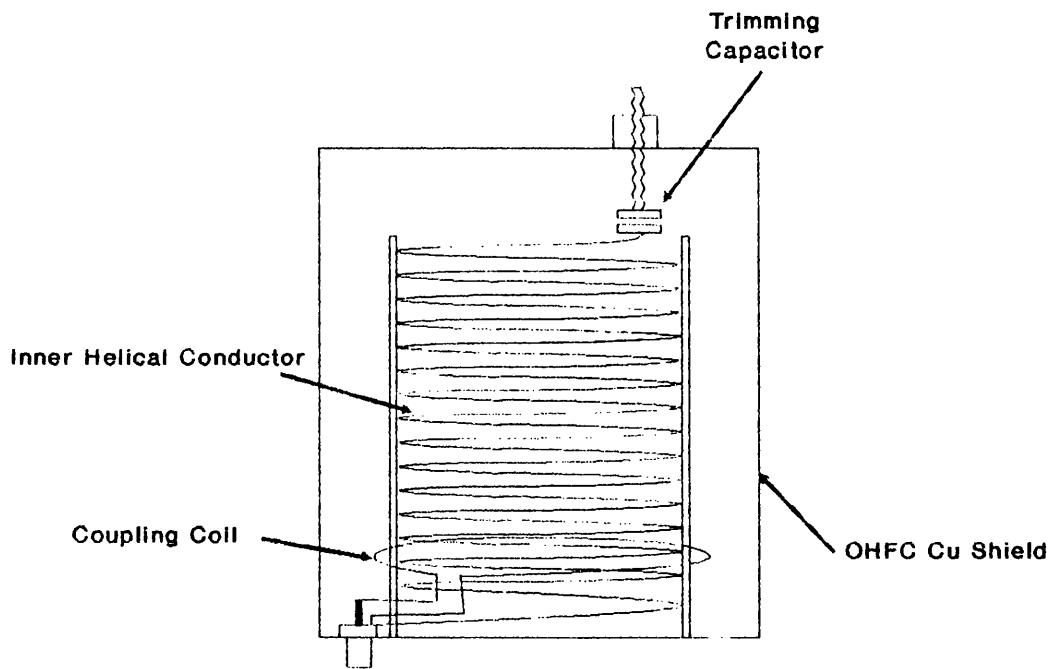


**Fig 3.7** A diagram of the resonator cavity cut away to show the helical inner conductor

feedthrough being a BNC bulkhead fitting sealed with a Viton O-ring.

### 3.4 The Ion Extraction System

Ions formed in the interaction region i.e. the region of overlap of the positron beam and the atomic jet are extracted and guided electrostatically to a detector; this extraction system is shown schematically in Figure 3.8. The system is similar to one used by Knudsen *et al* (1990) in that the electric field used to extract the ions is pulsed; this is to avoid any deflection or distortion of the beam by the potentials on the plates. In this way it differs from similar systems used for heavy particle ionization (Haugen *et al*, 1982 and Andersen *et al*, 1987) and previous positron ionization experiments (Charlton *et al*, 1989; Fromme *et al*, 1988 and Spicher *et al*, 1990). Positive and negative pulses of equal amplitude are supplied to two deflector plates either side of the scattering region by a pulser which is triggered by the shaped output pulse of the MCP at the end of the beam line. This ensures that detected ions will be in coincidence with a positron and thus enhances the probability that they were

were formed on positron impact. For reasons which will be made clear in the next chapter, ion extraction is augmented by a dc field applied between the plates, this being small in comparison to the beam energy. These 50mm square Al plates are 20mm apart with the point of intersection of the beam axes centrally between them. The pulses supplied to them have a rise time of 20ns for an amplitude of  $\pm 100\text{V}$ , their duration is then  $5\mu\text{s}$ . The delay between the MCP signal and the pulser output is  $\sim 175\text{ns}$ . It is important to minimize this delay since ions formed on positron impact will still have a velocity which will cause them to move out of the region of ion extraction-after dissociation a neutral H atom will have a kinetic energy of 2.2 eV, some of which it will lose in elastic collisions while exiting the discharge tube. In the period between the scattered positron leaving the interaction region and the onset of the full potentials on the extraction plates a  $\text{H}^+$  ion with the maximum possible kinetic energy of 2.2 eV will have moved  $\sim 3\text{mm}$  so, with an 8mm diameter hole in the negatively biased plate leading to the detector it is unlikely that any ions formed on positron impact will be lost in this manner. To maintain the uniformity of the field this hole is covered with 90% transmission W mesh.

After passing through the aperture in the deflection plate the ions drift through two 20mm internal diameter tubes, the first of length 40mm and the second 36mm. The first tube is held at a potential equal to that of the deflector plate (-100V) and the second is at -437V, this potential was selected for the purpose of focussing ions as they travel through the tube (after Harting and Read, 1976) so these tubes form a two element electrostatic lens. The focussing properties of this lens are further demonstrated by the computer simulation of ion trajectories shown in Figure 3.9, this was done using the SIMION PC/AT software package (Dahl and Delmore, 1987).

The ions are focussed into the cone of a Murata Ceratron detector; this is a ceramic single channel electron multiplier. Secondary electrons released on the impact of a charged particle on the inside of the entrance cone are accelerated by a potential difference down a tube, further secondary electrons are produced when they impinge

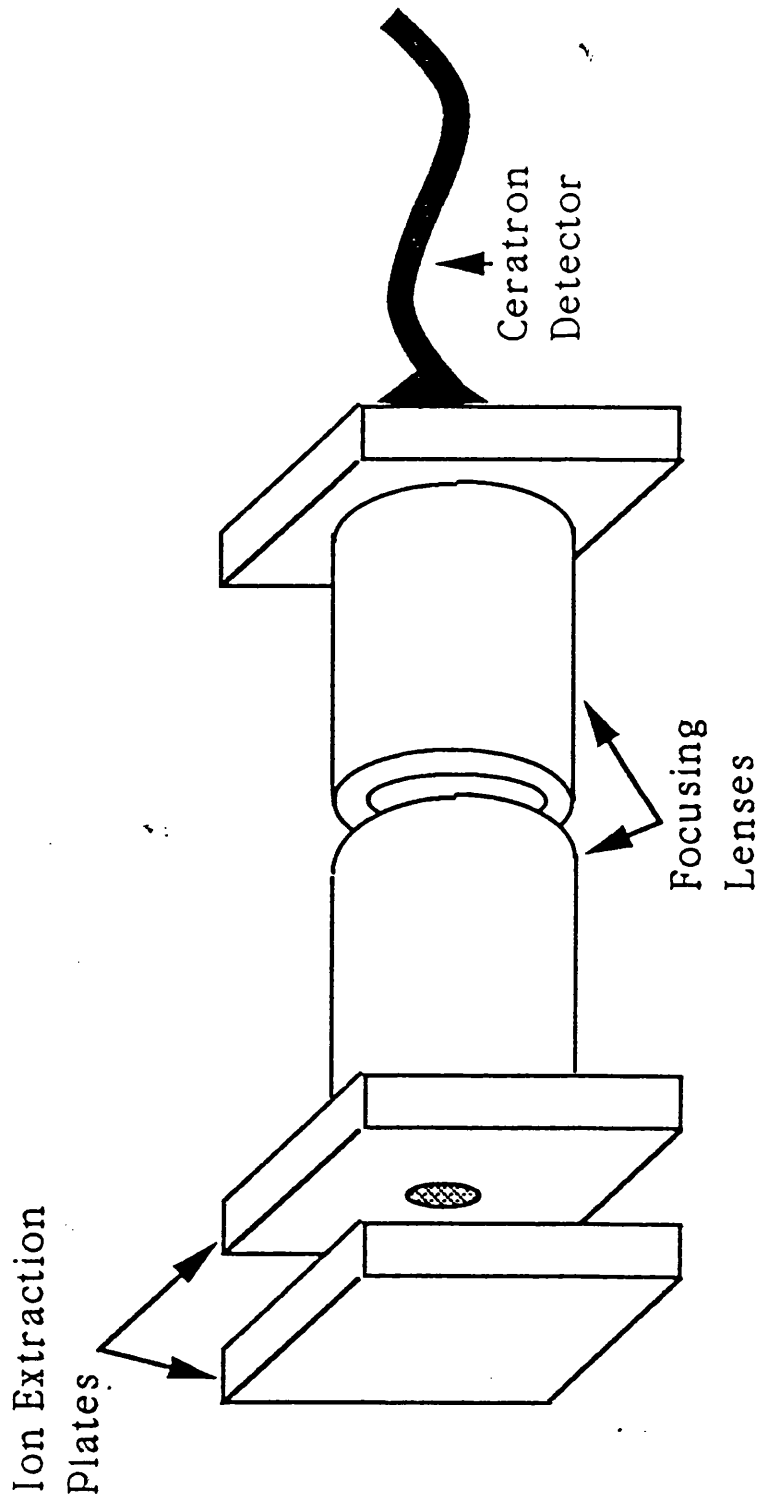


**Fig 3.8** A schematic diagram of the electrostatic ion extraction system, the nozzle of the RF discharge tube lies centrally between the ion extraction plates.

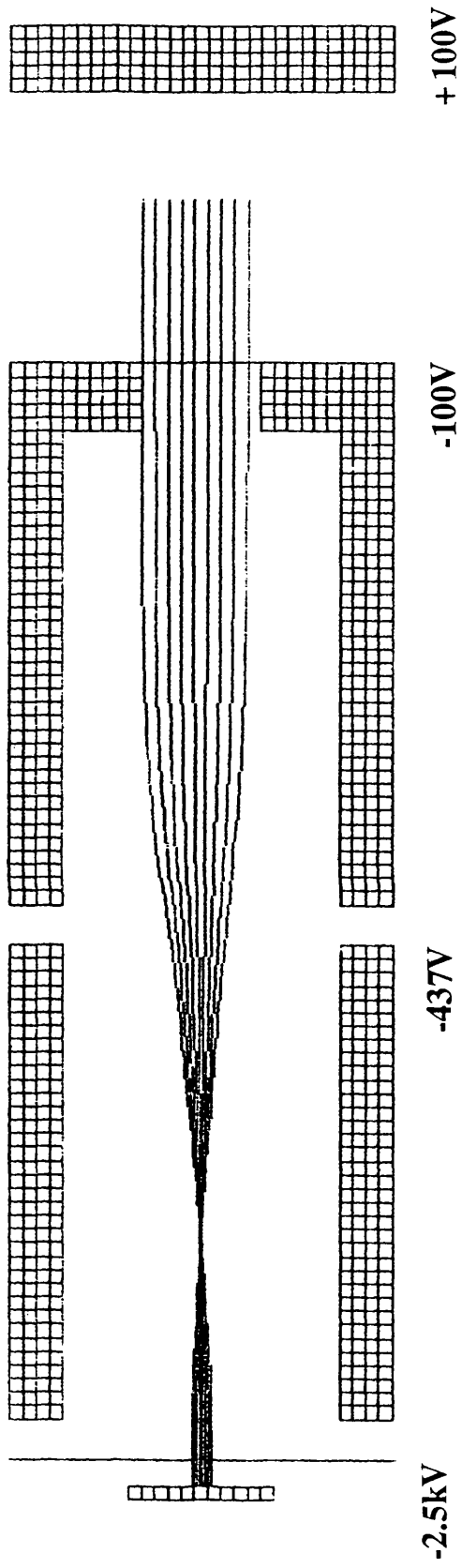


**Fig 3.9** A diagram of the trajectories of  $H^+$  ions after extraction from different parts of the interaction region, showing the spatial focussing properties of the extraction optics.

on the inner surface of the tube producing a cascade effect. All electrons are then collected on a metal plate at the end of the tube. The potentials that are applied to the Ceratron in this experiment are: -2.5kV to the cone, +500V to the back end of the tube and +800V to the collecting plate. This configuration produces a gain approximately double that of an ordinary channeltron ( $\sim 6 \times 10^9$ ) and yields pulses of  $\sim 30$ mV. Such a detector was selected because its high gain allowed the setting of discriminator levels so that pulses that were being picked up on the detector when voltage pulses were applied to the deflection plate could be discriminated against.

The entire assembly was mounted by M3 threaded rods off a 90mm diameter brass flange and contained in a 150mm brass tube of internal diameter 75mm which was mounted on the Al scattering chamber.

### 3.5 Timing Electronics

A block diagram of the electronic units that record the time-of-flight spectra of ions and initiate the application of the ion extraction voltage pulse is given in Figure 3.10.

Positron detection pulses from the MCP detector are decoupled from the dc potential on the MCP collector by a 470pF capacitor and amplified 10x with an Ortec 474 Timing Filter Amplifier. The amplified pulses are then fed into an Ortec 473 Constant Fraction Discriminator. Pick-up from the RF generator is reduced to such a level that it can be discriminated against with a notch filter-this consists of a length of screened 50 $\Omega$  cable which is left open-ended to absorb RF standing waves, to do this efficiently its length must be exactly a quarter of the wavelength of the pick-up that is to be absorbed. The negative TTL pulses from the discriminator are then used to monitor the beam with a ratemeter or scalar counter and are input into an Ortec 437A Time-to-Amplitude Converter as the start signal. The output pulse of the discriminator is also

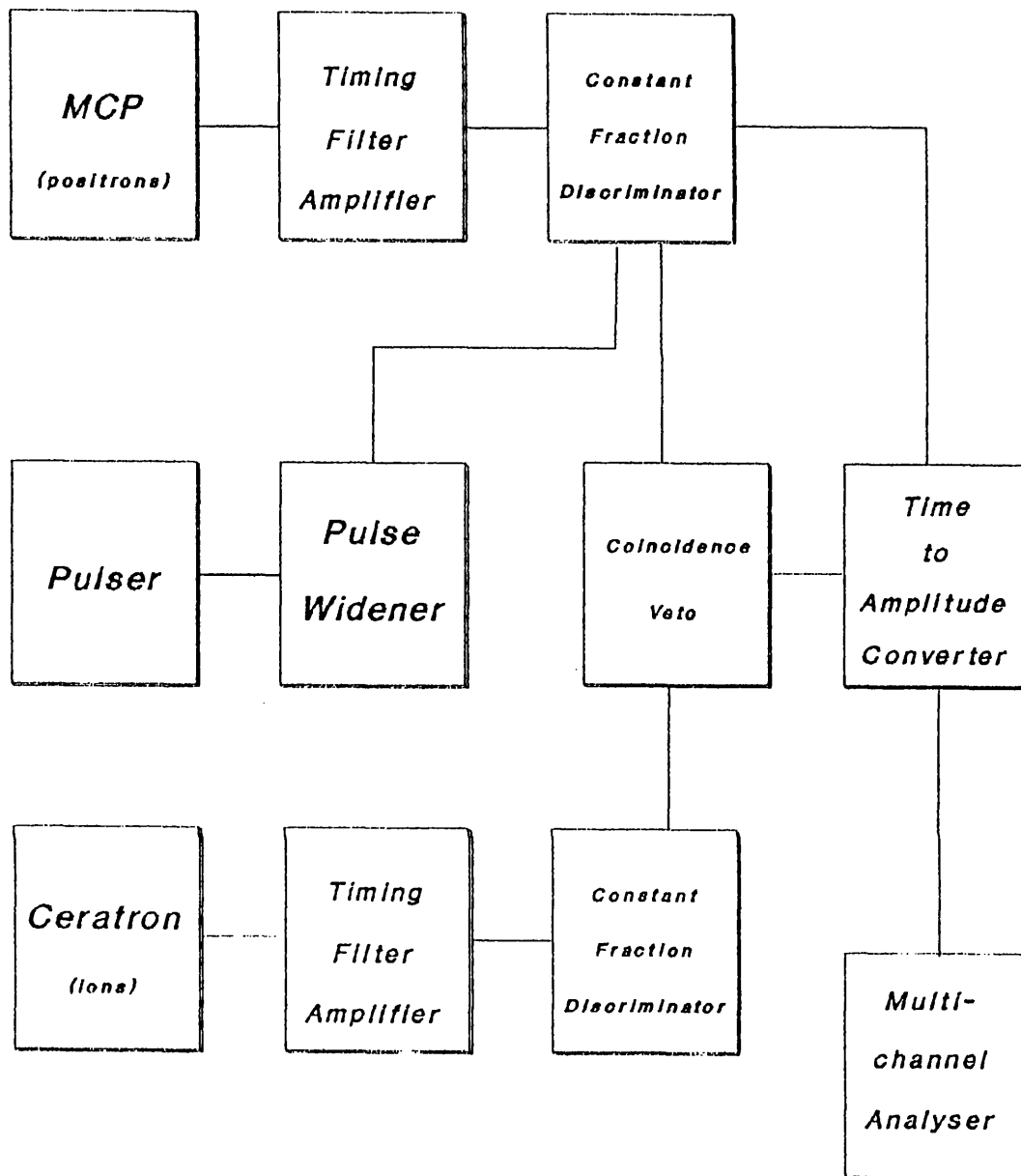
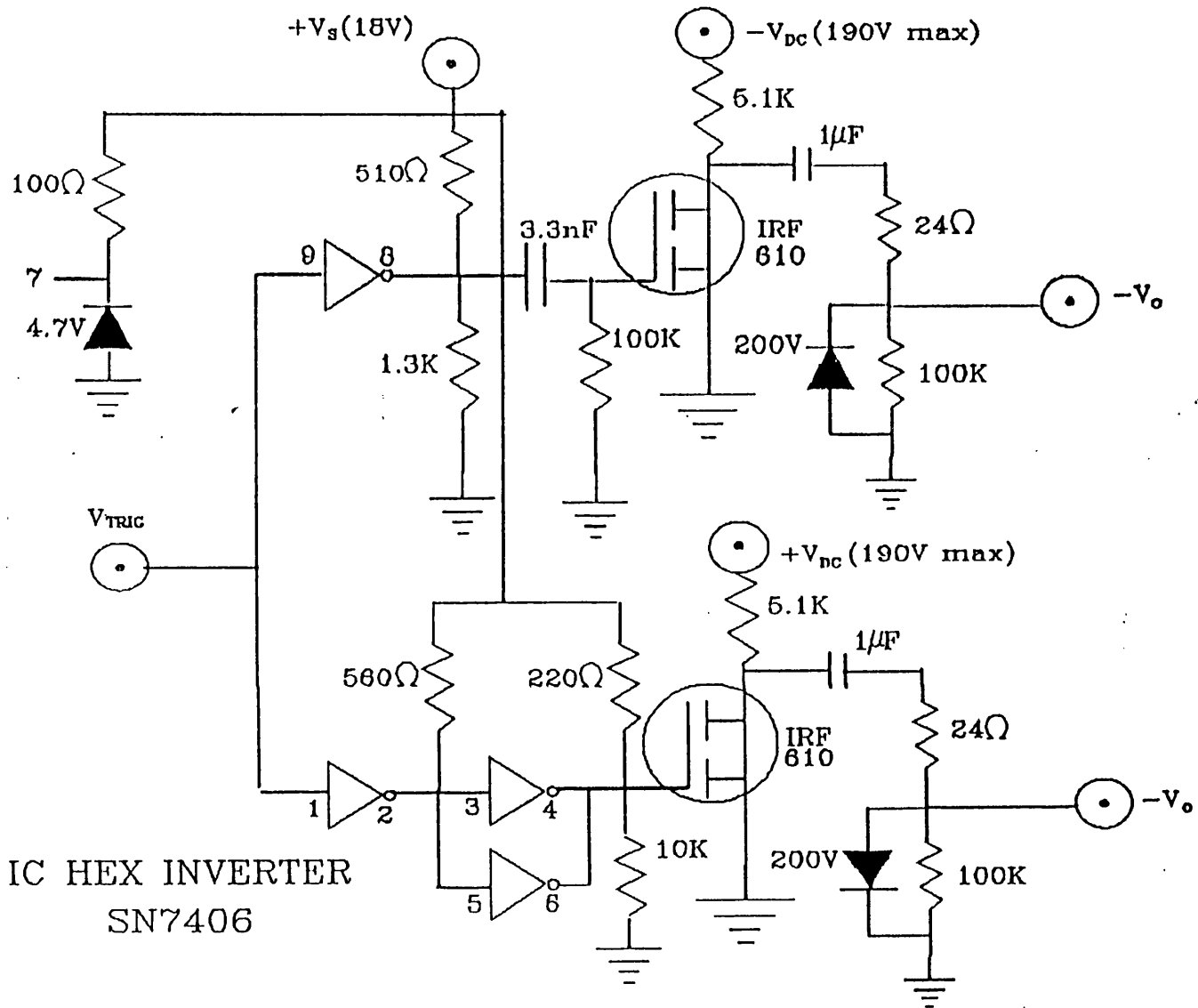


Fig 3.9 A block diagram of the timing electronics.



**Fig 3.10** The electronic circuit of the pulser unit that applied  $\pm 100V$  pulses to the ion extraction plates on the input of a shaped output pulse from the positron detector.

widened in a pulse widener and is used to trigger the pulser circuit shown in Figure 3.11, this circuit feeds pulses of  $\pm V_{ex}$  to the two plates either side of the interaction region. As discussed above  $V_{ex}=100V$  in this experiment. The trigger pulses for the circuit need to be positive and of height 2.5V with a duration greater than  $10\mu s$ . These conditions are met by widening and inverting the discriminator output.

Pulses from the discriminator are also used in a coincidence veto circuit, this consists of an Ortec T105N discriminator which widens the output of the previous discriminator which is delayed and fed into the veto input of an Ortec C104A/N coincidence unit. Also input into this unit are the output pulses of the Ceratron detector which have again been amplified (by 20x) and discriminated by similar units to those described above. The veto pulses are delayed so that they coincide with pulses the Ceratron has "picked-up" on the application of the extraction voltage to the plates thus not allowing their being input into the time-to-amplitude converter as a stop signal and halting the timing sequence at a time zero before ions can be counted. The discriminator level for the amplified Ceratron pulses is set so that most pick-up from the pulser and all RF pick-up does not contribute to the timing, anomalously large pulser pick-up is vetoed by the circuit described above.

The output signal of the time-to-amplitude converter is then collected by an Ortec 580-1 General Interface/ Controller for an MCA programme for the BBC Microcomputer.

## CHAPTER 4

# POSITRON AND ELECTRON IMPACT IONIZATION OF ATOMIC AND MOLECULAR HYDROGEN

### 4.1 Preliminary Remarks

The experiments which have been performed on the system described in Chapter 3 to measure ionization cross-sections will be discussed now. Modifications which have been made to the apparatus discussed above will be considered in the context of those experimental results which prompted them.

Initial experimentation was done with the radio-frequency discharge tube not in operation, the target was thus entirely molecular. This was for the purpose of checking measured cross-sections against previously published values thus allowing sources of error inherent in the experiment to be identified and eliminated.

### 4.2 Results for Molecular Hydrogen

#### *4.2.1 Positron Impact Ionization*

Experimental runs using the apparatus described in Chapter 3 involved the collection of data in the form of 512 or 1024 channel time of flight spectra. These spectra were histograms of pulses of different heights - their heights being dependent on the time interval between the output pulses of the positron and ion detectors.

Time-of-flight spectrum for positron impact ionization of  $H_2$  were similar to that shown for ionization of H and  $H_2$  in Figure 4.8 with a peak around channel number

287 due to the coincidental detection of a positron and a  $H_2^+$  ion. The peak at channel 209 was however absent as this corresponds to the charge-to-mass ratio of  $H^+$ . Its absence in the  $H_2$  should be noted as it is indicative of the paucity of dissociative ionization. This is significant when the ionization cross-section of atomic hydrogen is being measured by observing the ionic fragments of an incompletely dissociated target as dissociative ionization of  $H_2$  would be a source of spurious  $H^+$  ions. Due to the width of the  $H_2^+$  peak a "region-of-interest" of 40 channels centered on channel 287 was chosen to integrate over to obtain the total number of  $H_2^+$  ions,  $N_{H_2^+}$ . To allow comparison between different experimental runs the total number of ions detected in each run was normalized to positron beam intensity and target gas pressure,  $p$ . Due to the possibility of fluctuations in the beam intensity over a period of time the total number of positrons that were detected by the end detector,  $N_e$ , was used in the normalization. The resulting yield of  $H_2^+$  ions is then defined

$$Ion\ Yield = \frac{N_{H_2^+}}{pN_e} \quad (4.1)$$

To assess systematic effects this quantity has been measured as a function of various parameters, these measurements are discussed below.

Initially measurements of the ion yield, as defined in equation (4.1), were made at different pressures of  $H_2$  gas to investigate the dependence, if any, of the yield on target pressure. Such a dependence could be indicative of a changing gas distribution or of multiple collisions since normalizing the total ion count to target pressure in (4.1) removes the simple proportionality of yield to target number density. The dependence of ion yield on target pressure was investigated at different incident positron beam energies. Marked differences in the variation of yield with pressure at different beam energies would require taking several measurements at the same energy and different pressures and then extrapolating these results to zero pressure

for each energy before drawing valid conclusions about the energy dependence of the ion yield.

Ion yields measured at different pressures and energies are shown in Figures 4.1 (a) and (b). The error bars shown are the square-root standard deviation of a random sample, errors quoted on ion yields throughout this work have been calculated in this manner. It is clear from the graphs that a straight line with a small slope can be drawn through the sets of data points at each energy. The slopes of these lines are similar (typically  $\sim 0.45$  arbitrary units/torr) so it can be assumed that although the ion yield has a pressure dependence it is not variable with energy. At a fixed pressure the ion yield is therefore proportional to the ionization cross-section if the efficiency of detection of ions is also independent of energy.

The pressure was therefore kept constant by maintaining a reading of 1.5 Torr on an MKS Baratron Capacitance Manometer attached to the gas handling system and the ion yield was measured at various incident positron beam energies. The beam intensity was approximately  $5 \times 10^2 \text{ e}^+ \text{ s}^{-1}$  and run times were between 1 and 3 hours so as to obtain a statistical accuracy of  $\sim 7\%$ . The results of these measurements are shown in Figure 4.2 having been normalized at 100eV to the ionization cross-sections measured by Knudsen *et al* (1990). The smoothed results of Knudsen *et al* are shown for comparison. It can be seen that the present results were significantly lower than the published data for positron energies below 80eV. This was thought to be due to a change in the efficiency of detection of ions with energy possibly resulting from the drift of ions out of the field-of-view of the detector.

The potential pulse that extracts ions is triggered by the detection of a positron at the end detector as discussed earlier (see section 3.3), and is delayed in the electronics used to shape the trigger pulse by  $\sim 100\text{ns}$ . A further delay before the onset of this extraction pulse arises from the flight time of the positron from the scattering region to the detector - clearly this is dependent on the kinetic energy of

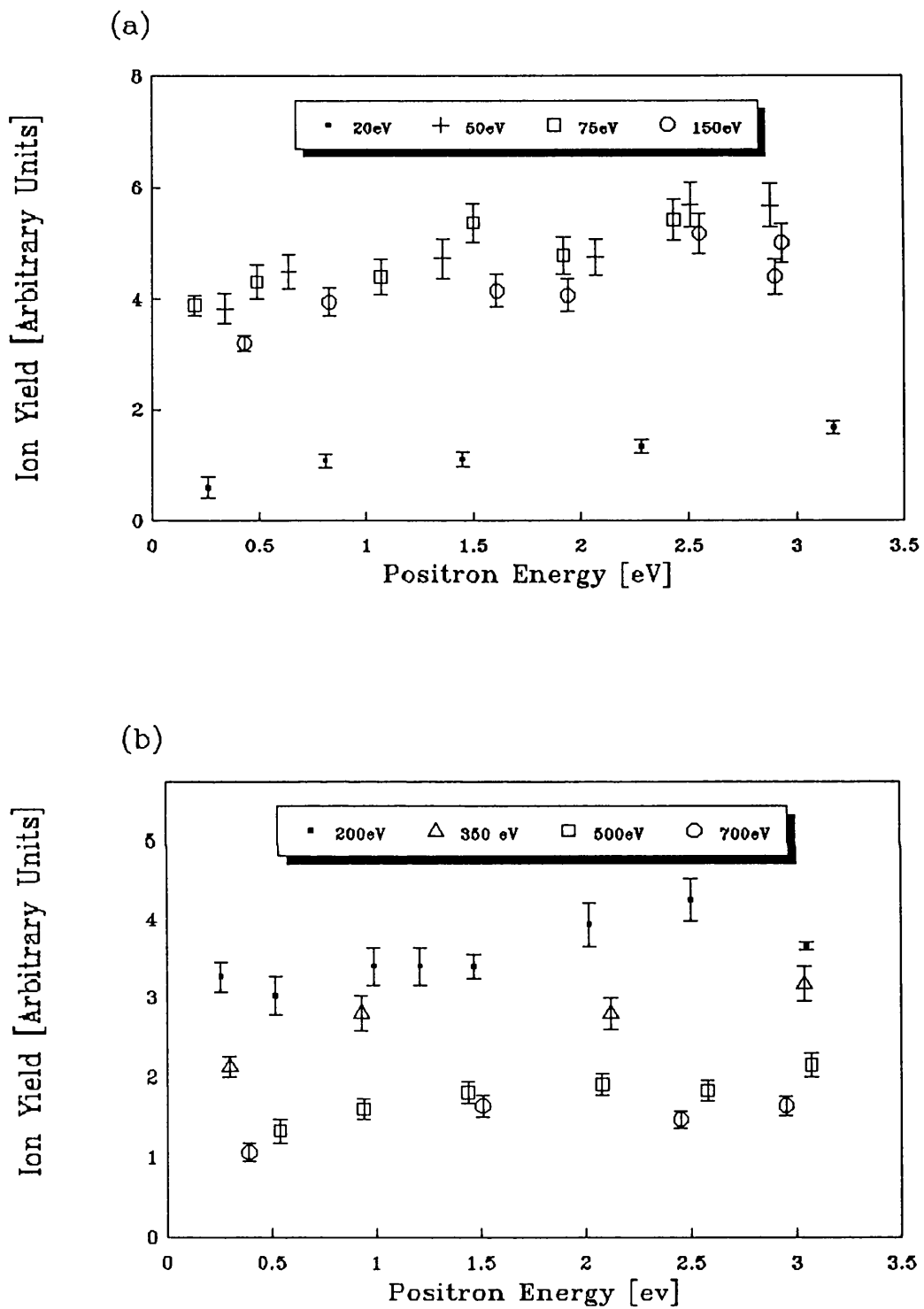


Fig 4.1 The measured ion yield as a function of gas pressure at different positron energies (a) below 150eV, (b) above 200eV.

the positron. The end detector is situated 0.445m from the centre of the interaction region - a 100eV positron will take  $\sim 75$ ns to reach it. Taking into account the electronic delay, the extraction pulse will therefore be applied  $\sim 175$ ns after the formation of a  $\text{H}_2^+$  ion, in this time a thermal  $\text{H}_2^+$  ion will have travelled  $\sim 0.5$ mm. The region over which ions are extracted extends 8mm below the nozzle from which molecules emanate and since the molecules drift at close to  $90^\circ$  to the axis of the detector, it is quite possible that some ions will be lost from the lower part of the extraction region. This will of course be more likely at lower positron energies where the delay before the onset of the extraction pulse is correspondingly longer. Thus the efficiency with which ions are detected at lower incident positron energy may be impaired. A systematic study of this effect was made.

The variation of observed ion yield with the onset time of the extraction pulse was studied by delaying the trigger pulse to the pulser circuit for different lengths of time. This was done by inserting known lengths of  $50\Omega$  co-axial cable between the constant fraction discriminator and the pulser (see Figure 3.8). Ion yields were measured with different amounts of delay and at different energies since the onset time is clearly energy-dependent. The measured yields are plotted in Figure 4.3. Although the statistical accuracy of the data is poor, the slope of a best-fit line through the points at each energy can be inferred from their scatter. It can be seen that, at incident positron energies above 80eV the data exhibits a negative slope above a certain delay but none below that - a plateau region. This is not the case for the sets of data below 80eV which have no plateau region. The plateau on these graphs indicates that all  $\text{H}_2^+$  ions that are formed by positron impact ionization are detected. A decrease in the ion yield for greater delay is due to some ions escaping the extraction region before the extraction pulse is applied. For energies below 60eV, the absence of a plateau at shorter lengths of delay is indicative that the delay imposed on the onset pulse by the time-of-flight of the positrons to the end detector is large enough for some ions to have escaped detection.

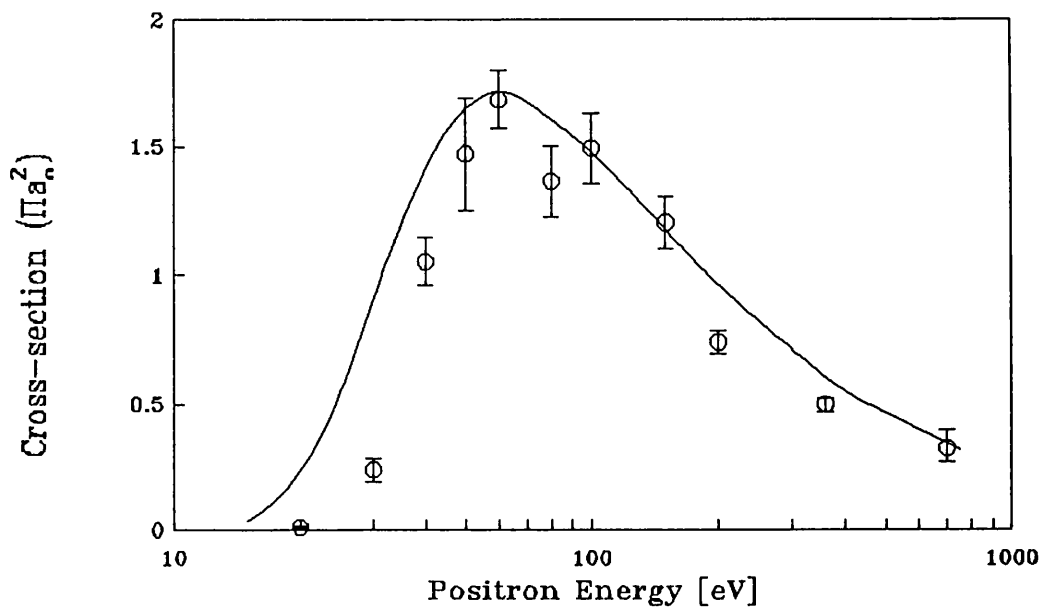


Fig 4.2 A plot of the measured ion yield against positron energy, having normalized all points to the data of Knudsen *et al* (1990) at 100eV which is shown smoothed (—).

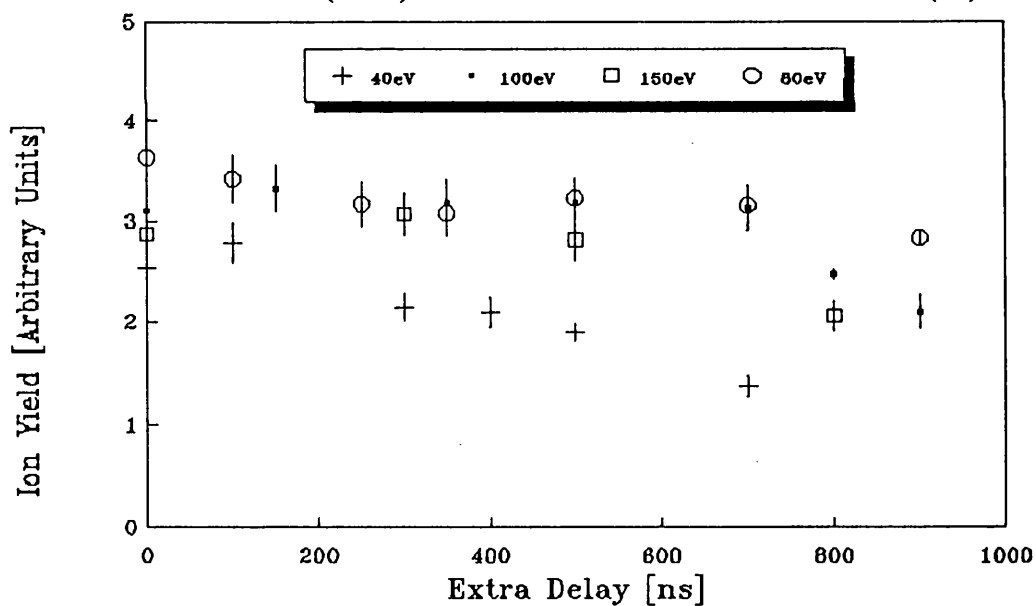


Fig 4.3 The  $H_2^+$  ion yield shown as a function of extra delay added to the onset time of the extraction pulse.

To obtain meaningful results at low incident positron energy it had to be ensured that the flight time of all positrons, regardless of their energy, was such that the number of ions that drifted out of the extraction region was negligible. This was done by electrostatically accelerating positrons between the interaction region and the end detector: two brass tubes of internal diameter 40mm were inserted in the beam tube as shown in Figure 3.2. Both were isolated from the chamber but the one immediately after the interaction region (of length 80mm) was earthed to the system, the second (of length 300mm) was connected to a BNC vacuum feedthrough on the end flange. The negative potential applied to the second extraction tube served to accelerate positrons to the end detector thus reducing their flight times and consequently the delay before the application of the ion extraction pulse. The ion yield was measured at different values of this potential so as to determine a single value which was sufficient for all ions to be detected. This was done for a range of energies and the results are shown in Figure 4.4. At a positron energy of 100eV it can be seen that the yield does not vary greatly with increasing positron extraction potential, this is as expected since all ions were being detected without any reduction of the onset time of the ion extraction pulse. At lower energies though the ion yield is seen to increase to a constant value with increasing potential - the lower the positron energy the greater the potential needed to attain a constant value of the ion yield. When the ion yield becomes constant all ions formed by positron impact ionization are being detected - the number of ions lost before extraction increases with decreasing positron extraction potential as the delay in their extraction increases.

To ensure the detection of all ions at all positron energies a positron extraction potential of -100V was selected since no further increase in ion yield was obtained in increasing extraction potentials beyond this at any positron energy. Ion yields were then measured with this positron extraction potential and normalized at 500eV to the results of Knudsen *et al* (1990); these are plotted in Figure 4.5.

#### 4.2.2 *Electron Impact Ionization*

To confidently measure the positron impact ionization cross-section of atomic hydrogen with this apparatus it was important to be able to compare other measured ionization cross-sections with published values. Other cross-sections that could be measured included the electron impact ionization cross-sections of both atomic and molecular hydrogen. If previously measured values which are generally accepted as accurate could be reproduced with this system then one could give greater credence to the positron cross-sections that are also determined.

An electron beam was derived by reversing the polarities on the source and moderator. This served to extract those secondary electrons that were produced in the impact of  $\beta^+$  particles on the moderator. They would be of low energy and could be accelerated to the required energy as with positrons. However, a problem with using an electron beam was that one could no longer be certain that all particles detected with the MCP beam detector were actually projectile particles. Secondary electrons could be emitted in all collisions of beam electrons with the internal surfaces of the apparatus (e.g. meshes, apertures etc.). Modifications had to be made to the system to overcome this - the grids in front of the MCP assembly were removed and the apertures on which they were mounted were used to retard and accelerate the projectile particles as before. The beam locating aperture before the interaction region was replaced with three successive apertures, the second two being of a slightly larger diameter than the first. The central one was held at a negative potential small compared to the beam energy to repel any secondary electrons coming from the narrower aperture and passing through the gas target and possibly causing ionization. The possible effects of the major sources of secondary electrons in the system were thus reduced. The beam intensity attainable with electrons was much greater than with positrons because of the low efficiency of positron moderation. Intensities of over  $10^5$  were possible with electrons; clearly it would have been desirable to use as high an intensity as possible if another problem had not

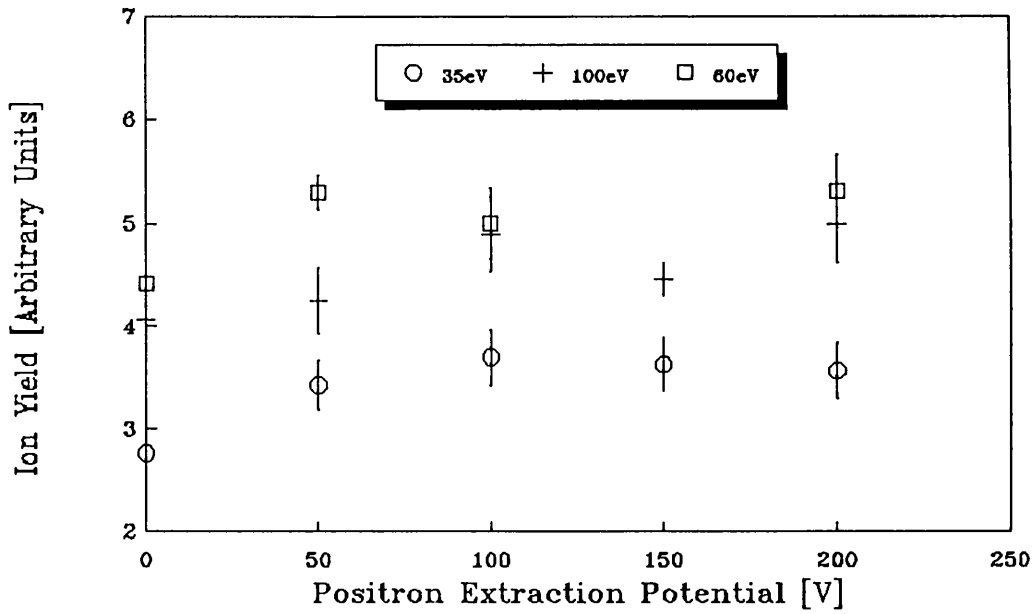


Fig 4.4 The  $H_2^+$  ion yield shown at different energies as a function of the potential applied to the positron extraction tube.

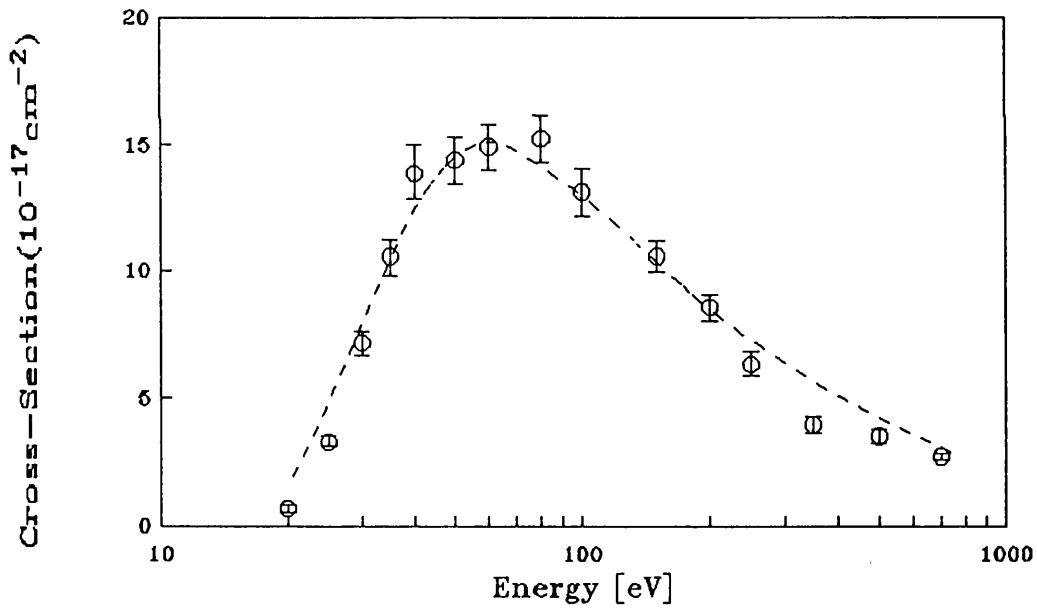
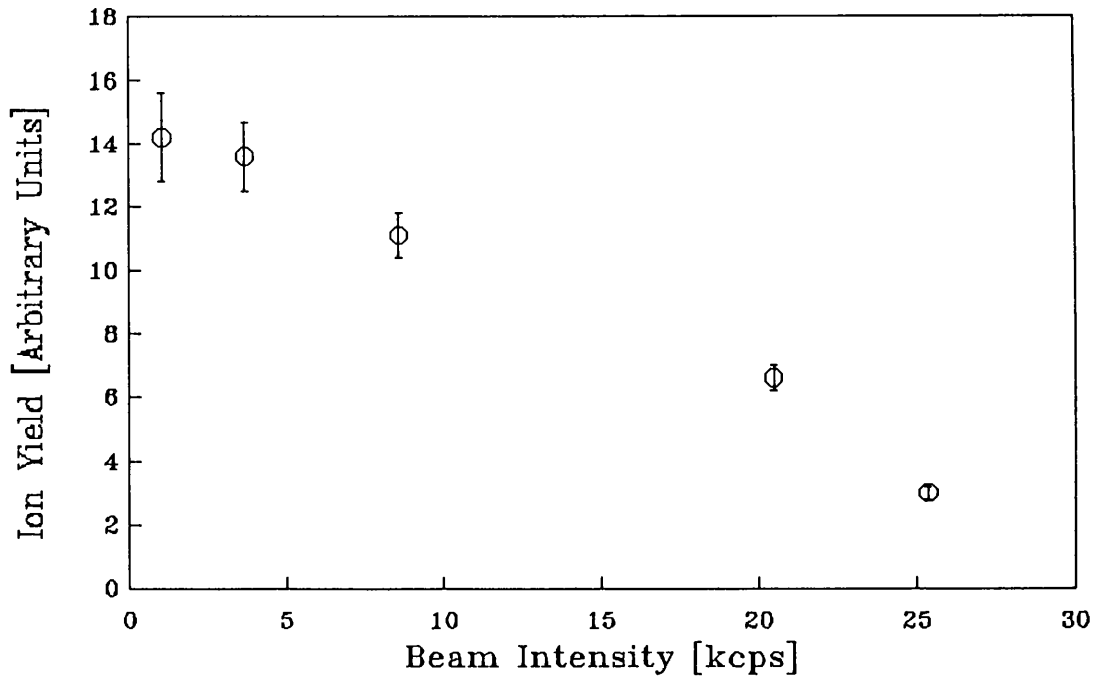
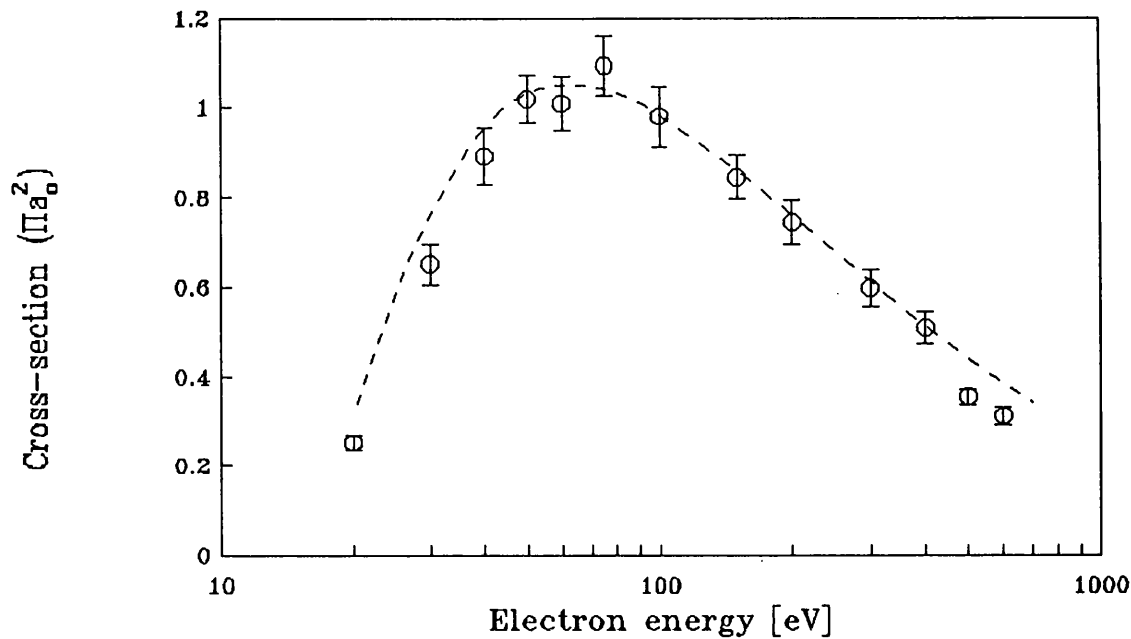


Fig 4.5 The  $H_2^+$  ion yield plotted over a range of energies having normalized it to the data of Knudsen *et al* (1990) at 100eV, this being shown smoothed (- -).



**Fig 4.6** The  $H_2^+$  ion yield plotted against electron beam intensity for an electron energy of 300eV.

arisen. This is displayed in Figure 4.6 which shows the  $H_2^+$  yield obtained with a 300eV electron beam as a function of beam intensity. The observed decrease in ion yield is a consequence of the pulsed ion detection system - the extraction pulses are of a fixed width which depends on the width of the trigger input to the pulser. If these pulses are too long a "dead-time" is effectively imposed upon the detection system: if ions are created whilst the extraction pulse associated with an unrelated positron is still on then the ion will be extracted but will not necessarily be accelerated to its full velocity and will have a different time-of-flight and will thus not fall in the region-of-interest on the spectrum. Inspection of the ion extraction pulses with an oscilloscope revealed that the pulses had a total duration of  $21\mu s$ , by changing the shape of the trigger pulse their total duration was reduced to  $1.4\mu s$ . The ion yield then showed little variation up to an intensity of about  $2 \times 10^5$  counts per second.



**Fig 4.7** Ion yields measured over a range of energies with an electron beam; the data has been normalized to the corrected data of Rapp and Englander-Golden (see text) which is shown smoothed (- - -).

Resolving these problems allowed the  $\text{H}_2^+$  ion yield to be measured as a function of electron energy. This study again revealed that at projectile energies below about 75eV, the ion yield was reduced as a result of ions drifting out of the interaction region before the onset of the extraction pulse. As above, an extraction potential was used to accelerate the electrons to the end MCP. The resulting data is shown in Figure 4.7; it should be noted that the extraction potential for electrons was only applied for the results below 75eV although the ion yield was measured at higher energies and found to be consistent with measurements taken without this potential. The data chosen to normalize the present results to was that of Rapp and Englander-Golden (1965) who repeated a previous experiment by Tate and Smith (1932) to a much greater degree of accuracy. Several authors have noted its consistency with the earlier work and the precautions that were taken to avoid systematic errors (Kieffer

and Dunn, 1966 and de Heer and Inokuti, 1982). However, as this experiment measured the cross-section for the production of all ions the results had to be corrected for dissociative ionization. This was done by subtracting the cross-section for dissociative ionization of  $H_2$  measured on the same apparatus by Rapp, Englander-Golden and Briglia (1965). The present results were then normalized to this corrected cross-section at 100eV as shown in Figure 4.7.

### 4.3 Preliminary Studies with Atomic Hydrogen

Having successfully reproduced previously measured values of total ionization cross-sections of molecular hydrogen with this system attention was focussed on the ionization of atomic hydrogen. In preparation for actually measuring its total positron impact ionization cross-section efforts were made to identify and resolve problems that arose from the operation of the RF discharge tube. This was done initially with positrons as projectiles and then, due to the higher beam intensity attainable, electrons. These studies will now be discussed.

#### 4.3.1 Positron Impact Ionization

The most immediate problem that was encountered in switching on the gas discharge was the extremely high count-rate observed on the Ceratron ion detector ( $\sim 2000$  counts per second). Such a count-rate in the stop channel of the timing system led to a large random background on the ionic time-of-flight spectrum which swamped the ion peaks making them indistinguishable from the background.

The count-rate was independent of the polarity of the potentials on the ion extraction optics but disappeared when the discharge was turned off. An examination of the output pulses of the Ceratron revealed that they were considerably larger in magnitude than pulses originating from RF pick-up which were successfully

discriminated against. This led to the conclusion that the observed count-rate was due to Lyman- $\alpha$  photons striking the Ceratron and being detected. The possibility that it may be due to photons from the visible part of the spectrum was excluded as these were of insufficient energy to be detectable by the Ceratron, the threshold for this being approximately 10eV. Attempts were then made to ascertain the exact origin of these photons - it was unclear whether they emanated from the discharge itself or were emitted in the de-excitation of resonantly excited H atoms that had left the discharge tube. If the latter was true then they would be emitted on the line-of-sight of the detector. Modifications to the ion extraction optics would then be necessary if the count-rate was to be reduced.

Initially, aluminum foil was used to block off the entrance aperture to the ion extraction optics and the region around the Ceratron cone. The Ceratron count-rate was then reduced to  $\sim 400$  counts per second, still considerably more than the count-rate with the discharge off. This implies that photons are travelling around the sides of the extraction lenses and being reflected off the graphite covered surface of the tube in which they are housed into the Ceratron. To make the internal surface of this tube less reflective it was coated with carbon in the form of soot. Removal of the foil from the aperture and subsequent operation of the discharge tube revealed that this had served to reduce the count-rate of Lyman- $\alpha$  photons to only 10 per second. This was sufficiently low for ion peaks to be seen on the time-of-flight spectra. It also demonstrates that some photons escape the plasma and the discharge tube and that fluorescence of the hydrogen target outside the discharge tube is negligible.

A typical time-of-flight spectrum that was obtained with the discharge on is shown in Figure 4.9; the peak at shorter time (centered on channel 209) is that due to the detection of protons and at longer times the  $H_2^+$  peak can be seen. This time difference between the two ionic species is a result of their different charge-to-mass ratios and correspondingly different velocities in the electrostatic extraction field. It is therefore not necessary in this experiment to have a gas target which is entirely

atomic hydrogen as the atomic and molecular forms are distinguishable in this manner.

As explained in section 3.3.2 the inelastic processes that occur in the plasma include ionization - in a mixture of atomic and molecular hydrogen one would therefore expect protons to be formed on the ionization of atomic hydrogen in the discharge. Clearly neutral species can diffuse out of the plasma and the discharge tube and it is not inconceivable that protons could do the same. If this occurred then it is quite possible that these protons would be detected after the extraction field was initiated by a positron which had not been involved in an ionizing collision. It had to be ensured therefore that all detected protons resulted from the ionization of atomic hydrogen by the positron beam.

This was tested by substituting for the MCP detector output pulses created by a pulse generator. These were of an amplitude sufficient to trigger the discriminator and pulser shown in Figure 3.9 and to start the timing sequence. By switching the positron beam off there would then be no ionization of the neutral gas by positrons and any ions which were detected must have come from the plasma.  $H^+$  yields obtained with this arrangement were negligible and it was concluded that these protons were being formed in the plasma and then diffusing out of the discharge tube - they were then present when an uncorrelated positron was detected and the extraction voltage pulse was applied. Thus they were being detected in coincidence with a positron in exactly the same way as those protons which were formed in positron impact ionization of atomic hydrogen.

#### *4.3.2 Electron Impact Ionization*

Having demonstrated that the observation of  $H^+$  ions formed on positron impact with this system was not without its attendant problems, their resolution was tantamount if an accurate determination of the total ionization cross-section was to

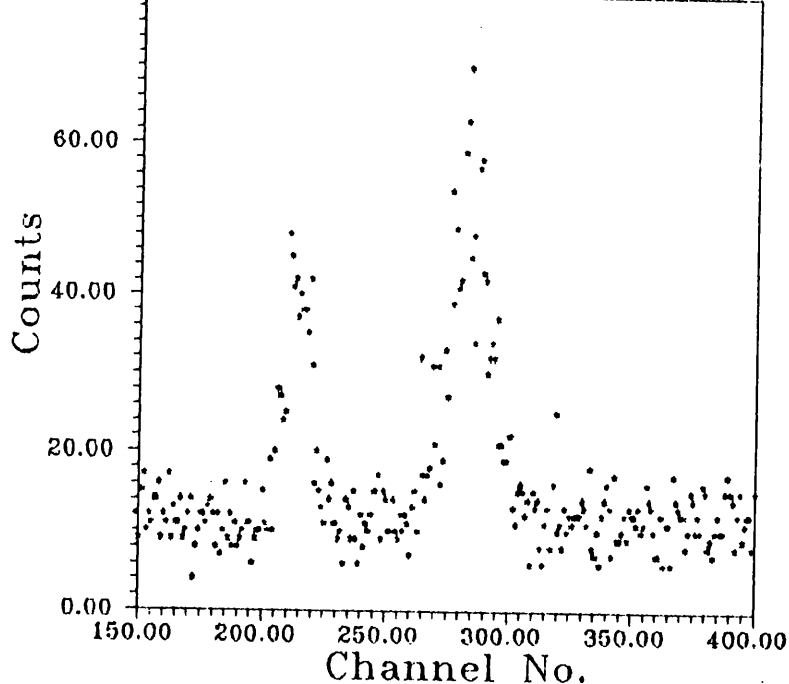


**Fig 4.8** A coincidence spectrum taken with the discharge on and a 100eV positron beam showing the peaks due to  $H^+$  ions and, at longer time,  $H_2^+$ .

be made. For convenience, an electron beam was used for the ensuing investigation due to the much higher intensity attainable than with a positron beam. As an additional check on the accuracy of the determined positron total ionization cross-section the electron total ionization cross-section could be measured with this system and compared with published values.

The resolution of problems which arose from the use of an electron beam are discussed above but a further, unexpected difficulty was encountered when the discharge was operated - the background count-rate of the MCP when the beam was switched off which was approximately  $10^4$  counts per second as opposed to the 500 counts per second with positrons which resulted from Lyman- $\alpha$  radiation from the discharge tube. This anomalously high count-rate was found to be dependent on whether the discharge was on or not - switching the discharge off reduced it to its usual value. Moreover it was independent of the level of RF power being input into

the resonator cavity be it zero or at its maximum, noting that at zero power the discharge was extinguished and the count-rate thus reduced. This implied that the count-rate was actually due to the detection of a large number of particles, the polarity of the plates requiring they be negatively charged or neutral. Their charge sign was determined by changing the polarity of the first aperture on the MCP assembly (the grid shown in Figure 3.3). The count-rate was observed to reduce to ~500 per second when a negative potential was applied to this grid even for as low a potential as -20V. It was concluded that these particles were negatively charged and came from the plasma - electrons were escaping the discharge. All measurements with electrons and the discharge on were therefore made with a potential of -20V on this grid.

The next investigations made with an electron beam were in order to resolve the problem of protons coming out of the discharge tube. Precautions had to be taken that protons which had not originated in impact ionization by the projectile were not detected in coincidence with an electron. This was achieved by applying a small dc potential to both ion extraction plates. With a negative field gradient towards the ion detector protons coming from the discharge tube would then be extracted and detected independently of the detection of an electron. They would therefore not appear on the time-of-flight spectrum, if such a proton was to be detected coincidentally with an electron then it would only appear on the spectrum as part of the random background. Furthermore, if the magnitude of the dc potential was kept as low as possible in comparison to the beam energy then the spatial displacement of the beam in the  $\text{ExB}$  field that results would be negligible. Different magnitudes of the potential gradient across the interaction region were used at a beam energy of 400eV to test for any effects on the beam - these would then change the gas overlap and the proton yield would change. The results of this investigation are shown in Figure 4.9; the increase in the proton yield on the initial application of a potential difference indicates that  $\text{H}^+$  ions are detected more efficiently when a small potential difference is applied. This is a result of ions which have a component of

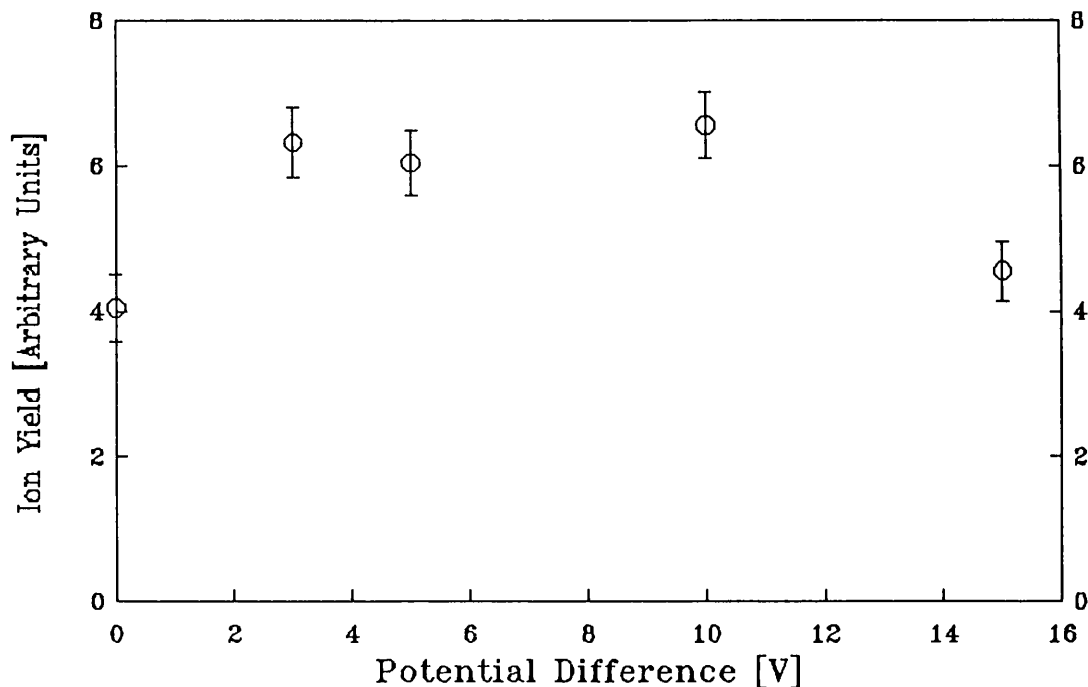


**Fig 4.9** The  $H^+$  ion yield plotted as a function of the magnitude of the dc offset potential applied to the ion extraction plates.

kinetic energy away from the detector being drawn towards the detector in the dc field and being detected whereas otherwise they would not. The decrease in ion yield at higher dc potentials that is seen in Figure 4.9 indicates that the potential is high enough to affect the beam transport noticeably. The chosen value of the potential difference was then taken to be the lowest possible at which the ion yield was enhanced, namely 3V. This was achieved by applying an offset of -3V to the negative output of the pulser. It was ensured that this potential difference successfully removed protons coming from the discharge tube from the region of interest for  $H^+$  ions by replacing the MCP output with the output of a pulse generator and switching the beam off as before. The resulting yield of  $(0.96 \pm 0.11)$  is clearly negligible compared to those measured for  $H^+$  ions shown in Figure 4.9.

#### 4.4 Summary

The experimental studies discussed in this chapter were carried out as tests preliminary to measuring the positron impact ionization cross-section of atomic hydrogen. It has been demonstrated that after slight modifications the apparatus described in Chapter 3 is suitable for measuring ionization cross-sections with positrons and electrons. To this end these cross-sections for molecular hydrogen have been measured and, as shown in Figures 4.5 and 4.7, agree well with the most accurate results that were previously obtained.

Measuring the ionization cross-section of atomic hydrogen with either particle has revealed several unexpected difficulties arising from the operation of the discharge tube in a magnetic field. It seems however that the effects of electrons and protons coming out of the discharge tube and being trapped in the magnetic field and then detected have been successfully negated. This in combination with the successful reproduction of previously obtained results discussed above indicates that the determination of the desired cross-sections for atomic hydrogen is possible with this apparatus.

## CHAPTER 5

# ELECTRON CAPTURE TO THE CONTINUUM IN POSITRON- ARGON COLLISIONS

### 5.1 Introduction

The ionization of gas atoms by positively charged particles takes different forms characterized by the fate of the ejected atomic electron. If, in the final state, the electron is free then the process is called direct ionization. However, if it is bound to the projectile charge transfer will have taken place for proton or heavy ion collisions and positronium formation for positron impact.

Classically, impact ionization can be viewed as an energy transfer from the projectile to the atomic electron sufficient to raise it from a potential well of depth  $E_I$ , the ionization potential, to the continuum. If the energy gained by the atomic electron is slightly less than  $E_I$  then ionization will not have taken place and the atom will be in a highly excited state. If the energy gained is slightly greater  $E_I$  though then the electron will be ejected with a very low kinetic energy. It follows therefore that direct ionization with the ejection of a slow electron is merely a natural continuation of excitation to a state with a high principal quantum number. One can view charge transfer to a highly excited state of the projectile in a similar fashion: the same reaction will extend beyond the ionization limit giving electrons with very low kinetic energy in the rest frame of the projectile. In the laboratory frame their velocity vectors will be almost equal and their relative motion will indicate a high degree of correlation between the particles. Such a reaction is referred to as electron capture to a continuum state of the projectile. In their study of the velocity and angular distributions of electrons ejected in proton impact ionization of hydrogen and helium Rudd *et al* (1966) observed that the distributions were distinctly peaked at  $0^\circ$  to the incident proton beam and at a velocity equal to that of the scattered proton. Following

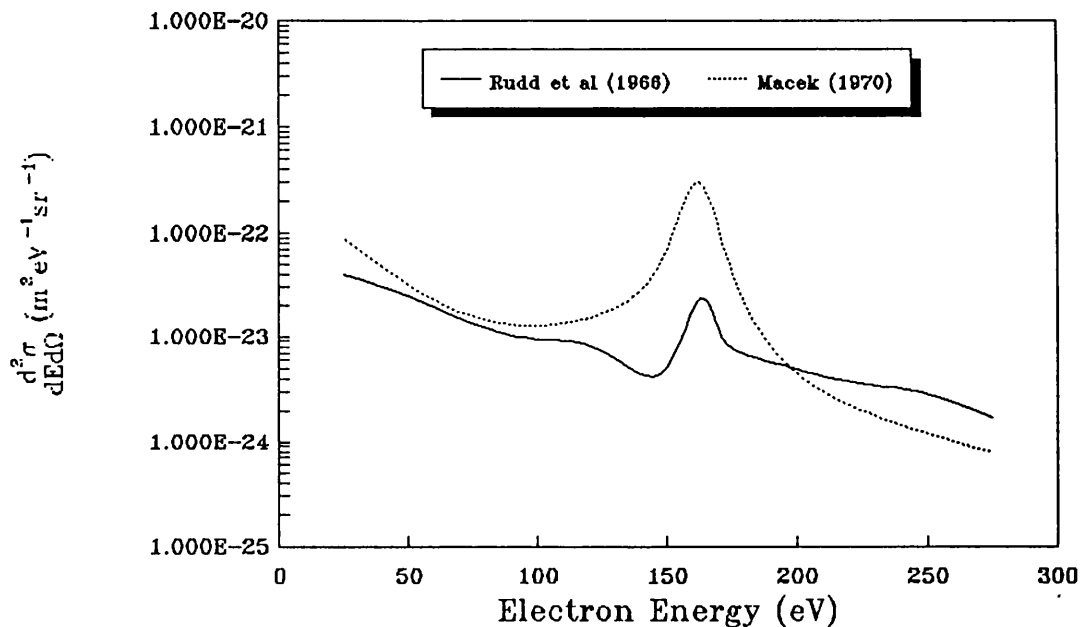


Fig 5.1 The calculated doubly differential cross-section for electron emission of Macek (1970) for 300 keV protons incident on He. The experimental data of Rudd et al (1966) is shown for comparison.

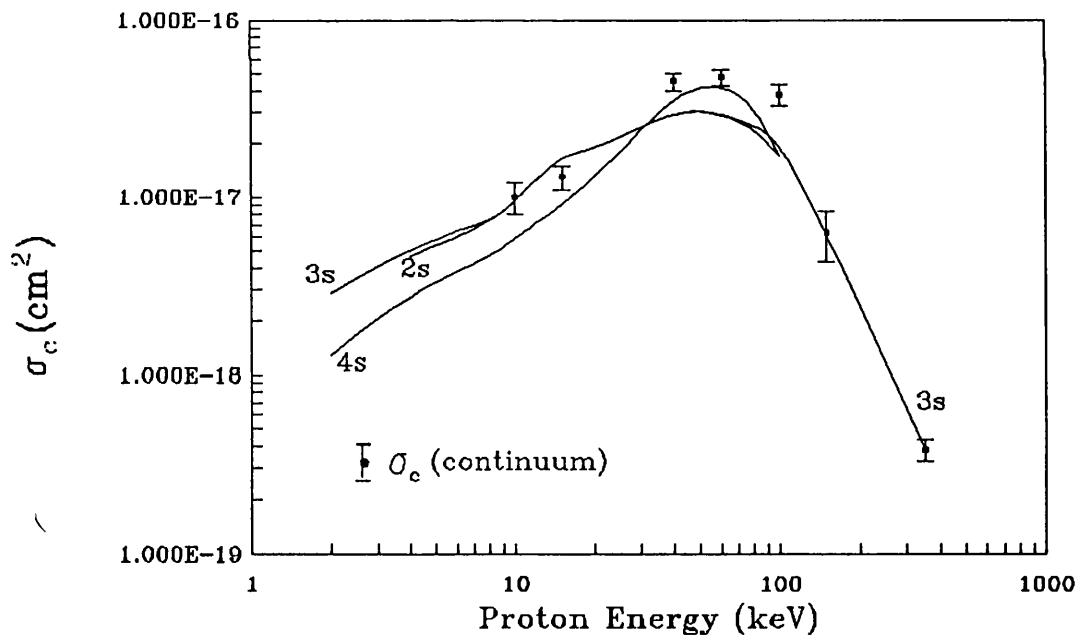


Fig.5.2 The reduced cross-section  $\sigma_c$  for capture to a continuum state of Rodbro and Andersen (1979) compared with reduced cross-sections for capture to bound states derived from literature.

Oldham (1967) it was proposed that these results were characteristic of electron capture to the continuum. A theoretical framework to describe this phenomenon was then sought. Macek (1970) proposed a modification to the first Born approximation (see section 2.2.1) in which the final state was an eigenstate of the projectile-electron system rather than the target-electron system. The justification for this was that, asymptotically, the electron and proton were moving with approximately equal velocities. Using an expression proposed by Faddeev (1961) for the wave function of three asymptotically free particles

$$\Psi = \phi + \psi^{(1)} + \psi^{(2)} + \psi^{(3)} \quad (5.1)$$

where  $\phi$  is the plane wave

$$\phi = (2\pi)^{-3/2} \exp i(k_1 \cdot r_1 + k_2 \cdot r_2 + k_3 \cdot r_3) \quad (5.2)$$

Macek retains only the first order terms of  $\psi^{(i)}$  ( $i=1,2,3$ ). This gives

$$\psi_f = \phi^{(23)} + \phi^{(31)} + \phi^{(12)} - 2\phi \quad (5.3)$$

where  $\phi^{(ij)}$  satisfies the Schrödinger equation

$$\left( -\frac{1}{2m_1} \nabla_1^2 - \frac{1}{2m_2} \nabla_2^2 - \frac{1}{2m_3} \nabla_3^2 + V_{ij} \right) \phi^{(ij)} = E \phi^{(ij)} \quad (5.4)$$

and  $V_{ij}$  is the interaction potential between particles  $i$  and  $j$ . The first Born approximation is then included by substituting for the final state projectile-target wave function  $\psi^{(31)}$  the plane-wave  $\phi$  given by (5.2). This gives

$$\psi_f = \phi^{(23)} + \phi^{(12)} - \phi \quad (5.5)$$

The ionization amplitude can then be written

$$f_{ion} = (2\pi)^{-3} \left\langle \psi_f \left| \frac{1}{|\mathbf{r}_1 - \mathbf{r}_2|} \right| F(\mathbf{r}_1) \phi_0(\mathbf{r}_2) \right\rangle \quad (5.6)$$

where  $F(\mathbf{r}_1)$  is a plane wave representing the incident proton and  $\phi_0(\mathbf{r}_2)$  is the wave function of the initial bound state of particles 2 and 3. The potential is taken as the Coulomb interaction between the electron and the projectile as prescribed by Macek's initial assumption on the relative significance asymptotically of the electron-projectile and electron-ion interactions. Substituting for  $\psi$  from (5.5)

$$f_{ion} = f_{23} + f_{12} - f_0 \quad (5.7)$$

where  $f_{23}$  is the Born amplitude for direct ionization,  $f_{12}$  the amplitude for electron capture to the continuum and  $f_0$  is the amplitude for an ejected electron which is described by a plane wave.

It is of interest to consider the behaviour of  $f_{12}$  as the relative momentum of the electron and the projectile,  $\kappa_{12}$  goes to zero. It can be written

$$f_{12} = \frac{\exp\left(\frac{\pi}{2\kappa_{12}}\right) \Gamma\left(1 - \frac{i}{\kappa_{12}}\right) \sqrt{2} Z_3^{\frac{3}{2}}}{\pi^3 q^2 [Z_3^2 + (q - \kappa_{12})]} \quad (5.8)$$

where  $q$  is the momentum transfer of the projectile. This differs from the plane wave amplitude  $f_0$  by the multiplicative Coulomb distortion factor  $\exp(\pi/2\kappa_{12})\Gamma(1-i/\kappa_{12})$ . This can be re-written, and, in the limit  $\kappa_{12} \rightarrow 0$

$$\frac{2\pi}{\kappa_{12} \left[1 - \exp\left(-\frac{2\pi}{\kappa_{12}}\right)\right]} \rightarrow \frac{2\pi}{\kappa_{12}} \quad (5.9)$$

which clearly tends to infinity as  $\kappa \rightarrow 0$ . Thus  $f_{12}$  becomes the dominant term in (5.8) when the relative momentum of the electron and projectile is small. This is borne out in the energy and angular dependence of the cross-section for electron emission doubly differential in electron energy and emission angle calculated from (5.8). This is shown in Figure 5.1 for proton scattering off helium, the experimental data of Rudd *et al* (1966) is shown for comparison. Macek's calculations reproduce the cusp in the experimental data which is indicative of electron capture to the continuum thus implying the validity of the physical basis for this approach.

Experimental studies of this reaction have since continued apace. These include the observation of electron capture to the continuum following the ionization of helium by fast, highly charged positive ions (Knudsen *et al*, 1986) and in the ionization of He, Ne, Ar and H<sub>2</sub> by proton impact (Rödbro and Andersen, 1979). In their study of capture to the continuum they consider the behaviour of the reduced cross-section

$$\sigma_c \sim n^3 \sigma_n \quad (5.10)$$

where  $\sigma_n$  is the cross-section for capture to an excited state  $n$  of the projectile. For proton impact ionization of He they derive  $\sigma_c$  from previously measured values of  $\sigma_n$  for a range of values of  $n$ . These they compare with their own results for capture to the continuum. The ensuing  $\sigma_c$  values are shown in Fig 5.2 from which the similarity of results for different  $n$  and for continuum states suggests that the treatment of electron capture to the continuum as an extension of capture to highly excited states of the projectile is justified. Shakeshaft and Wadehra (1980) speculate that this implies that the formation of bound states by charge transfer could be studied indirectly by studying electron capture to the continuum. Specifically, they suggest positronium formation since the finite lifetime of this bound state can complicate its direct detection. It is informative, therefore to assess the degree of correlation between a positron and an ejected

atomic electron following positron impact ionization as it indicates the likelihood of electron capture to the continuum occurring in this interaction.

## 5.2 Electron capture to the continuum in positron impact ionization

In this section the limited theoretical considerations of electron capture to the continuum following positron impact ionization will be reviewed.

### 5.2.1 Quantum Mechanical Theory

The quantum mechanical treatment of positron impact ionization leading to capture to the continuum has consisted of adopting Macek's approach to the proton case. Mandal *et al* (1985, 1986) repeat the procedure described in section 5.1 for positron impact ionization of atomic hydrogen and obtain the doubly differential cross-section shown in Fig 5.3 for 100eV positrons. Their results show a cusp in the ejected electron distribution in the forward direction and at a velocity equal to that of the scattered positron. Again, this follows from the relative momentum dependence of the Coulomb distortion factor given in (5.9). Since this calculation utilizes the first Born approximation it is worthwhile noting that Brauner and Briggs (1986) have repeated the calculation for 1keV incident energy, within the range of validity of the approximation (see section 2.2.1) and achieve similar results as shown in Fig 5.4. This shows that although a simple treatment of capture to the continuum based on the first Born approximation may not necessarily give quantitatively accurate values of the cross-section, it can predict the position of the cusp in the doubly differential cross-section at all energies. This has been noted previously in proton scattering and is in accordance with experiment (Rudd and Macek, 1972). Furthermore a recent T-matrix calculation by Sil *et al* (1991) shows cusp structures in the doubly differential cross-section at zero relative momentum for all scattering angles.

Quantum mechanical calculations thus predict a pronounced cusp in the energy

and angular distributions of ejected electrons in the forward direction and at an energy equal to that of the scattered positron. This indicates a very high degree of correlation between the outgoing particles and that electron capture to the continuum occurs in positron impact ionization.

### 5.2.2 Classical Theory

Following its success in reproducing the total ionization cross-section of protons incident on atomic hydrogen, the Classical Trajectory Monte Carlo method (Abrines and Percival, 1966a) has been used to calculate the doubly differential cross-section for electron emission for the same reaction (Reinhold and Olson, 1989). To this end the more rigorous CTMC theory developed by Olson and Salop (1977) and discussed fully in section 2.2 has been used. Good agreement was found with both experimental results and previous quantum mechanical calculations and both the position and the magnitude of the cusp were accurately predicted by Reinhold and Olson's calculations. This has prompted the use of the CTMC method to calculate the doubly differential cross-section for electron emission in positron impact ionization by Schultz and Reinhold (1990). The resulting variation of the cross-section with electron energy is shown in Fig 5.5 for several ejection angles. As can be seen by comparison with the scaled  $0^\circ$  results of Mandal *et al* (1986) also shown in Figure 5.5 the classical results do not display a pronounced cusp in the forward direction as the quantum mechanical results.

Schultz and Reinhold consider the corresponding proton results and interpret the near absence of a cusp in the positron data as being a consequence of the smaller mass of the positron. This will increase the likelihood of positrons being scattered at large angles. Therefore although electron capture to the continuum may occur the doubly differential cross-section will not be strongly peaked in the forward direction but will exhibit a ridge-like structure extending in both angle and energy.

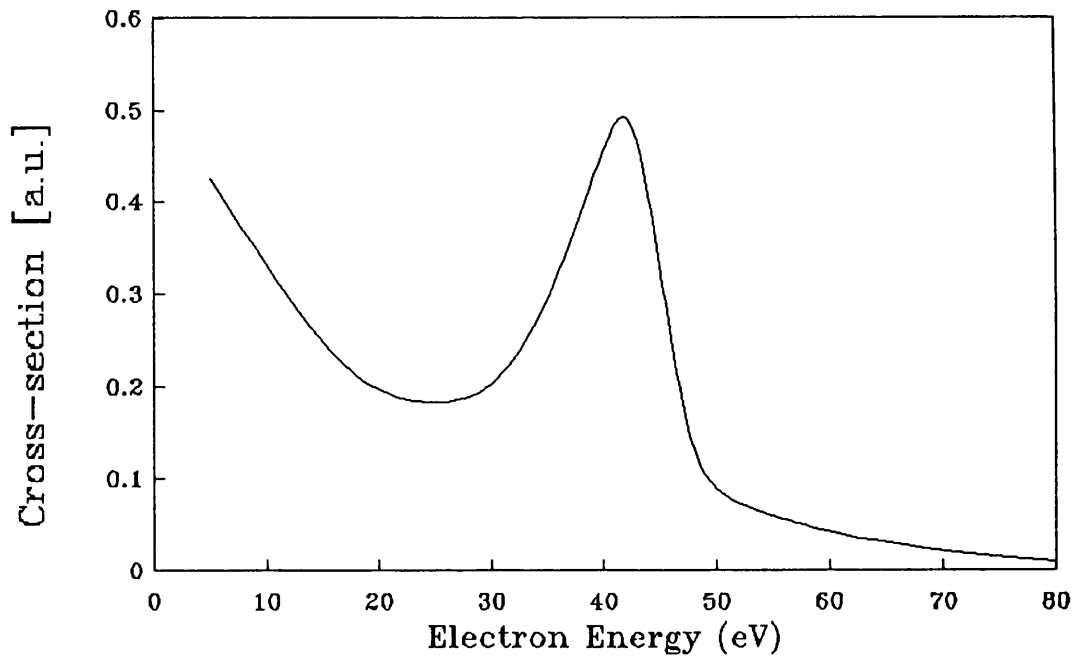


**Fig 5.3** The energy distribution of electrons emitted at  $0^\circ$  in positron impact ionization of H at 100eV as calculated by Mandal *et al* (1986).

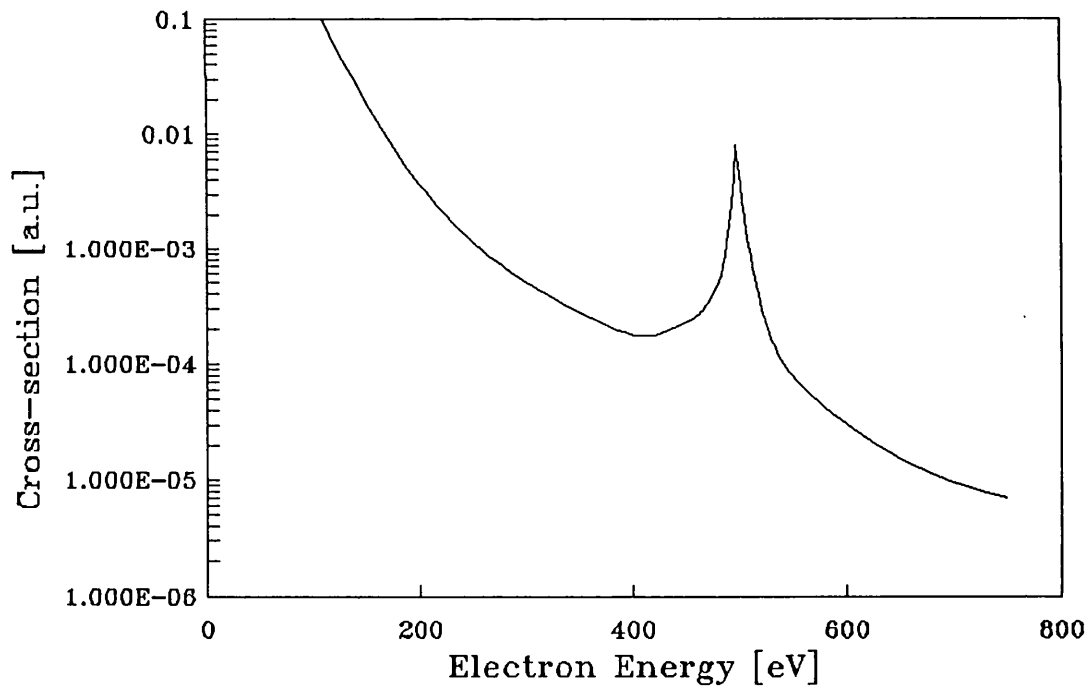


**Fig 5.4** The triply differential cross-section for electron emission at  $0^\circ$  in the ionization of H atoms by 1keV positrons, as calculated by Brauner and Briggs (1986).

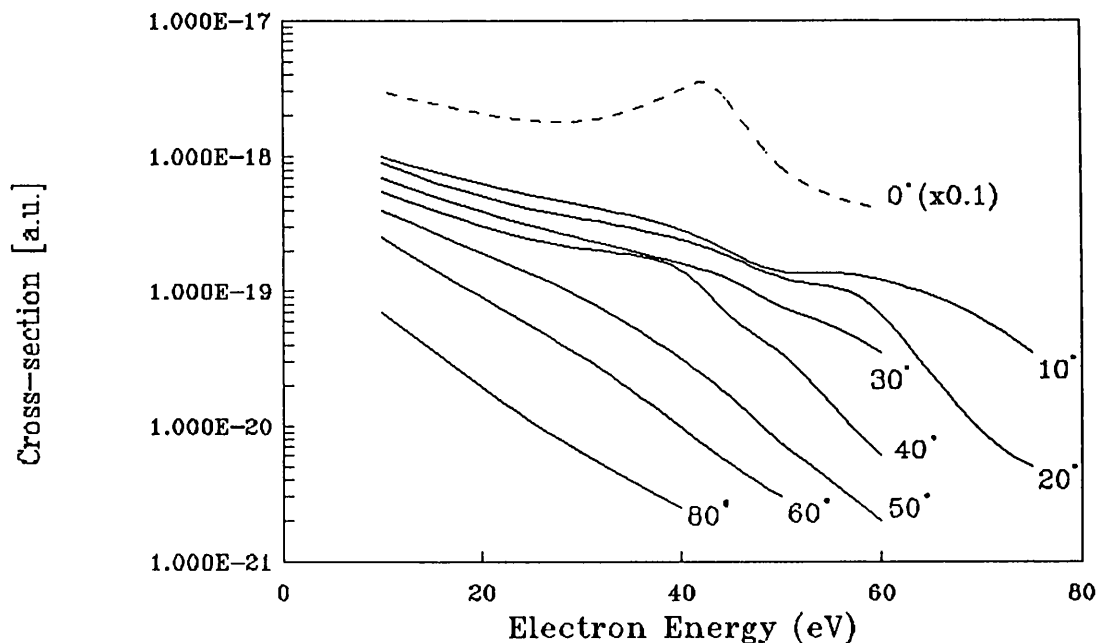


Fig 5.5 The energy distribution of electrons emitted in the ionization of H by 100eV positrons, calculated at various angles by Schultz and Reinhold (1990). Also shown are the scaled 0° results of Mandal *et al* (1986).

### 5.2.3 Experimental Studies of Capture to the Continuum after Positron Impact

In measuring the ionization cross-section of He, Coleman (1986, for experimental details see section 1.3) observed a retarding spectrum for electrons ejected in positron impact ionization: this is shown in Figure 5.6. It was done by varying the potential applied to a grid in front of a channeltron detector thus only allowing electrons with energy greater than a certain value to be detected. It is, essentially, the integrated energy distribution of ejected electrons. Charlton *et al* (1987) have performed a similar experiment with Ne giving the results shown in Figure 5.7. Also shown for the purpose of comparison are the results of Brauner and Briggs' (1986) calculation which are discussed above, these have been integrated and normalized to the experimental results. Although these calculations are made for 1keV positrons incident on He, the shapes of the curve for Ne at 200eV should

not differ greatly and normalization removes numerical differences. Of note in the diagram is the cut-off of the theoretical data near the energy expected for the capture to the continuum cusp. Unlike the results of Coleman (1986) this cut-off is reproduced in the experimental data of Charlton *et al* (1987) showing that some electrons are emitted with energy close to that expected. Any assessment of the significance of electron capture to the continuum with this method were difficult though and an investigation in which electron emission could be observed as a function of energy was clearly required.

### **5.3 An Experiment to Study Electrons Ejected Following Positron Impact Ionization of Argon**

In an attempt to ascertain the likelihood of electron capture to the continuum occurring after positron impact ionization an investigation has been made of the times of flight of electrons ejected in such collisions. The electrons' energies are clearly related to their times-of-flight and the distances they have travelled so their energy spectra can be computed. Although this method is crude in that the origin of many detected electrons is uncertain, gross features of the actual energy distributions of electrons ejected on ionization can be deduced from the derived energy spectra.

The apparatus employed to perform this experiment is a slightly modified form of that used by Laricchia *et al* (1988) to produce a timed positronium beam. A magnetically guided positron beam produced in the conventional manner is remoderated and allowed to pass through a scattering cell containing gas. Positrons and electrons are then confined by the magnetic field and detected at the end of the beam path, the particle to be detected being specified by electrostatic biasing of the end detector. Times of flight are measured by "tagging" the beam in the manner developed by van House *et al* (1984). This involves detecting secondary electrons produced by positron impact on the remoderator and using the detection pulse as one signal for a timing circuit for which the other signal is a pulse from the end detector. The component parts of the experimental

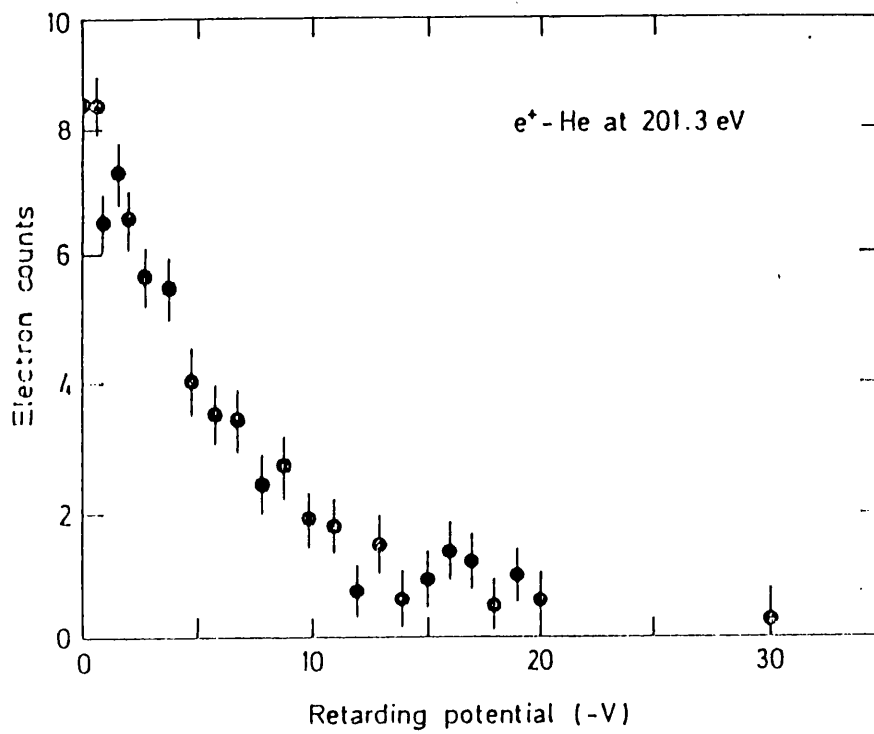


**Fig 5.6** The emitted electron count versus retarding potential reported by Coleman (1986) for positron impact ionization of Helium.

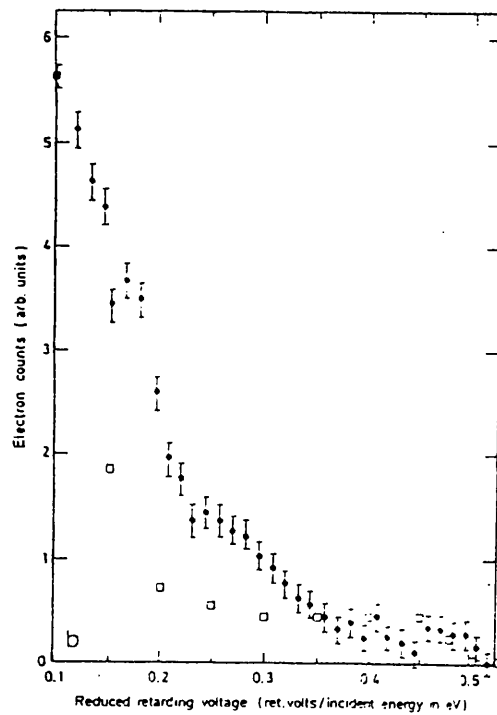


**Fig 5.7** Electron count versus retarding potential for positron impact ionization of neon reported by Charlton *et al* (1987) (●) shown with the integrated results of Brauner and Briggs' (1986) (□).

apparatus will now be considered in more detail.

### *5.3.1 The Primary Positron Beam*

As discussed in section 1.3 a slow positron beam was produced by the moderation of fast  $\beta^+$  particles from a  $^{22}\text{Na}$  source. The source, described in section 3.2, was mounted on a mobile shaft via a stainless steel jig. The shaft could be moved linearly through a 70mm flange mounted on a cylindrical vacuum chamber partially filled with Pb. The source can then be moved up to the moderator assembly and retracted to safety when access to this region is necessary.

The moderator comprises of four layers of annealed 90% transmission W mesh of 13mm diameter, the annealing procedure being that described in section 3.2. These meshes were held in a recessed PTFE ring by a push-fit brass ring to which the moderator potential was applied. An unannealed 90% transmission W mesh was held 1mm away from the moderator in a similar mounting, this was earthed to extract positrons. Another annealed mesh, again in a similar mounting, was placed between the moderator and the source. A potential slightly more positive than that applied to the moderator was applied to this mesh to turn back those slow positrons emitted towards the source-this results in a doubling of the beam intensity. The ensemble of mesh mountings was inserted into a 9mm long brass cylinder of outer diameter 20mm, they were insulated from each other by PTFE washers. This cylinder was mounted on the base of a Pb plug attached to a flange removable for the purpose of installing the moderator. The chamber which housed this assembly was evacuated by an Edwards E02 diffusion pump backed by an Edwards ED35 rotary pump. A diagram of the source area is shown in Figure 5.8.

The moderator is held at a potential so that 400eV positrons emerge from the source region, these are then transported along the beam line, shown schematically in Figure 5.9, and are constrained to move axially along it by a series of Helmholtz coils. A curved solenoid transports positrons through an angle

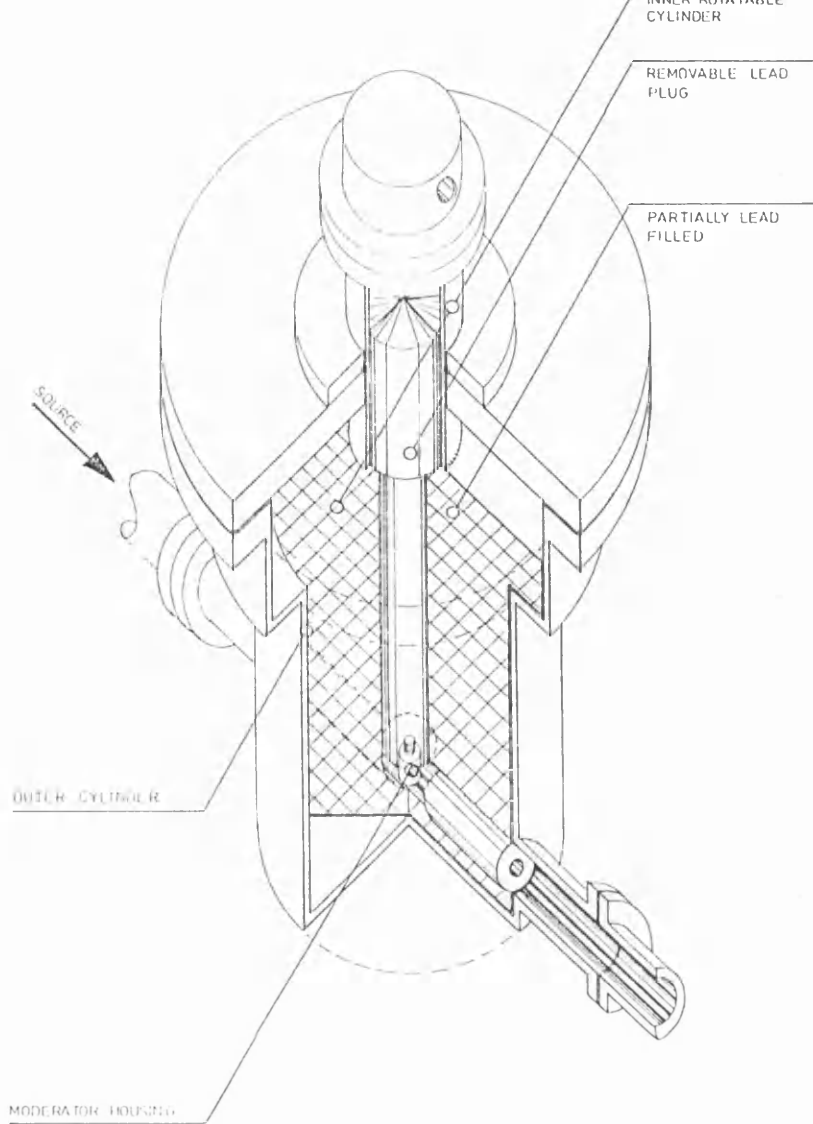
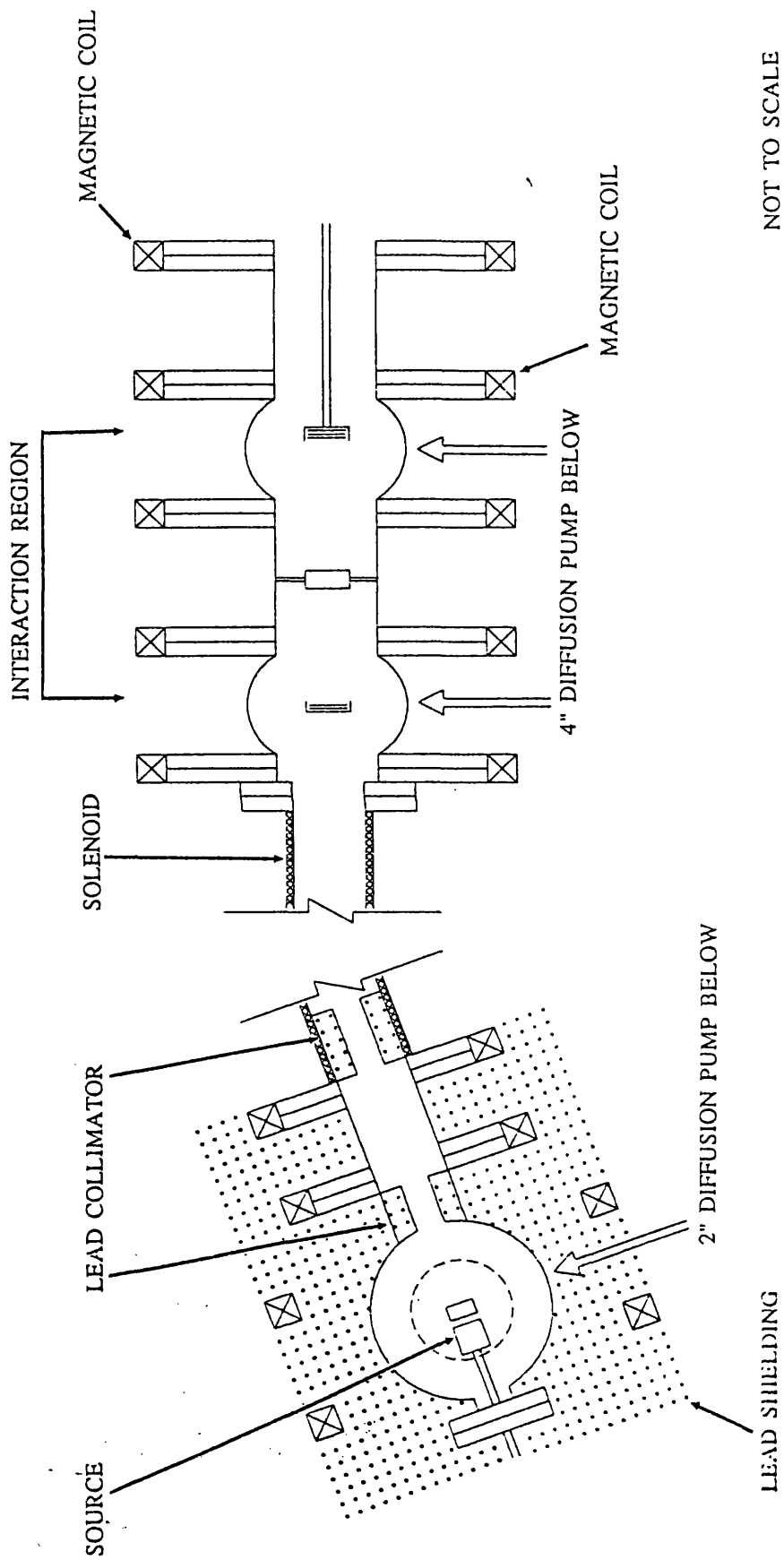


**Fig 5.8** A cut-away diagram of the source region

of  $15^\circ$  and causes the removal from the beam of many of its fast components such as high energy positrons and electrons. This bend in the beam line, together with the Pb collimators shown in Figure 5.9 also prevent annihilation  $\gamma$ -rays from the source region passing through the interaction region to the detectors. The magnetic field strength along the beam varied from approximately 100 Gauss near the source to about 20 Gauss in the interaction region. The purpose of this decrease was twofold - the reduction in the field strength will cause the pitch of the positrons' helical paths to increase and the beam will thus be "parallelized" on reaching the scattering region since their velocities will be predominantly longitudinal. It also serves to reduce the acceptance angle of the detection system-



NOT TO SCALE

Fig 5.9 A schematic diagram of the experimental apparatus showing the primary positron beam transport and electron collection and detection systems.

for a given transverse momentum transfer on collision this is the maximum angle a particle can scatter at and still move in a path with a helical radius small enough to allow it to impinge on the detector. Given that the aim of the experiment was to observe the forward cusp in the electron distribution it was thought prudent to minimize the acceptance angle so that only electrons ejected close to or at  $0^\circ$  to the incident beam were detectable. The variation of acceptance angle with electron emission energy is shown in Figure 5.10 for the two magnetic field strengths employed in this experiment; this has been calculated from the expression for the radius,  $r$  of a charged particles' helical path in a magnetic field of strength  $B$  which can be re-written

$$r = \frac{1}{B \sin \theta} \sqrt{\frac{2mE}{e}} \quad (5.11)$$

where, for an electron,  $E$  is its energy. If one sets  $r$  as the maximum possible radius at which the particle can travel then  $\theta$  will be the acceptance angle.

### 5.3.2 The Interaction Region and Timing System

As pointed out above, particle timing was by means of the "tagging" method. The primary positron beam is here remoderated by implantation into a set of annealed W meshes. The energy of the ensuing slow  $e^+$  beam is determined by the sum of the potential applied to these meshes and their positron work function (found to be  $2.5 \pm 0.5 \text{ eV}$  by Zafar, 1990). An earthed unannealed W mesh is employed to extract the remoderated positrons. The stop signal for the inverted timing sequence is obtained by the detection of secondary electrons released when positrons strike the remoderator. The primary  $e^+$  beam passes through an 8mm diameter tube in the centre of a pair of micro-channel plates (henceforth referred to as CEMA1) These Galileo MCP10 48-208 plates are 1mm thick and have an active diameter of 32.5mm, the central tube passes through a 10mm hole drilled in each. Their principle of operation is similar to that of the MCP's described in section 3.2. This pair of plates was mounted in a machined ceramic holder with

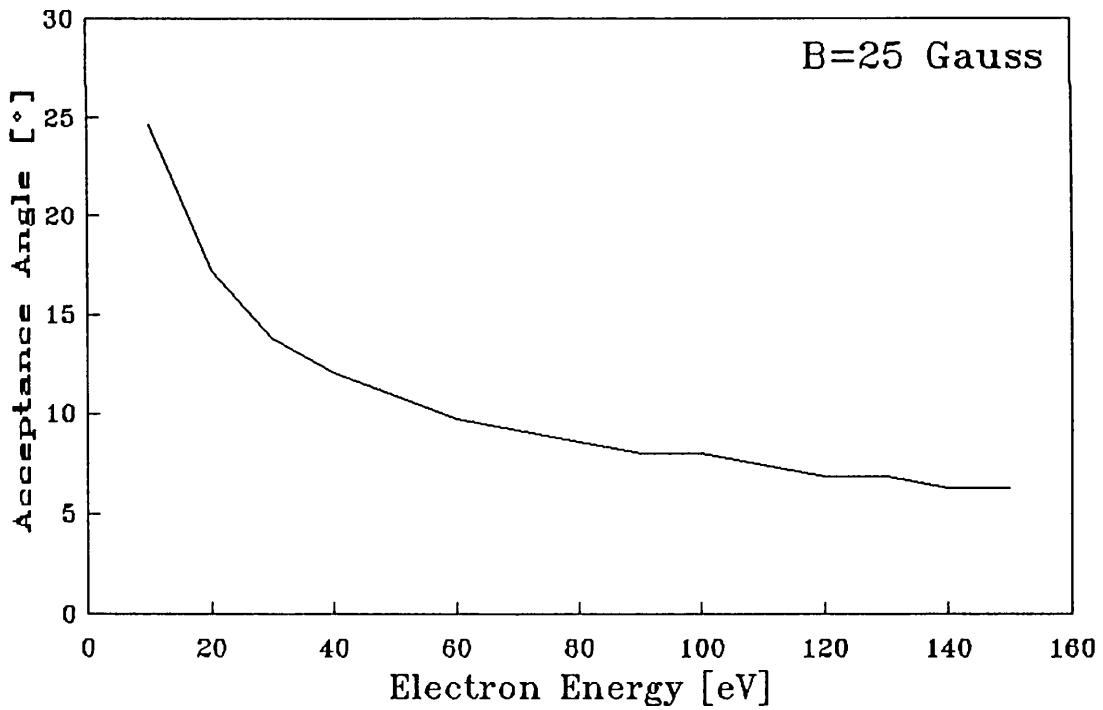
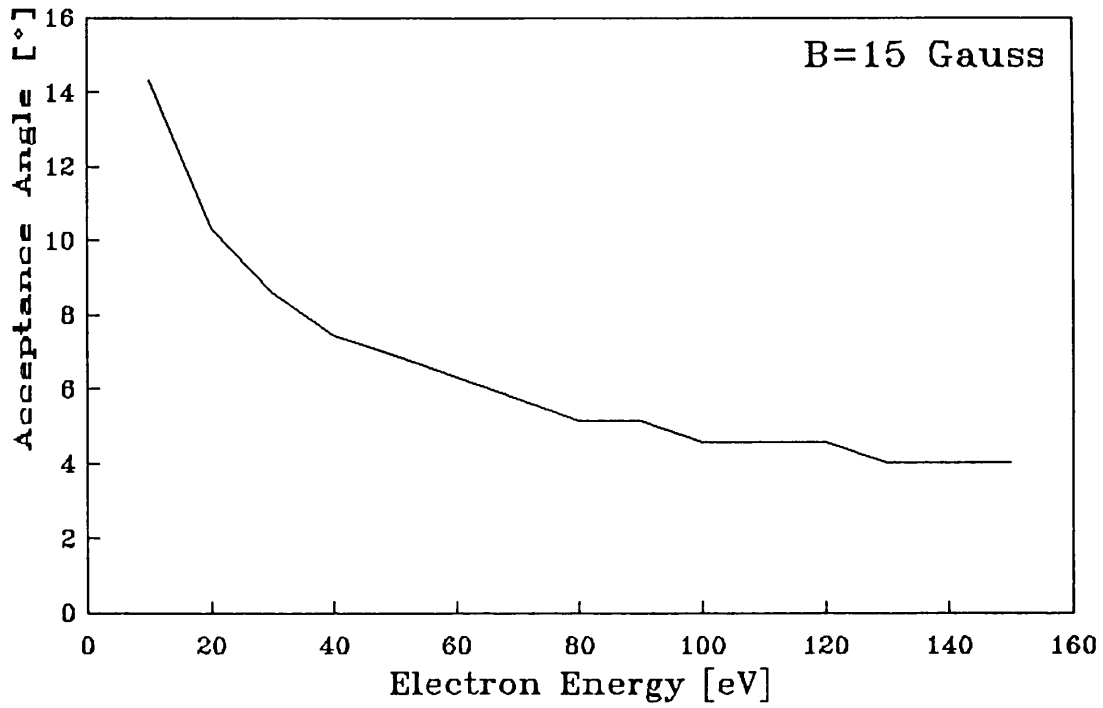


**Fig 5.10** A graph showing the acceptance angle of the electron detection system used in this experiment for both magnetic field strengths (a) 15 Gauss and (b) 25 Gauss.

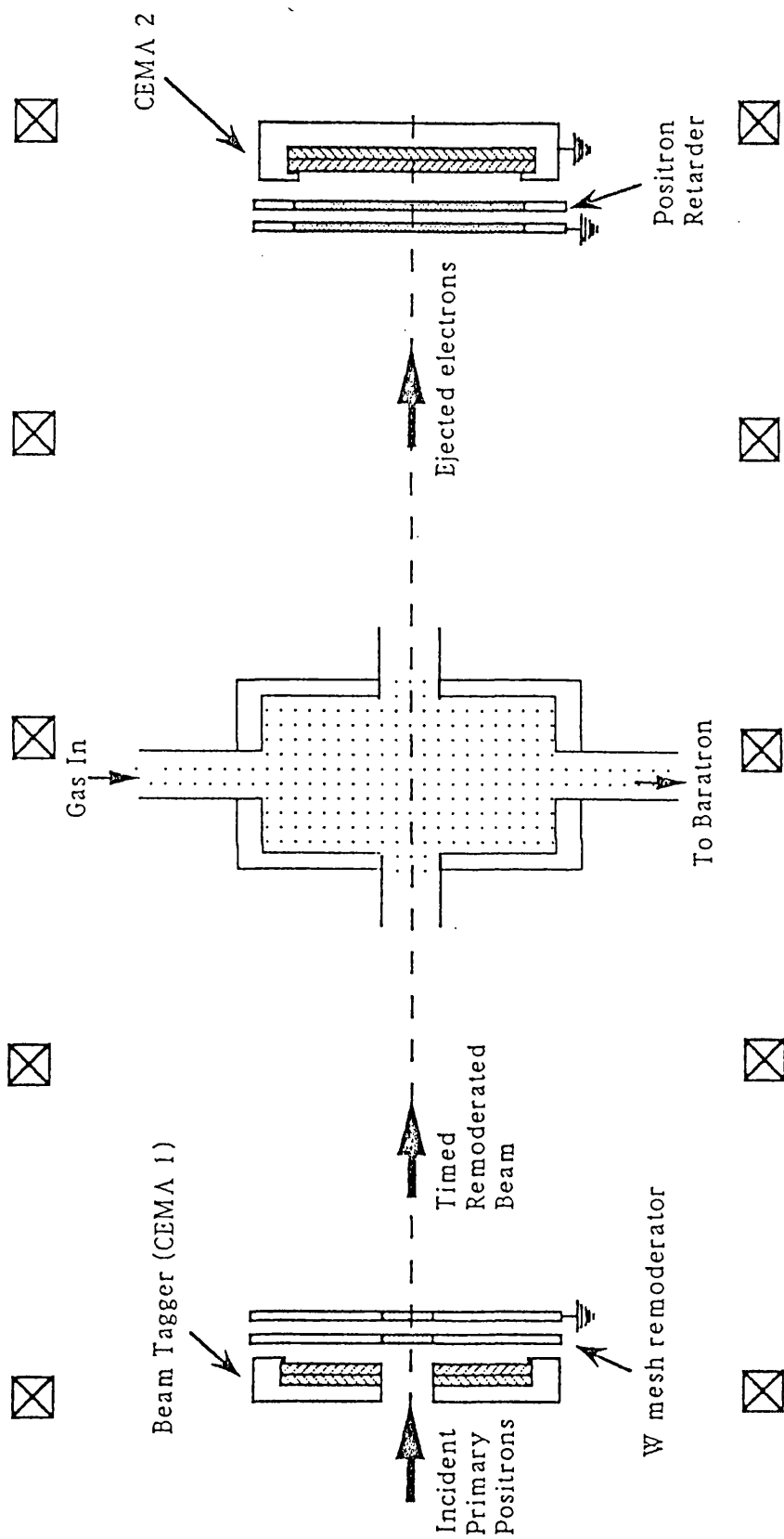


Fig 5.11 A schematic diagram of the interaction region.

	$e^-$	$e^+$
Front,CEMA2	+400	-400
Back,CEMA2	+2800	+2200
Collector,CEMA2	+3000	+2400
Retarder	+500	Earth

Table 5.1 A table showing the potentials that are applied to parts of the CEMA2 assembly when detecting  $e^-$  or  $e^+$ .

an Al coated recess which served as the charge collector, the inner surface of the central tube was coated with Al paint and connected to a stainless steel base on which the ceramic was mounted. The tube and base were held at -325V. The remoderator meshes were held between stainless steel apertures mounted off the ceramic MCP holder at a distance of 14mm from the first plate. The front of the MCP arrangement was at +275V to attract electrons emitted from the remoderator on positron impact and to repel positrons re-emitted in the backward direction. A potential of +3.5keV on the back of the plates and +3.7keV on the collecting screen provided a gain in excess of  $10^8$  with this detector. In Figure 5.11 the remoderator and CEMA1 arrangement can be seen, this assembly was held off a brass flange by a movable shaft which allowed it to be moved linearly perpendicular to the beam axis and rotated about its line of motion-this enabled its accurate location by maximizing the observed count-rate.

The timed, remoderated  $e^+$  beam then passes through the interaction region, this consists of two brass pumping ports connected by a brass tube which contains the scattering cell. This cell is 200mm long and has an internal diameter of 30mm, it

is held on the axis of the beam by two ¼" Cu pipes screwed into the body of the cell and soldered onto the external brass tube. Gas is admitted into the cell via one of these tubes, its flow being controlled with an Edwards LV5 leak valve and the pressure being monitored with an MKS 220-1 Baratron capacitance manometer attached to the other tube. To reduce the conductance of the entrance and exit apertures of the cell and thus maintain a fairly high number density of gas atoms within the cell, two cylindrical brass tubes of diameter 7mm and length 11.8mm were placed at the apertures. This region of the vacuum system was evacuated with Edwards E04 diffusion pumps backed with Edwards ED250 rotary pumps attached to both pumping ports. The interaction region is shown schematically in Figure 5.11. Charged particles emanating from the gas cell, be they scattered positrons or electrons ejected in ionizing collisions, are confined by the axial magnetic field and travel towards another MCP detector (CEMA2) placed 0.3826m from the centre of the cell. CEMA2 consisted of three Varian VUW8926 MCP's of 25mm active diameter, again their operation is fully described in section 3.2. An arrangement of three W grids placed in front of these plates was incorporated, following Zafar (1990), to electrostatically retard unwanted particles and prevent them reaching the detector and to return to the detector secondary electrons released by particles incident on a non-active part of the plate surface (e.g. between channels) thus increasing the detection efficiency. This was achieved by earthing the front grid, applying to the second grid a potential sufficient and of the correct polarity to retard those particles that are not required for detection and applying to the third grid -520V. The plate potentials for positron or electron detection are shown in Table 5.1. The grids were mounted directly on the CEMA2 assembly which itself was attached to a linear shaft mounted on a brass flange.

The timing sequence employed was inverted in that the start signal was taken as the output pulse of CEMA2 with the stop signal being the delayed output pulse of CEMA1. This system was used because the higher count rate of CEMA1 ( $\approx 10^4$ ) compared to CEMA2 ( $\leq 10^2$ ) could lead to pulses from CEMA2 being lost due to the dead time of the Time to Amplitude Converter. A block diagram of

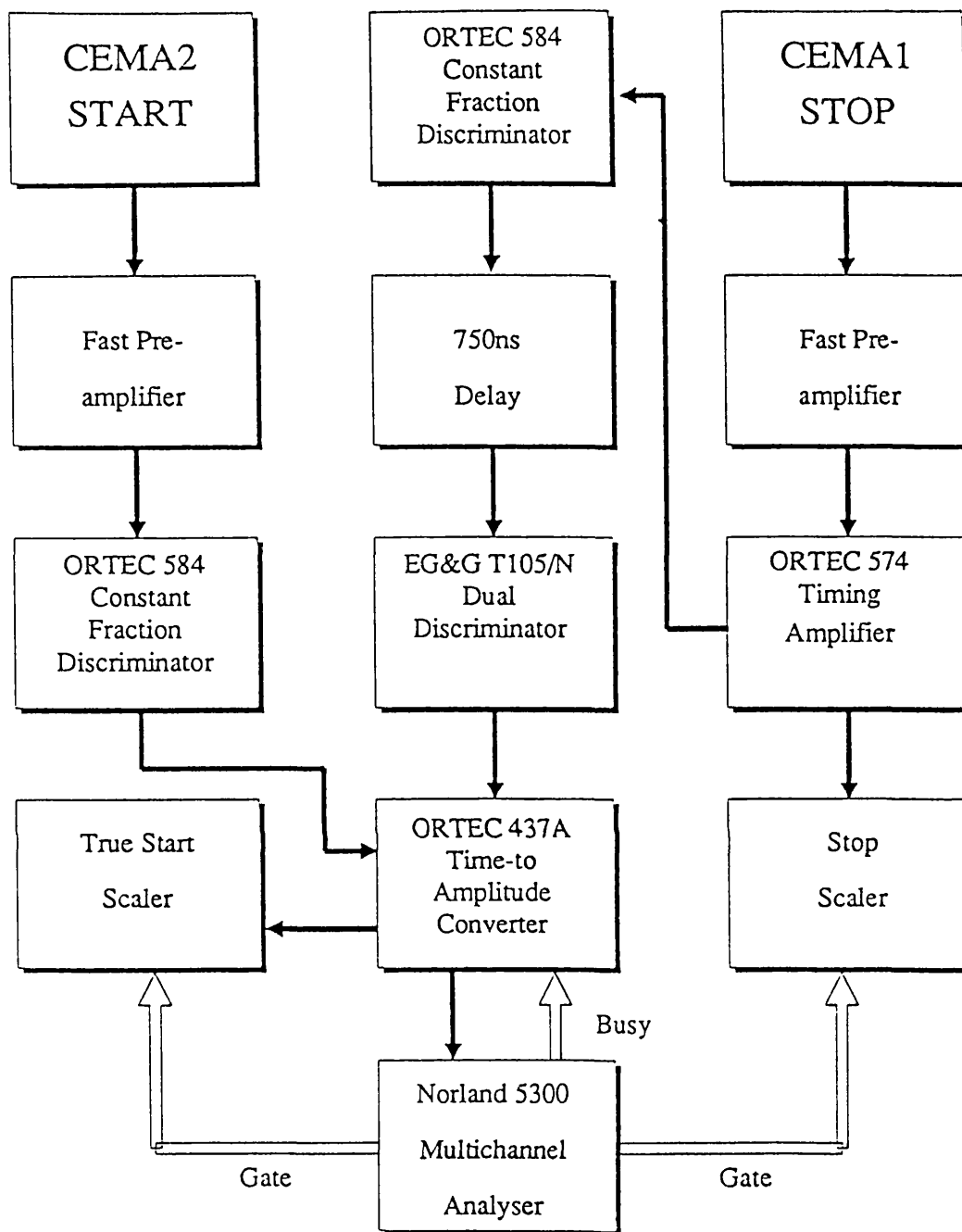


**Fig 5.12** A schematic diagram of the timing electronics.

the timing electronics is given in Figure 5.12.

### *5.3.3 Experimental Procedure*

Measurements were made over a positron energy range of 10-150 eV and at two magnetic field strengths 15 Gauss and 25 Gauss. At each energy the same procedure of beam optimization, experimental runs and beam checking was carried out. Beam optimization was done, with suitable potentials on CEMA2, by adjusting the positions of the Helmholtz coils so that the count-rate of timed positrons going into a peak on their time-of-flight spectrum was at its maximum. The potentials on CEMA2 were then changed so that electrons could be observed. As has been stated, one of the main sources of uncertainty in this experiment is the exact origin of the electrons that are detected - some will be produced in the impact ionization of Ar by positrons but many will arise from positron impact on metal surfaces in the interaction region. To eradicate this problem as well as accounting for any remnants of the primary or remoderated positron beam being detectable two experimental runs were made at each energy - one with gas in the scattering cell and one without. Random coincidences produced an uniform background in each spectrum which was ascertained by averaging over 50 channels in a flat part of the spectrum, this was then subtracted from the signal in each channel. Channel numbers were converted to times-of-flight using values for the time-per-channel (1.15ns) and the zero time channel (number 689) that were previously determined for the same system by Zafar (1990). The time-of-flight spectrum obtained in the vacuum run was then subtracted from that obtained in the gas run to get an ejected electron time-of-flight spectrum. Examples of the spectra obtained in this way are shown in Fig 5.11 for both magnetic field strengths used, these will be discussed in more detail in the following section.

### *5.4.4 Results and Discussion*

The time-of-flight spectra obtained by the method described above all exhibited

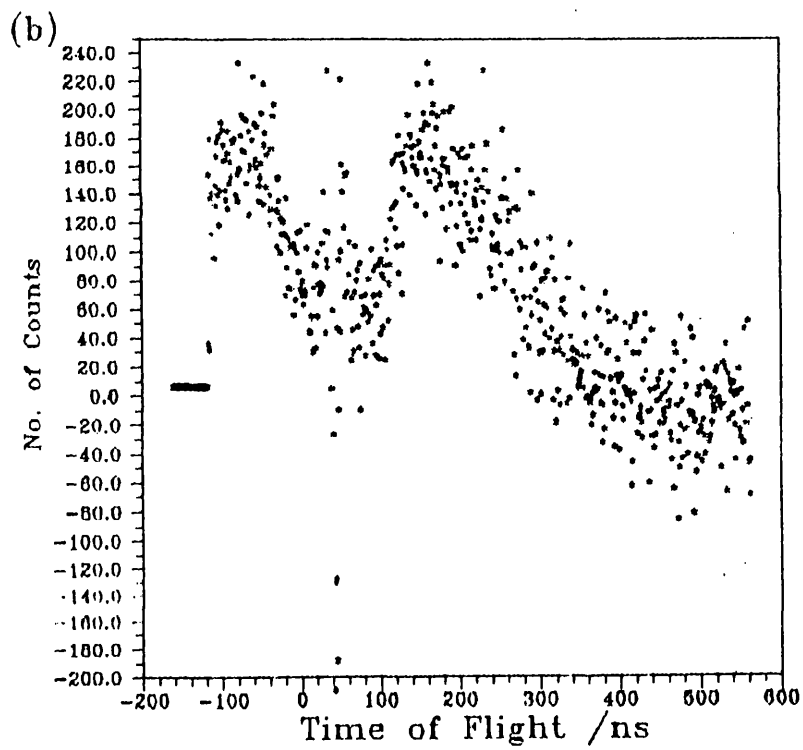
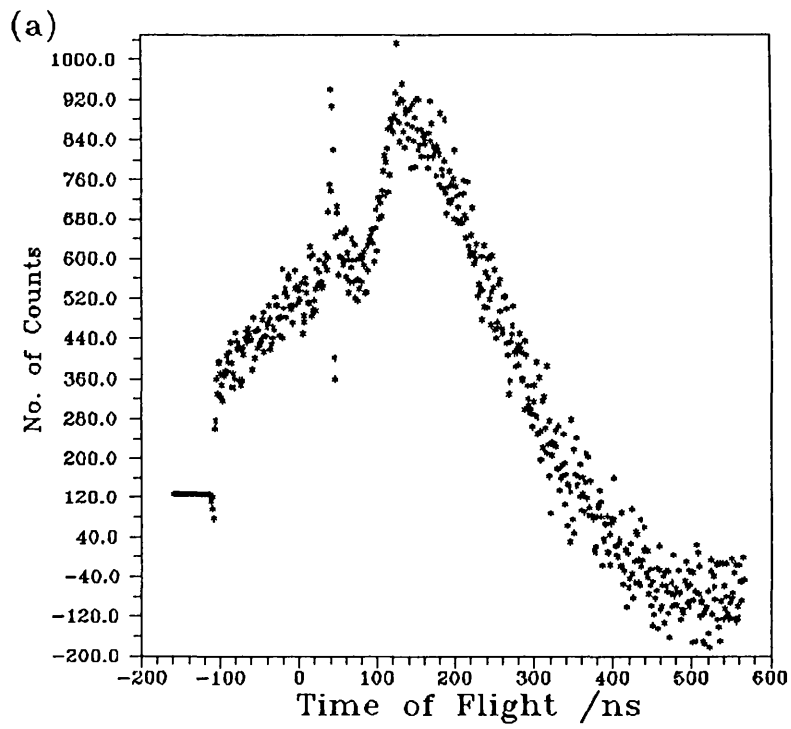


**Fig 5.13** The time-of-flight spectra of electrons detected after the ionization of Argon atoms by  $\text{ }^0_+1\text{eV}$  positrons in magnetic fields of (a) 15 Gauss and (b) 25 Gauss

peaks similar to those in Figure 5.11. The peak at negative time in Figure 5.11 (a) is due to the coincidental detection of electrons by CEMA2 and electrons liberated at CEMA2 travelling down the flight tube to CEMA1. The structure which shows a sharp maximum and a sharp minimum adjacent to each other at a small positive time are as a result of incorrect matching of the zero time channels of the vacuum and gas spectra resulting in the peaks for energetic positrons in the two spectra not cancelling out exactly. It can be seen from the spectra that negative values are obtained at long flight times - this is because, when gas is present, many slow electrons will scatter off the atoms at angles greater than the acceptance angle of the system and will thus not be detected. Since these electrons will be unscattered in the vacuum run they will appear at their proper times-of-flight therefore on subtraction of the spectra negative values will be obtained.

The broad peak at a larger positive time is taken to be that due to electrons originating in the ionizing collisions of positrons on Ar atoms. This being the case, one can then deduce the electrons' time of flight from

$$T = t_{e+} + t_{e-} \quad (5.12)$$

where T is the measured time of flight,  $t_{e+}$  is the time of flight of the positron from the remoderator to the mid-point of the scattering cell and  $t_{e-}$  is the time of flight an electron ejected on ionization from the mid-point of the scattering cell to the CEMA2 detector. The positrons' flight times can be calculated from a knowledge of their energies' and distance travelled. Equation (5.11) can then be written

$$t_{e-} = T - l_e \cdot \sqrt{\frac{m}{2eE_{e+}}} \quad (5.13)$$

where  $l_{e+}$  is the distance from the remoderator to the mid-point of the scattering cell and  $E_{e+}$  is the positrons' energy set with the remoderator.  $l_{e+}$  was measured to be 0.1328m.

Having calculated  $t_{e-}$  from equation (5.12) the electrons' energy can be obtained from the relation

$$E_{e-} = \frac{1}{2}m\left(\frac{l_{e-}}{t_{e-}}\right)^2 \quad (5.14)$$

where  $l_{e-}$  is the distance from the mid-point of the scattering cell to the CEMA2 detector and is 0.4296m in this experiment. Thus the energy of electrons which contribute to the peaks in the time of flight spectra can be determined if one assumes that the acceptance angle of the detection system is small so that more energetic electrons which scatter at small angles are not detected with the same flight time as those travelling on axis. The energy which corresponds to the position of the peak was then calculated for each spectrum taken. The peak position was simply taken as the channel with the maximum number of counts. The error bars assigned to this value were derived by considering the standard deviation of a number of random counts ( $\sqrt{N}$  for a number  $N$ ) for the peak number and finding the extreme channels either side whose similarly derived errors overlap with those of the peak value.

After making the assumptions listed above it can be inferred that these energies are those of electrons which have been ejected on ionization and travel in the forward direction (i.e. at  $0^\circ$  to the path of the incident positron). If such electrons exhibit a high degree of correlation with the scattered positron quantum calculations predict that they will have the same energy as the positron (see previous section). The energy of each outgoing particle is then given by

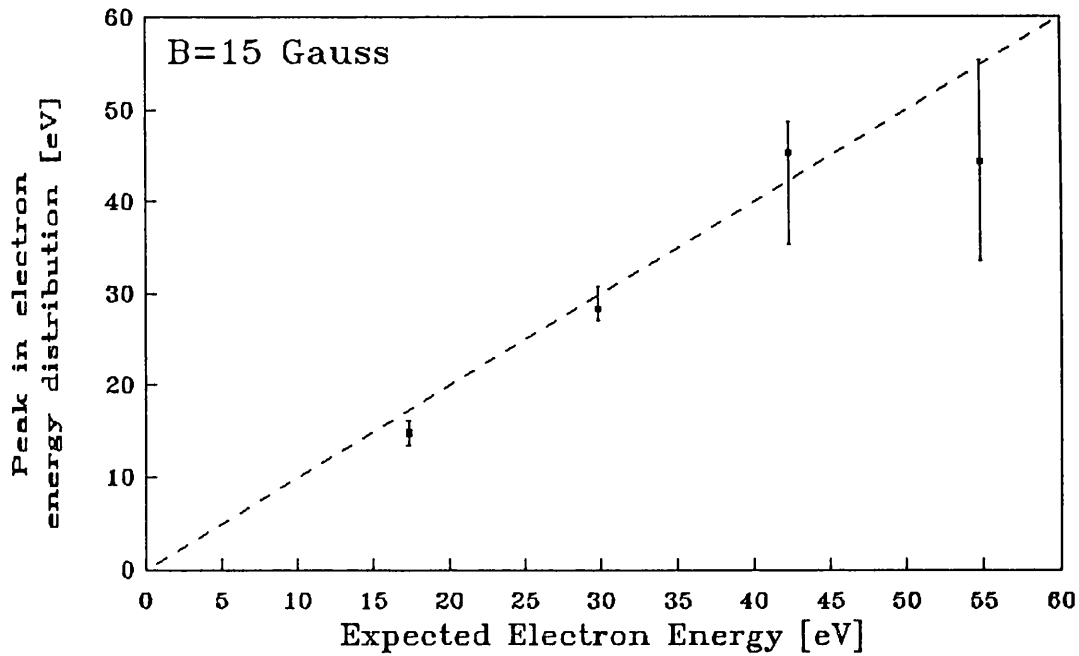


Fig 5.12(a) A plot of the observed positions of the peaks in the electron energy distributions against those values of electron energy expected from theory at 15 Gauss.

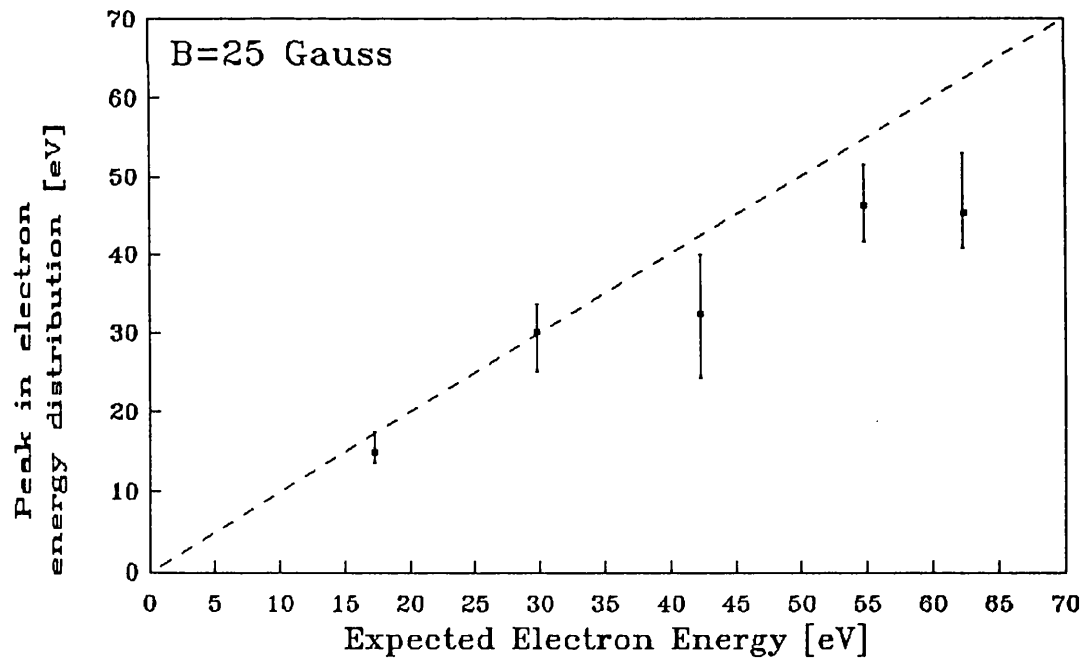


Fig 5.12(b) A plot of the observed positions of the peaks in the electron energy distributions against those electron energies expected from theory at 25 Gauss.

$$E = \frac{E_e - E_I}{2} \quad (5.15)$$

where  $E_I$  is the energy required for ionization of the target gas ( $E_I = 15.4\text{eV}$  for Ar). This has been calculated for each positron energy and Fig 5.12 shows the observed position of the peak in the electron energy spectrum plotted against this expected energy for both magnetic field strengths used. The broken line on each graph indicates the positions of the points that would be expected from theory.

It can be seen there is slightly better agreement with theoretical predictions for data taken at 15 Gauss than at 25 Gauss. The data taken at the higher field strengths tends to fall below the line but this can be understood if one considers the generally larger acceptance angle at the higher field. This would result in the collection of more electrons which are travelling near to but not on axis. Their longer flight path would lead to their having longer flight times-they would then appear to have less energy than expected even if they did have this energy.

Given the sources of error inherent in this experiment and the resulting large error bars in the graphs in Figure 5.12 one cannot make any quantitative conclusions about the post-collision dynamics of the system under study. The broad agreement of the experimentally determined electron energies with the theoretically predicted data does however suggest that the number of electrons ejected with energies characteristic of those captured into continuum states is not negligible. Some enhancement of the doubly differential cross-section for electron ejection in positron-Ar ionization might therefore be expected at these energies. This preliminary work therefore lends some support to the premisses of the quantum calculations which emphasise the importance of the Coulomb interaction between the ejected electron and the scattered positron.

## CHAPTER 6

### CONCLUSION

The work presented in this thesis is a study of impact ionization processes in gases. The main body of work has been an investigation of positron and electron impact ionization of molecular hydrogen as part of the development of an experiment to measure the positron impact ionization cross-section of atomic hydrogen. To date there has been one measurement of this quantity over a range of incident positron energies (Spicher *et al*, 1990) and the results differ considerably from the predictions of existing theory. The magnitude of the measured ionization cross-section was also twice that for electron impact ionization at intermediate energies - an observation consistent with previous measurements of the ionization cross-sections of other gaseous targets. As has been discussed, a recent theoretical calculation by Campeanu (1990) on the  $e^+$ -H system which incorporates an interaction between the scattered positron and the ejected electron in the final state yields results closer to those observed than any previous calculation. This would appear to indicate the importance of such an interaction in positron impact ionization of atomic hydrogen. One would infer therefore that the attractive positron-electron interaction increases the likelihood of ionization occurring in positron scattering off bound state systems as opposed to electron scattering. To draw such conclusions about the fundamental aspects of collision dynamics require accurate experimental thus enabling comparison with theoretical models. Possible sources of uncertainty in the only experiment to measure the positron ionization cross-section of atomic hydrogen have been discussed in Chapter 1 so a further measurement of this cross-section, for one of the simplest three-body scattering processes, is clearly warranted.

Thus far, in the present work, it has been demonstrated that relative cross-sections can be measured with the experimental apparatus that has been constructed. The

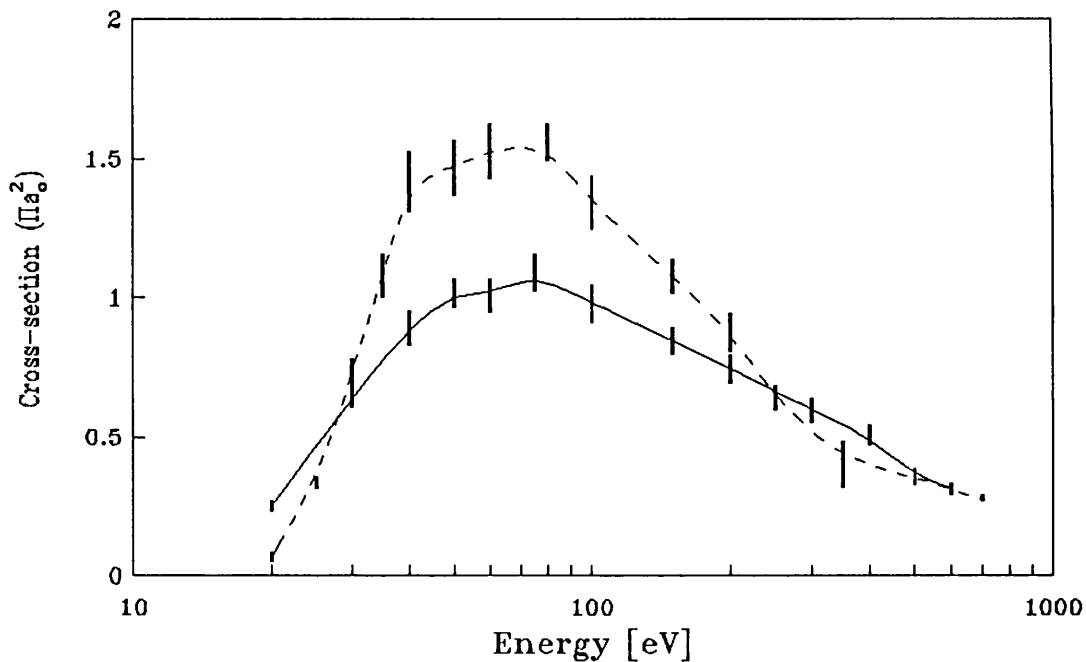


**Fig 6.1** Curves drawn through the relative positron (- - -) and electron (—) ionization cross-sections of  $H_2$  measured in this experiment to illustrate comparisons made in the text.

ionization cross-sections of positrons and electrons incident on molecular hydrogen have been measured and are in agreement with the results of the experiments of Fromme *et al* (1988) and Knudsen *et al* (1990) for positrons and Rapp and Englander-Golden (1965) for electrons, the latter having been corrected for dissociative ionization. Their observations are consistent with the present data as illustrated in Figure 6.1 which shows curves drawn through the data points obtained in this experiment for both electrons and positrons. At intermediate energies the positron ionization cross-section exceeds that for electrons; several contributory effects have been postulated to explain this. These include the reduction of the electron cross-section due to the possibility of exchange as was demonstrated by Peterkop (1962); polarization of the target charge cloud which can increase the positron cross-section and decrease the electron cross-section and, finally, saddle-

point ionization which can only occur for positive particles and has been predicted for protons (Pieksma *et al*, 1991) and would serve to increase the positron ionization cross-section should it occur. Within about 10eV of the ionization threshold the opposite case occurs and the electron ionization cross-section exceeds that for positrons, this is an energy range where the positronium formation cross-section is still significant so this process will compete with ionization for positrons with the possible consequence of a reduction in the ionization cross-section. At high energies (greater than about 600eV) the cross-sections are seen to merge as expected from the Born approximation (see section 2.3.1.1).

Preliminary studies with the atomic hydrogen source in operation have revealed several unforeseen difficulties arising from its use, these have included photons, electrons and protons being emitted from the discharge tube in fluxes sufficient to make it impossible to detect  $H^+$  ions. Coating the inside of the system with a non-reflective substance (soot) and using electrostatic fields to prevent the charged particles from being detected has allowed protons created on positron impact to be detected. The next investigation that will be made with this apparatus is of the energy dependence of the yield of  $H^+$  ions (as defined in section 4.2.1) using an electron beam. This can then be compared with the well-known electron impact ionization cross-section of atomic hydrogen as a further test on the suitability of this experimental arrangement to determine the positron ionization cross-section. If, as anticipated, no insoluble systematic sources of error are discovered then the positron impact ionization cross-section of atomic hydrogen can be measured.

In the second part of this work another ionization process was studied - electron capture to the continuum (ECC). This is complementary to the other experimental work as its presence indicates a high degree of correlation between the scattered positron and ejected electron, which is thought to be the case in positron-atomic hydrogen ionization (Campeanu, 1990). The experimental work involved studying the energy distributions of electrons ejected in positron impact ionization of Argon, the

distributions being derived from the electrons' time-of-flight spectra. Electrons which are captured to the continuum states of projectiles will have identical velocity vectors to the projectile and, in the case of positron scattering, each outgoing particle will share equally the residual kinetic of the projectile after ionization. The energy distributions of these electrons are therefore indicative of the extent of ECC. Given the uncertainty surrounding the origin, and therefore energy, of many detected electrons, conclusions drawn from the results of this experiment can at best be tentative. It is certain however that a large number of electrons have velocities close to that expected for those which are in continuum states of the scattered positron. This does imply that ECC is a process which occurs to some extent in positron ionization but to what degree, which is the contentious issue that has arisen from different methods of calculation, is difficult to assess. This is because of the ambiguity surrounding the cause of the peaks being quite broad around the expected velocities in the time-of-flight spectra. The peaks are broadened in this manner either because they reflect a broad structure in the energy dependence of the doubly differential cross-section (as predicted by Schultz and Reinhold's CTMC calculation, 1989) or are due to the detection of equivelocity electrons emitted over a wide range of angles because of the finite magnetic field present. This therefore does not rule out the possibility that the recent calculation of Sil *et al* (1991), which predicts cusps in energy in the doubly differential cross-section at all energies, is accurate. Recent results from a modified form of the same apparatus (Moxom *et al*, 1991) which support the classical results are not entirely free of this ambiguity either and a proposed study of this process with an electrostatic system (Köver, 1991) is awaited to resolve this.

Both pieces of experimental work discussed in this thesis therefore study the post-collision dynamics of the outgoing particles in positron impact ionization. The experiment with atomic hydrogen, which appears to be nearing completion, will give an indication of the degree of correlation between the scattered positron and ejected electron in positron impact ionization of atomic hydrogen - one of the most

fundamental collision systems. These results may then give an indication of the significance of ECC in positron impact ionization of heavier atoms, as was studied in the second experiment.

## REFERENCES

- Abrines R and Percival I C (1966a) Proc Phys Soc **88**, 861  
(1966b) Proc Phys soc **88**, 873
- Adachi S, Chiba M, Hirose T, Nagayama S, Nakamitsu Y, Sato T and Yamada T,  
(1990) Phys Rev **A65**, 2634
- Amusia M Ya, Cherepkov N A, Chernysheva L V and Shapiro S G, (1976) J Phys B  
**9**, L531
- Andersen L H, Hvelplund P, Knudsen H, Moller S P, Elsener K, Rensfelt K G and  
Uggerhoj E, (1986) Phys Rev Lett **57**, 2147
- Andersen L H, Hvelplund P, Knudsen H, Møller S P, Sørensen A H, Elsener K,  
Rensfelt K G and Uggerhoj E, (1987) Phys Rev **A36**, 3612
- Andersen L H, Hvelplund P, Knudsen H, Moller S P, Pedersen J O P, Tang-Petersen  
S, Uggerhoj E, Elsener K and Morenzoni E, (1990) Phys Rev **A71**, 6536
- Anderson C D, (1932) Phys Rev **41**, 405
- Andrikoupoulos K, Avdi E and Laricchia G, (1991) *Private Communication*
- Basu M, Mazumdar P S and Ghosh A S, (1985) J Phys B **18**, 369
- Basu M and Ghosh A S, (1988) J Phys B **21**, 3439
- Bethe H A, (1930) Ann Physik **5**, 325
- Bhatia A K, Temkin A, Drachman R J and Eiserike H, (1971) Phys Rev **A3**, 1328
- Bhatia A K, Temkin A and Eiserike H, (1974) Phys Rev **A9**, 219
- Blackett P M S and Occhialini G P S, (1933) Proc Roy Soc **A139**, 699
- Born M, (1926) Z für Physik **38**, 803
- Boyd R L F and Boksenberg A, (1961) in "Proceedings of the Fourth International  
Conference on Ionization Phenomena in Gases" (North Holland, 1960) p.253  
Boyd R L F and Green G W, (1958) Proc Phys Soc **71**, 351
- Brandes G R, Canter K F, Horsky T N, Lippel P H and Mills A P, (1988) Rev Sci  
Instrum **59**, 228
- Brandes G R, Mills A P and Zuckerman D M, (1991) in "Book of Abstracts, 9th  
International Conference on Positron Annihilation", p.K5
- Bransden B H and Joachain C J, (1983) "Physics of Atoms and Molecules"
- Bransden B H, McCarthy I E and Stelbovics A T, (1985) J Phys B **18** 823

- Brauner M and Briggs J S, (1986) *J Phys B* **19**, L325
- Brown C J and Humberston J W, (1985) *J Phys B* **18**, L401
- Brun-Nielsen L, (1990) Masters Thesis, Aarhus University
- Brunings J, (1934) *Physica* **1**, 996
- Burke P G and Taylor A J, (1965) *Proc Roy Soc* **A287**, 105
- Byron F W, (1978) *Phys Rev* **A17**, 170
- Byron F W, Joachain C J and Potvliege R M, (1981) *J Phys B* **14**, L609  
(1985) *J Phys B* **18**, 1637
- Campeanu R I, (1990) *Private Communication*
- Campeanu R I, Fromme D, Kruse G, McEachran R P, Parcell L A, Raith W, Sinapius G and Stauffer A D, (1987a) *J Phys B* **20**, 3557
- Campeanu R I, McEachran R P and Stauffer A D, (1987b) *J Phys B* **20**, 1635
- Canter K F, Coleman P G, Griffith T C and Heyland G R, (1972) *J Phys B* **5**, L167
- Caswell W E and Lepage G P, (1979) *Phys Rev* **A20**, 36
- Charlton M, (1985) *Rep Prog Phys* **48**, 737  
(1989) in "Positron Annihilation" (World Scientific, 1989) eds Dorikens-Vanpraet L, Dorikens M and Segers D, p181  
(1990) *Physica Scripta* **42**, 464
- Charlton M, Clark G, Griffith T C and Heyland G R, (1983) *J Phys B* **16**, L465
- Charlton M, Griffith T C, Heyland G R and Twomey T R, (1980) *J Phys B* **13**, L239
- Charlton M, Laricchia G, Zafar N and Jacobsen F M, (1987) in "Atomic Physics with Positrons" eds Humberston J W and Armour E A G (Plenum, 1987) p.15
- Charlton M, Andersen L H, Brun-Nielsen L, Deutch B I, Hvelplund P, Jacobsen F M, Knudsen H, Laricchia G, Poulsen M R and Pedersen J O, (1988) *J Phys B* **21**, L545
- Charlton M, Brun-Nielsen L, Deutch B I, Hvelplund P, Jacobsen F M, Knudsen K, Laricchia G and Poulsen M R, (1989) *J Phys B* **22**, 2779
- Chen D M, Lynn K G, Pareja R and Nielsen B, (1985) *Phys Rev* **B31**, 4123
- Cherry W, (1958) PhD Thesis, Princeton University
- Coleman P G, (1986) in "Proceedings of the 3rd International Workshop on Positron (Electron)-Gas Scattering (World Scientific, 1986) eds Kauppila W E, Stein T S and Wadehra J M, p.25
- Coleman P G and Hutton J T, (1980) *Phys Rev Lett* **45**, 2017

Coleman P G, McNutt J D, Diana L M and Burciaga J R, (1979) *Phys Rev A* **20**, 145

Coleman P G, Hutton J T, Cook D R and Chandler C A, (1982) *Can J Phys* **60**, 584

Coleman P G and McNutt J D, (1979) *Phys Rev Lett* **42**, 1130

Costello D G, Groce D E, Herring D F and McGowan J W,  
 (1972a) *Phys Rev B* **5**, 1433  
 (1972b) *Can J Phys* **50**, 23

Dahl D A and Delmore J E, (1988) "The SIMION PC/PS2 User's Manual" (Idaho National Engineering Laboratory, 1988)

Dale J M, Hulett L D and Pendyala S, (1980) *Surf Int Anal* **2**, 199

Dalgarno A and Lynn N, (1958) *Proc Phys Soc* **223**, 223

de Heer F J and Inokuti M, (1982) in "Electron Impact Ionization" eds Märk T D and Dunn G H, (Springer-Verlag, 1982) p.232

Deutsch M, (1951) *Phys Rev* **82**, 455

Dewangan D P and Walters H R J, (1977) *J Phys B*, **10**, 637

Diana L M, Fornari L S, Sharma S C, Pendleton P K and Coleman P G, (1985a) in "Positron Annihilation" (World Scientific, 1985) eds Jain P C, Singru R M and Gopinathan K P, p 342

Diana L M, Sharma S C, Fornari L S, Coleman P G, Pendleton P K, Brooks D L and Seay B E, (1985b) in "Positron Annihilation" (World Scientific, 1985) eds Jain P C, Singru R M and Gopinathan K P, p 428

Diana L M, Chaplin R L, Brooks D L, Coleman P G and Howell J P, (1989) in "Positron Annihilation" (World Scientific, 1989) eds Dorikens-Vanpraet L, Dorikens M and Segers D, p308

Ding A, Karlan J and Weise J, (1977) *Rev Sci Instrum* **48**, 1002

Dirac P A M, (1930a) *Proc Roy Soc A* **126**, 360  
 (1930b) *Proc Camb Phil Soc* **26**, 361

Donnelly A, (1991) *Private Communication*

Drachman R J, (1966) *Phys Rev* **144**, 25

Drachman R J, Omidvar K and McGuire J H, (1976) *Phys Rev A* **14**, 100

Faddeev L D, (1961) *Zh Eksperim i Teor Fiz*, **39**, 1459

Fite W L and Brackmann R T, (1958) *Phys Rev* **112**, 1141

Fock V, (1935) *Z Physik* **98**, 145

Fornari L S, Diana L M and Coleman P G, (1983) *Phys Rev Lett* **51**, 2276

Frieze W E, Gidley D W and Lynn K G, (1985) *Phys Rev* **B31**, 5628

Fromme D, Kruse G, Raith W and Sinapius G, (1986) *Phys Rev Lett* **57**, 3031

Fromme D, Kruse G, Raith W and Sinapius G, (1988) *J Phys B* **21**, L261

Fulton T and Martin P C, (1954) *Phys Rev* **95**, 811

Funk H, (1930) *Ann Physik* **4**, 149

Gailitis M, (1965) *Sov Phys JETP* **20**, 107

Geltman S and Hidalgo M B, (1974) *J Phys B* **7**, 831

Ghosh A S, Majumdar P S and Basu M, (1985) *Can J Phys* **63**, 621

Gidley D W, Rich A, Sweetman E and West D, (1982) *Phys Rev Lett* **49**, 525

Gien T T, (1977) *Phys Rev* **A16**, 1736

Glauber R J, (1959) *Lec Notes in Th Phys* **1**, 315

Golden J E and McGuire J H, (1974) *Phys Rev Lett* **32**, 1218

Griffith T C and Heyland G R, (1978) *Phys Rep* **39C**, 169

Griffith T C, Heyland G R, Lines K S and Twomey T R, (1979) *App Phys* **19**, 431

Griffith T C and Heyland G R, (1978) *Phys Rep* **39C**, 169

Groce D E, Costello D G, McGowan J W and Herring W F, (1968) *Bull Am Phys Soc* **13**, 1397

Gryzinski M, (1959) *Phys Rev* **115**, 374  
(1965) *Phys Rev* **A138**, 305

Gullikson E M and Mills A P, (1986) *Phys Rev Lett* **57**, 376

Gullikson E M, Mills A P, Crane W S and Brown B L, (1985) *Phys Rev* **B32**, 5484

Harris I and Brown L, (1957) *Phys Rev* **105**, 1656

Harting E and Read F H, (1976) "Electrostatic Lenses" (Elsevier Scientific Publishing, 1976) p.A1.7

Haugen H K, Andersen L H, Hvelplund P and Knudsen H, (1982) *Phys Rev* **A26**, 1962

Higgins K, Burke P G and Walters H R J, (1990) *J Phys B* **23**, 1345

Higgins K and Burke P G, (1991) in "Abstracts of Contributed Papers, 17th International Conference on the Physics of Electronic and Atomic Collisions" eds McCarthy I E, MacGillivray W R and Standage M C, p347

Humberston J W, (1979) in "Advances in Atomic and Molecular Physics" eds Bates

DR and Bederson B (Academic Press, New York) **15**, 101

Humberston J W, (1984) J Phys B **17**, 2353

Humberston J W and Campeanu R I, (1980) J Phys B **13**, 4907

Hutchins S M, Coleman P G, Stone R J and West R N, (1986) J Phys E **19**, 282

Inokuti M and McDowell M R C, (1974) J Phys B **7**, 2382

Jacobs S, (1951) Phys Rev **84**, 877

Jacobsen F M, Charlton M, Chevallier J, Deutch B I, Laricchia G and Poulsen M R,  
(1990) J App Phys **67**, 575

Kauppila W E and Stein T S, (1990) Adv At Mol Phys **26**, 1

Kauppila W E, Stein T S, Smart J H, Dababneh M S, Ho Y K, Downing J P and  
Pol V, (1981) Phys Rev **A21**, 725

Kauppila W E, Stein T S and Jeison G, (1976) Phys Rev Lett **36**, 580

Khan P and Ghosh A S, (1983) Phys Rev **A28**, 2181

Khan P, Mazumdar P S and Ghosh A S, (1985) Phys Rev **A31**, 1405

Kieffer L J and Dunn G H, (1966) Rev Mod Phys **38**, 1

Kingston A E, (1964) Phys Rev **A135**, 1537

Kövér Á, (1991) in "Book of Abstracts, 9th International Conference on Positron  
Annihilation", p.E24

Knudsen H, Andersen L H and Jensen K E, (1986) J Phys B **19**, 3341

Knudsen H, Brun-Nielsen L, Charlton M and Poulsen M R, (1990) J Phys B **23**, 3955

Landau L D and Lifshitz E M, (1959) "Statistical Physics", (Pergamon Press, 1959)  
p.11

Lang N D and Kohn W, (1971) Phys Rev **B3**, 1215

Laricchia G, Davies S A, Charlton M and Griffith T C, (1988) J Phys E **21**, 886

Laricchia G, Charlton M, Davies S A, Beling C D and Griffith T C, (1987) J Phys B  
**20**, L99

Lynn K G, (1980) *Unpublished, taken from Schultz and Lynn, 1988*

Lynn K G, Nielsen B and Quateman J H, (1985) Appl Phys Lett **47**, 239

MacAlpine W W and Schildknecht R O, (1959) Proc I R E, Dec 1959, 2099

Macek J M, (1970) Phys Rev **A1**, 235

Madansky L and Rasetti F, (1950) Phys Rev **79**, 397

Madey J M J, (1969) Phys Rev Lett **22**, 784

Makowski A J, Raczyński A and Staszewska G, (1986) *J Phys b* **19**, 3367

Mandal P and Guha S, (1979) *J Phys B* **12**, 1603

Mandal P, Guha S and Sil N C, (1979) *J Phys B* **12**, 2913

Mandal P, Roy K and Sil N C, (1985) in "Positron Annihilation" eds Jain P C, Srivastava R M and Gopinathan K P (World Scientific, 1985) p.395

(1986) *Phys Rev A* **33**, 756

Mandal P, Guha S and Sil N C, (1979) *J Phys B* **12**, 2913

Mapleton R A, (1966) *Proc Phys Soc* **87**, 219

Massey H S W and Mohr C B O, (1933) *Proc Roy soc A* **140**, 613

Massey H S W and Burhop E H S, (1938) *Proc Roy soc A* **167**, 53

McCarroll R, (1957) *Proc Phys Soc A* **70**, 460

McEachran R P, Morgan D L, Ryman A G and Stauffer A D, (1977) *J Phys B* **10**, 663

McGuire J H, Hidalgo M B, Doolen G D and Nuttall J, (1973) *Phys Rev A* **7**, 973

Mills A P, (1980) *App Phys* **23**, 189

Mills A P, Platzman P M and Brown B L, (1978) *Phys Rev Lett* **41**, 1076

Mizogawa T, Nakayama Y, Kawaratani T and Tosaki M, (1985) *Phys Rev A* **31**, 593

Mohorovicic S, (1934) *Astron Nachr* **235**, 94

Moliere G, (1947) *Z für Naturforschung* **2A**, 133

Morgan L A, (1982) *J Phys B* **15**, L25

Mori S and Sueoka O, (1984) *At Col Res Jpn* **12**, 8

Mott N F and Massey H S W, (1965) "The Theory of Atomic Collisions" 3rd ed., p.380

Moxom J, Jones G O, Kövér À, Laricchia G and Charlton M, (1991) in "Abstracts of Contributed Papers, 17th International Conference on the Physics of Electronic and Atomic Collisions" eds McCarthy I E, MacGillivray W R and Standage M C, p330

Mukherjee K K, Ranjit Singh N and Mazumdar P S, (1989) *J Phys B* **22**, 99

Murray C A and Mills A P, (1980) *Solid State Comm* **34**, 789

Nico J S, Gidley D W, Skalsey M and Zitzewitz P W, (1991) in "Book of Abstracts, 9th International Conference on Positron Annihilation", p.I32

O'Malley T F, Spruch L and Rosenberg L, (1961) *J Math Phys* **2**, 491

Ohsaki A, Watanabe T, Nakanishi K and Iguchi K, (1985) Phys Rev **A32**, 2640  
Oldham W J, (1967) Phys Rev **161**, 1  
Olson R E and Salop A, (1977) Phys Rev **A16**, 531  
Omidvar K, (1965) Phys Rev **140**, A26  
Ore A and Powell J L, (1949) Phys Rev **75**, 1696  
Parcell L A, McEachran R P and Stauffer A D, (1983) J Phys B **16**, 4249  
(1987) J Phys B **20**, 2307  
Peach G and McDowell M R C, (1983) *Unpublished*  
Pendyala S, Bartell D, Girouard F E and McGowan J W, (1976) Can J Phys **54**, 157  
Percival I C and Valentine N, (1967) in "Abstracts of the Fifth International  
Conference on the Physics of Electronic and Atomic Collisions, Leningrad eds  
Flaks IP and Solovyov E S, p.121  
Peterkop R K, (1961) Proc Phys Soc **77**, 1220  
(1962) Sov Phys JETP **14**, 1377  
Poth H, (1989) Comments At Mol Phys **22**, 211  
Rapp D and Englander-Golden P, (1965) J Chem Phys **43**, 1464  
Rapp D, Englander-Golden P and Briglia D D, (1965) J Chem Phys **42**, 4081  
Reinhold C O and Olson R E, (1989) Phys Rev **A39**, 3861  
Rödbro M and Andersen F D, (1979) J Phys B **12**, 2883  
Rothe E W, Marino L L, Neynaber R H and Trujillo S M, (1962) Phys Rev **125**, 582  
Rudd M E and Macek J H, (1972) Case Studies in Atom Phys **3**, 47  
Rudd M E, Sautter C A and Bailey C L, (1966) Phys Rev **151**, 20  
Rudge M R H and Seaton M J, (1964) Proc Phys Soc **A283**, 262  
Rudge M R H, (1968) Rev Mod Phys **40**, 564  
Schrader D M, (1979) Phys Rev **A20**, 918  
Schultz D R and Olson R E, (1988) Phys Rev **A38**, 1866  
Schultz P J and Lynn K G, (1988) Rev Mod Phys **60**, 701  
Schultz D R and Reinhold C O, (1990) J Phys B **23**, L9  
Schultz D R, Olson R E and Reinhold C O, (1991) J Phys B **24**, 521  
Shah M B, Elliott D S and Gilbody H B, (1987) J Phys B **20**, 3501  
Shakeshaft R and Wadehra J M, (1980) Phys Rev **A22**, 968  
Sil N C, Roy K and Mandal P, (1991) in "Abstracts of Contributed Papers, 17th

Sinapius G, Raith W and Wilson W G (1980) J Phys B **13**, 4079

Slevin J A and Stirling W, (1981) Rev Sci Inst **52**, 1780

Sommerfeld (1931) Ann der Physik **11**, 257

Spicher G, Olsson B, Raith W, Sinapius G and Sperber W, (1990) Phys Rev Lett **64**,  
1019

Srivastava R, Katiyar A K and Khurana I, (1987) J Phys B **20**, 1853

Stabler R C, (1964) Phys Rev **A133**, 1268

Stein T S, Kauppila W E, Pol V, Smart J H and Jeison G, (1978) Phys Rev **A17**, 6

Stein T S, Kauppila W E and Roellig L O, (1974) Rev Sci Inst **45**, 951

Sueoka O, (1989) *Private Communication*

(1982) J Phys Soc Jpn **51**, 3757

Tate J T and Smith P T, (1932) Phys Rev **39**, 270

Temkin A and Lamkin J C, (1961) Phys Rev **121**, 788

Thomson J J, (1912) Phil Mag **23**, 449

Tong B Y, (1972) Phys Rev **B5**, 1436

Tripathi S, Sinha C and Sil N C, (1989) Phys Rev **A39**, 2924

van House J, Rich A and Zitzewitz P W, (1984) Origins of Life **14**, 413

Vehanen A, Lynn K G, Schultz P J and Eldrup M, (1983) App Phys **A32**, 163

Vehanen A and Mäkinen J, (1985) App Phys **A36**, 97

Viennet J, Petit P and Audoin C, (1973) J Phys E **6**, 257

Vogt H, Schuch R, Justiniano E, Schulz M and Schwab W, (1987) Phys Rev Lett **57**,  
2256

Wadehra J M, Stein T S and Kauppila W E, (1981) J Phys B **14**, L783

Walters H R J, (1988) J Phys B **21**, 1893

Watkin S, (1985) PhD Thesis, Stirling University

Westbrook C I, Gidley D W, Conti R S and Rich A, (1987) Phys Rev Lett **58**, 1328

Wetmore A E and Olson R E, (1986) Phys Rev **A34**, 2822

Weyl H, (1931) "Gruppentheorie und Quantenmechanik" 2nd ed., p234

Wheeler J A, (1946) Ann N Y Acad Sci **48**, 219

Wicke E and Brodowsky H, (1978) in "Hydrogen in Metals II: Application Oriented

- Properties" (Springer-Verlag, 1978) eds Alefeld G and Völkl J, p139
- Wilson W G, (1978) J Phys B **11**, L629
- Winick J R and Reinhardt W P, (1978) Phys Rev **A18**, 925
- Wood R W, (1922) Proc Roy Soc **A102**, 1
- Wood B J and Wise H, (1962) J Phys Chem **66**, 1049
- Yang C N, (1950) Phys Rev **77**, 242
- Zafar N, (1990) PhD Thesis, University of London

## ERRATA

Page 22, Line 16: 'shall' should be 'will'

Page 32, Line 22: 'without' should be 'by'

Page 33, Line 7: 'this' should be 'these'

Page 33, Line 15: 'n' should be 'p'

Page 38, Line 16: 'left' should be 'right'

Page 39, Figure 1.8: The legend caption should also include

— . — Mandal *et al* (1979)

\_\_\_\_\_ Sum of n=1 Khan and Ghosh (1983) and n=2 Khan *et al* (1985)

— — — Roy *et al* (1984)

Page 40, Line 23: 'partitioning' should be 'partitioning'

Page 46, Line 19: 'questin' should be 'question'

Page 48, Line 15: '1.15' should be '1.16'

Page 57, Line 4: '1.13' should be '1.12'

Page 64, Line 2: 'was' should be 'were'

Page 64, Line 18: 'shown in Figure 1.29' should be deleted

Page 77, Line 1: ' $G_0^{(+)}(\mathbf{r}, \mathbf{r}')$ ' should be ' $G_0^{(+)}(\mathbf{r}, \mathbf{r}')$ '

Page 86, Line 1: '2.2.1' should be '2.3.1.1'

Page 86, Line 13: ' $\chi_{kf}$ ' should be ' $\chi_{kf}$ '

Page 97, Line 16: '500m' should be '500mm'

Page 103, Figure 3.5 (b): Ordinate axis should be labelled 'Pressure (mbar)'

Page 105, Line 5: 'on' should be 'one'

Page 110, Figure 3.7: 'OHFC' should be 'OFHC'

Page 114, Line 5: 'approxiametaly' should be 'approximately'

Page 114, Line 23: 'scalar' should be 'scaler'

Page 115: '3.9' should be '3.10'

Page 116: '3.10' should be '3.11'

Page 118, Line 16: 'spectrum' should be 'spectra'

Page 119, Line 3: ' $H_2$ ' should be ' $H_2$  spectrum'

Page 122, Line 15: '3.8' should be '3.11'

Page 129, Line 24: 'origniating' should be 'originating'

Page 130, Line 24: '4.9' should be '4.8'

Page 131, Line 13: '3.9' should be '3.11'

Page 131, Line 26: 'tantamount' should be 'paramount'

Page 131, Line 16: 'negligible' should be 'not negligible'

Page 133, Line 7: '3.3' should be '3.4'

Page 136, Line 11: 'greater' should be 'greater than'

Page 138, Line 4: '2.2.1' should be '2.3.1.1'

Page 141, Line 17: '2.2.1' should be '2.3.1.1'

Page 150, Line 20: 'secodary' should be 'secondary'

Page 161, Line 13: 'reusultingly' should be 'resultingly'

Page 162, Line 20: 'experimental' should be 'experimental results'

Page 165, Line 20: 'energies' should be 'angles'

Page 167 should include Boksenberg A, (1961) PhD Thesis, University of London

Page 175 should include Peterkop R K, (1960) Sov Phys JETP **14**, 1377